Drilled Shaft Socket Connections for Precast Columns in Seismic Regions

Hung Viet Tran

A dissertation

submitted in partial fulfillment of the

requirements for the degree of

Doctor of Philosophy

University of Washington

2015

Reading Committee:

John F. Stanton, Chair

Marc O. Eberhard, Co-Chair

Laura N. Lowes

Program Authorized to Offer Degree:

Civil and Environmental Engineering

University of Washington

Abstract

Drilled Shaft Socket Connections for Precast Columns in Seismic Regions

Hung Viet Tran

Co-Chairs of the Supervisory Committee:

John F. Stanton
Civil and Environmental Engineering

Marc O. Eberhard
Civil and Environmental Engineering

A new type of connection between a precast concrete column and a drilled shaft has been developed for Accelerated Bridge Construction (ABC) in regions of moderate or high seismicity. This connection can be built quickly and allows generous placement tolerances. Three quasi-static tests of connections between a precast bridge column and a drilled shaft were performed (1) to investigate the seismic performance of this connection, and (2) to calibrate a new design methodology.

The test specimens represented the most critical geometry in which the difference between the diameters of the shaft and column was minimized. Large-scale, lateral-load tests to a drift ratio of 10% showed that, if adequate confining steel is included in the splice zone, the plastic hinging mechanism forms in the column, without inducing damage in the splice or shaft. If the confinement is insufficient, the strength of the splice zone deteriorates rapidly with cyclic loading.

A new design methodology, based on a strut-and-tie model of the transition region, allows the designer to proportion the connection to limit the strains in the connection transverse reinforcement.

Table of Contents

List of Figures

List of Tables

Notation

A_{tr} or A_{sp} = area of shaft transverse reinforcement or spiral (in.^{2})

A_l = total area of longitudinal column reinforcement (in.^{2})

$A_{l,sh}$ = total area of longitudinal shaft reinforcement (in.^{2})

c = concrete cover at the top of the connection

C_c = column compressive resultant force

C_s = shaft compressive resultant force

$d_{b,col}$ = diameter of column longitudinal reinforcing bars

e = distance from the inner bar to the outer bar

f_c' = concrete compressive strength (ksi)

f_{cc} = confined concrete strength (ksi)

f_r = concrete modulus of rupture (ksi)

f_{yt} = specified minimum yield strength of shaft transverse reinforcement (ksi)

f_{ul} = specified minimum tensile strength of column longitudinal reinforcement (ksi), 90 ksi for A615 and 80 ksi for A706

L = length of the transition

l_a = required anchorage length

$l_{a,eff}$ = effective anchorage length

l_d = development length of reinforcing bar

l_{ns} = total noncontact lap splice length

l_s = Class C tension lap splice length of the column longitudinal reinforcement (in.)

M_c = column moment at the interface

$M_{c,ult}$ = column ultimate moment

$M_{p,col}$ = plastic moment capacity of the column

$M_{po,col}$ = over-strength plastic moment capacity of the column

M_{sh} = design moment demand in the shaft at the bottom of the transition

N_{col} = the number of column longitudinal reinforcing bars

R = radius of shaft spiral (in.)

T_c = column tensile resultant force

T_s = shaft tensile resultant force

T_{sp} = spiral resultant force

$T_{sp,yield}$ = spiral resultant force when the strain of the top spiral turn reaches yielding strain

s = radial center-to-center distance between the longitudinal bars of the column and those of the shaft

s_{tr} = spacing of shaft transverse reinforcement (in.)

V = column shear force

V_{po} = column shear force corresponding to the over-strength plastic moment of the column

X_{Cc} = distance from compressive resultant force to the centroid of column

X_{cs} = distance from compressive resultant force to the centroid of shaft

X_{Tc} = distance from tensile resultant force to the centroid of column

X_{Ts} = distance from tensile resultant force to the centroid of shaft

ε_{cu} = ultimate concrete compressive strain

ε_{sh} = onset of strain hardening

ε_t = lateral strain at the top of the transition

λ_{mo} = overstrength moment factor, which is equal to 1.2 for ASTM A706 reinforcement

Φ = curvature (1/in.)

τ_u = ultimate bond strength of the column longitudinal reinforcing bars

CHAPTER 1.

INTRODUCTION

1.1 THE NEED FOR RAPID CONSTRUCTION

The bridge construction industry faces new challenges. The most recent version of the Federal National Bridge Inventory (FHWA 2013) classifies 63,522 bridges as “structurally deficient”, 84,348 bridges as ‘functionally obsolete” with many of them needing to be repaired, rehabilitated or replaced. The bridge construction activities that will be necessary to address these needs will exacerbate existing traffic congestion and have significant social impacts. To reduce these negative effects, the acceleration of bridge construction needs to be a high priority for the nation.

The use of precast concrete bridge elements is one strategy that can reduce on-site construction time, field labor requirement and traffic impacts. Precasting also improves the safety and quality of construction. Transportation agencies have been using precast superstructure elements (e.g., girders) for a long time, and they are gradually embracing precasting for the construction of bridge substructures. However, in high seismic regions, precast concrete substructures have seldom been used. It is a challenge to develop connections that must be moment resisting, robust under inelastic cyclic deformations, and easy to construct with high quality.

1.2 PAST RESEARCH AT UW ON PRECAST BENT SYSTEMS

Previous researchers at the University of Washington have developed, and experimentally investigated a variety of precast column-beam connection concepts. Pang et al. (2008) proposed using “Large-Bar, Large-Duct” connections to connect beams and columns. They proposed to connect the elements with a small number of large bars that would fit easily into large ducts. Steuck et al. (2008, 2009) showed that bars as large as #18 could be anchored within the typical depth of a cap beam. Cohagen et al. (2008) later proposed using un-bonded post-tension bars to help re-center the column after the earthquake. Haraldsson et al. (2011) developed the concept of using a socket connection to connect the base of a precast column with a cast-in-place spread footing. Chapter 2 provides more details on the relevant previous research, both at the University of Washington and elsewhere.

1.3 NEW CONNECTION CONCEPT

This thesis proposes and investigates a connection between precast columns and cast-in-place drilled shafts, which are often needed to support columns in soft-soil conditions.

In the proposed connection (Figure 1-1), the bottom of the precast column is intentionally roughened where it is embedded in the cast-in-place drilled shaft. The end of the longitudinal column reinforcement is terminated with mechanical anchors. This anchorage mechanism is more effective than the conventional detail and allows generous placement tolerances.

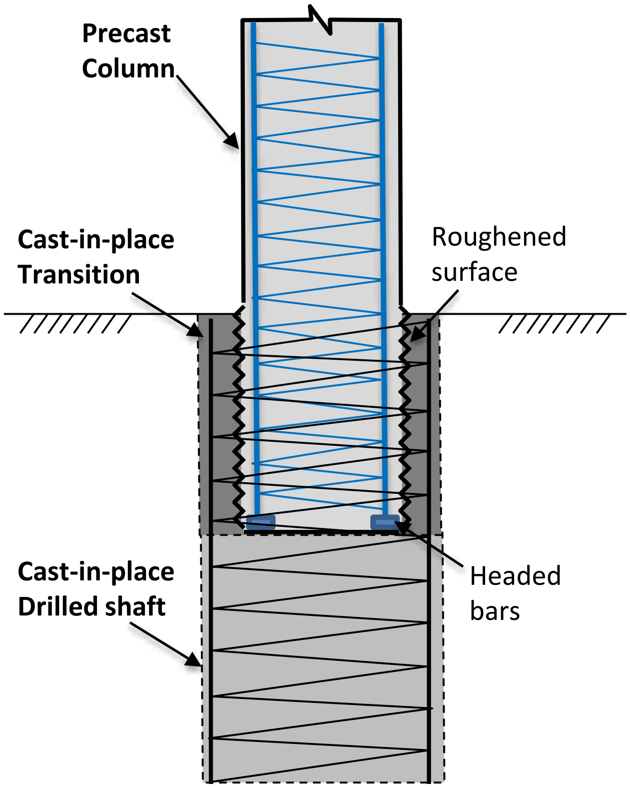

Figure 1-1. Column-shaft connection concept

The construction stages for the proposed connection, shown in Figure 1-2, are as follows:

1. Drill the shaft excavation, position the reinforcing cage, and place the concrete.

2. Position and brace the precast column
3. Cast the transition region
4. Position precast cross beam with ducts and grout to protruding column bars.

The connection needs to be strong enough to ensure that inelastic action in the column occurs above the transition region. Thus, it is necessary to ensure an adequate margin of the strength between the connection (i.e., non-ductile element) and the column (designed ductile element). Therefore, the plastic overstrength capacity of the column will be used to define the minimum seismic demands on the connection.

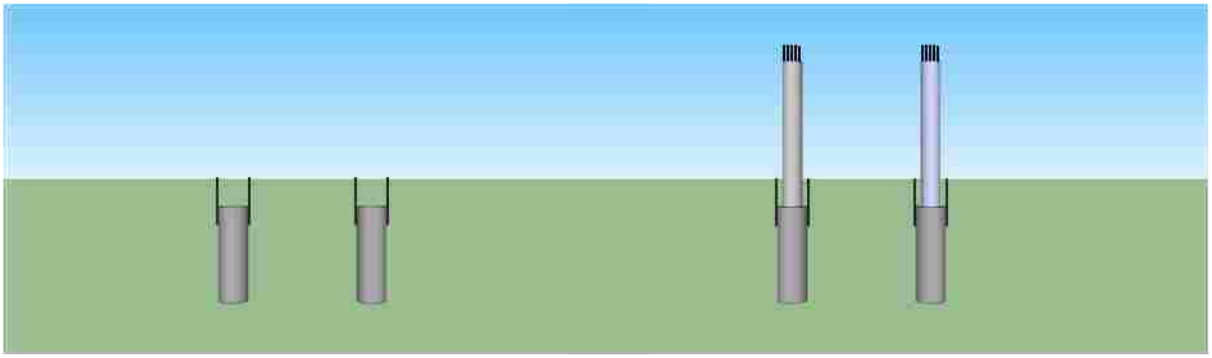

1. Dig and cast drilled shaft

2. Position and brace precast column

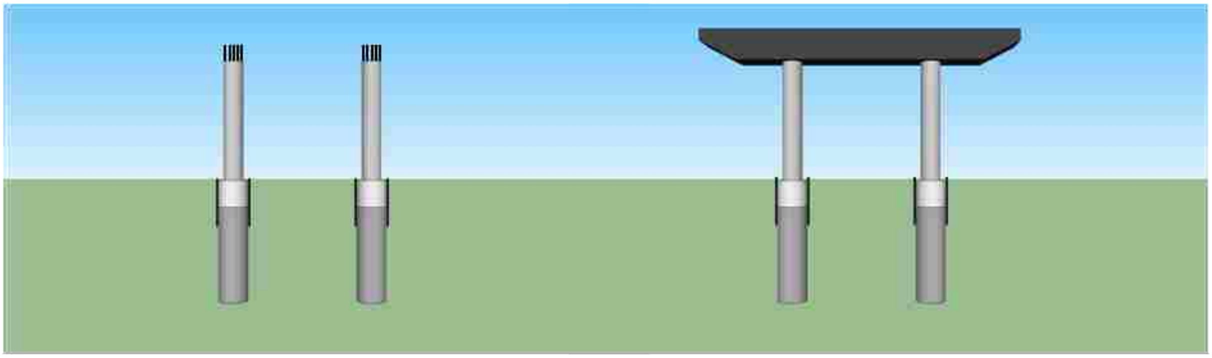

3. Cast transition

4. Position precast cross beam with ducts and grout to protruding column bars

Figure 1-2. Precast bridge bent construction stages

1.4 OBJECTIVES

The objectives of the research described in this thesis were to:

1. Develop a method for connecting a precast column to a cast-in-place drilled shaft.
2. Evaluate the performance of the precast column-to-shaft connections, and
3. Develop modeling and design recommendations for this type of connection in seismic regions.

1.5 SCOPE

To evaluate the behavior and performance of the system, three quasi-static tests were performed at the University of Washington to evaluate the seismic performance of the system experimentally. All the test specimens were designed according to the AASHTO Load Resistant Factor Design 2009, AASHTO Guide Specifications for LRFD Seismic Design 2009, and WSDOT Bridge Design Manual 2009 with the exception of the spirals in the transition region. Chapter 3 describes the test design procedures. The test setup, instrumentation and test program are presented in Chapter 4. The experimental results are discussed in Chapter 5

Force transfer models were determined to reproduce the responses of the connection, and a strut-and-tie model was proposed in Chapter 6. A design procedure, which is based on the proposed strut-and-tie model, is developed to guide designers in Chapter 7.

Chapter 8 summarizes the completed work and suggests future research needs.

CHAPTER 2.

LITERATURE REVIEW

In this chapter, the literature relevant to the behavior, analysis and design of column-to-shaft connections is reviewed. First, the chapter reviews the performance requirements of such connections in seismic regions. Then, the background for two analytical approaches are presented. One is based on models derived from tests of non-contact splices (Sec. 2.2), and the other is based on the behavior of column-to-socket connections (Sec. 2.3). Finally, some current specifications for designing column-shaft connections are presented and compared (Sec. 2.4).

2.1 CONNECTION PERFORMANCE REQUIREMENTS

Bridge columns located in high seismic regions are required to resist cyclic, lateral deformations. Depending on configuration of the bents and the direction of deformation, the columns may act as simple cantilevers or will be subjected to double bending as shown in Figure 2-1. In both cases, the column-shaft system is usually designed and detailed to force the plastic hinge to form just above the interface between the shaft and the column, where it can be inspected immediately following a seismic event.

In some states, such as California, the column and shaft usually have the same diameter, in which case careful detailing is necessary to force the plastic hinge to form in the column, because the maximum moment almost certainly occurs below the shaft-column interface. In the system considered here, the shaft is assumed to be larger than the column, which is common in Washington State. In this situation, even though the peak moment occurs below grade, the peak flexural demand/capacity ratio, which controls the location of yielding, most likely occurs just above the shaft-column transition.

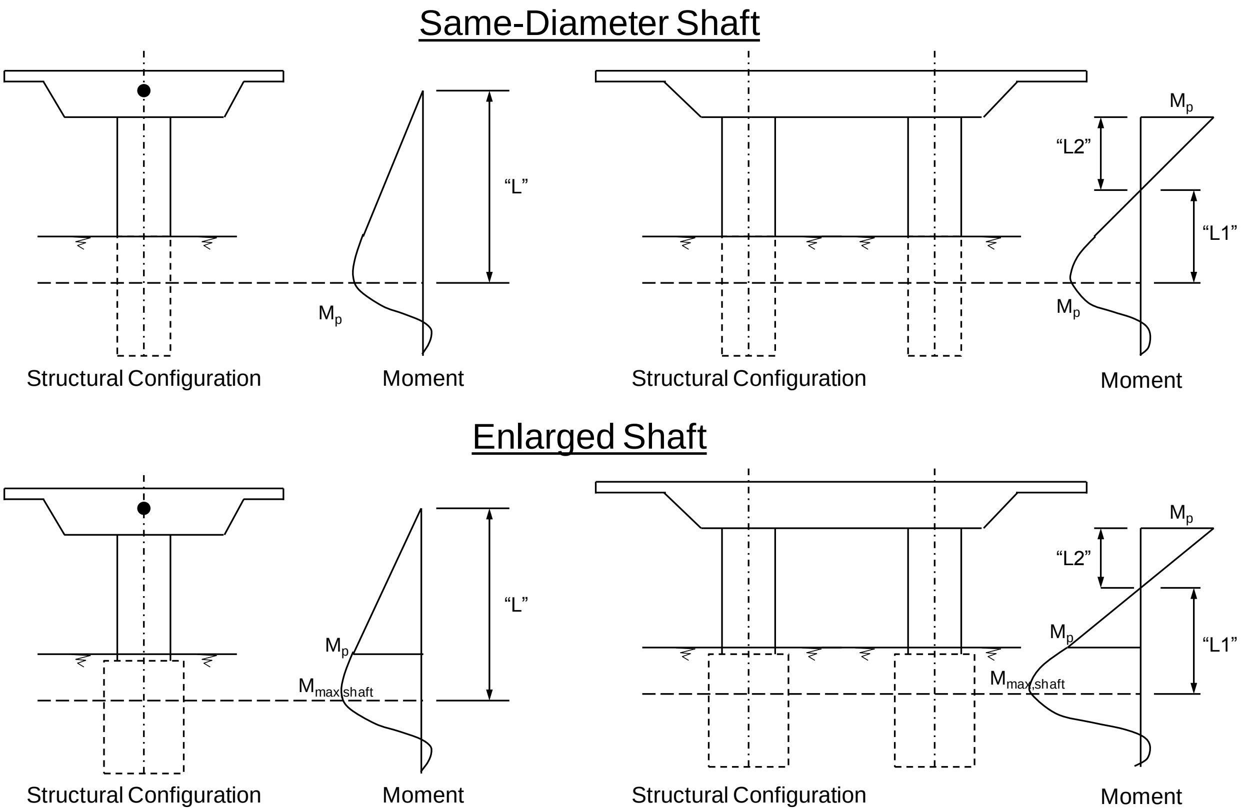

Figure 2-1. Moment diagram of bridge pier with column-shaft connections (Caltrans Seismic Design Criteria 2013)

To form a stable plastic hinge in the column without incurring damage elsewhere, the column must be ductile and the adjoining elements must be capacity protected. To be conservative it is necessary to ensure a margin of strength between the non-ductile elements (e.g., shafts) and ductile elements (e.g., columns). Several conditions must be fulfilled:

- The column should have sufficient transverse reinforcement to prevent shear failures, maintain the resistance of the core concrete, and delay buckling of the longitudinal bars under cyclic deformations.
- The column longitudinal reinforcement should be sufficiently anchored to allow the bars to yield cyclically without pulling out. The development length of column longitudinal reinforcement may need to be increased to account for the effect of the noncontact lap splice (McLean et al. 1997).

- The connection should be designed to withstand the cyclic force and moment demands that are placed on it, and it must be strong enough to prevent it from yielding.

Two analytical approaches are presented. One is based on the requirement that the column longitudinal reinforcement be spliced completely with the shaft longitudinal reinforcement in a non-contact mechanism, so the maximum tension in the column bars can be transferred to shaft bars (Sec. 2.2). The second approach is based on the behavior of column-to-socket connections in which the column and its embedded part are considered to interact with the socket shaft cast around the column (Sec. 2.3).

2.2 NONCONTACT LAP-SPLICE BEHAVIOR IN PLATE SPECIMENS

One approach to selecting the transverse reinforcement in the column-shaft connection is to treat it as a noncontact lap splice. A noncontact lap splice provides the continuity of reinforcement by placing bars next to each another without touching. This approach is the basis of the requirements of the WSDOT Bridge Design Manual (Section 2.4.3). In this section, previous experiments and proposed models are discussed.

2.2.1 Sagan, Gergely and White (1991)

Sagan et al. (1991) studied the behavior of noncontact lap splices under monotonic and repeated inelastic tensile loading up to the yield strength of the spliced bars. A total of 47 full-scale, flat-plate specimens were built with the geometry shown in Figure 2-2. They concluded that, for monotonic loading and for bar spacing up to six times the bar diameter, the strength of a splice did not depend on the bar spacing (Figure 2-3. When transverse reinforcement was provided, the splice strength of the monotonically loaded specimens increased (Figure 2-3). Under repeated loading up to the yield strength of the splice bars, the ultimate load (equal to the yield load) was also independent of the splice-bar spacing for up to eight bar diameters for both #6 and #8 bars.

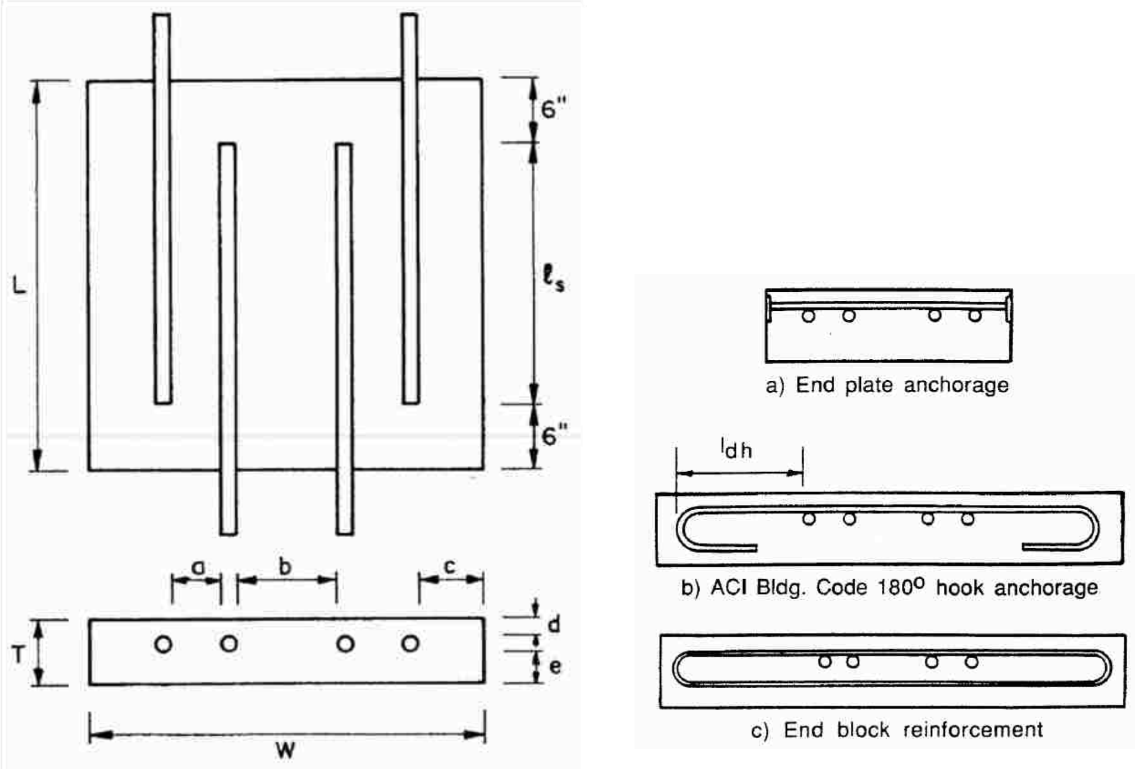

a) Typical spaced lap-spliced specimen *b) Transverse reinforcement details*

Figure 2-2. Noncontact lap splice flat-plate specimens (Sagan et al. 1991)

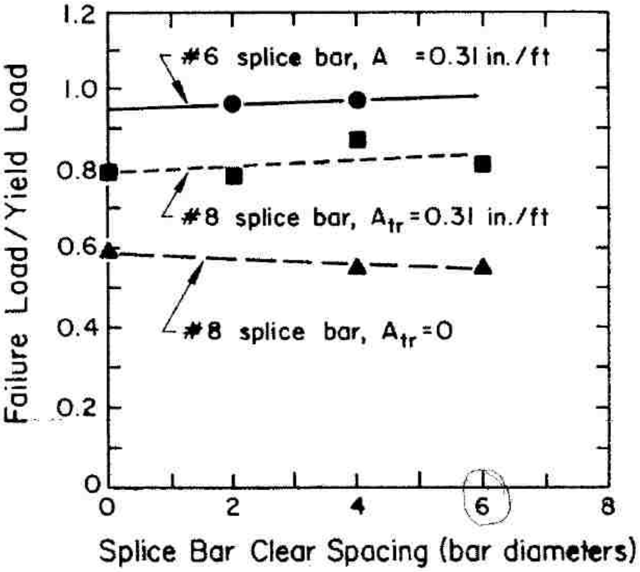

Figure 2-3. Normalized failure loads of monotonically loaded specimens (Sagan et al. 1991)

Based on the test results, Sagan et al. (1991) proposed a design method using compression-field theory, combined with the strut-and-tie method. According to the authors, the load is transferred from one bar to the diagonal concrete compressive struts and then to the other bar. The required transverse reinforcement is based on equilibrium of the strut-and-tie model. The capacity of strut elements was determined by the compression field theory, which takes into account the "softening" of the ultimate compressive strength of struts. A strut angle of 50 degrees was selected to characterize the compressive stress field. In a noncontact lap splice, the end splice crack is diagonal, so the transfer length is not equal, but shorter than the overall lap length. This reduced transfer length, shown in Figure 2-4, is referred to as the effective lap length.

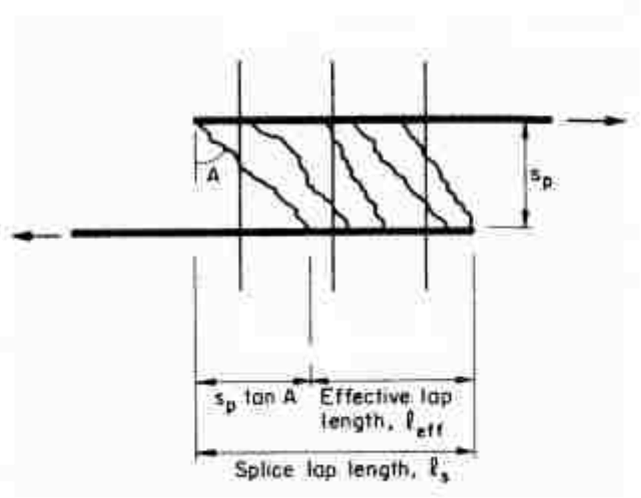

Figure 2-4. Effective lap length (Sagan et al. 1991)

According to Sagan et al., the required splice lap length,l_s, should be determined by adding to the effective lap length l_{eff} and the splice-bar clear spacing, s_p, multiplied by a factor of 1.2, which is approximately the tangent of 50 degrees, the angle of the compressive struts. In other words:

$$l_s = l_{eff} + 1.2s_p \tag{2-1}$$

The effective lap length l_{eff} is determined by

$$l_{eff} = \frac{3100 d_b}{\sqrt{f_c'}\left(1.5 + 0.2 s_p / d_b\right)} \tag{2-2}$$

where, the value of f_c' is in psi, and the value of s_p/d_b cannot be taken as greater than 3.0, even if the splice-bar clear spacing s_p may be greater.

2.2.2 McLean et al. (1997) – 2-Dimensional Model

In 1997, Mc Lean, et al. performed similar tests to investigate the behavior of noncontact lap splices under monotonic and cyclic loading. They performed 15 flat-panel tension tests (Figure 2-5). As opposed to Sagan's tests, most of the McLean specimens were tested to failure.

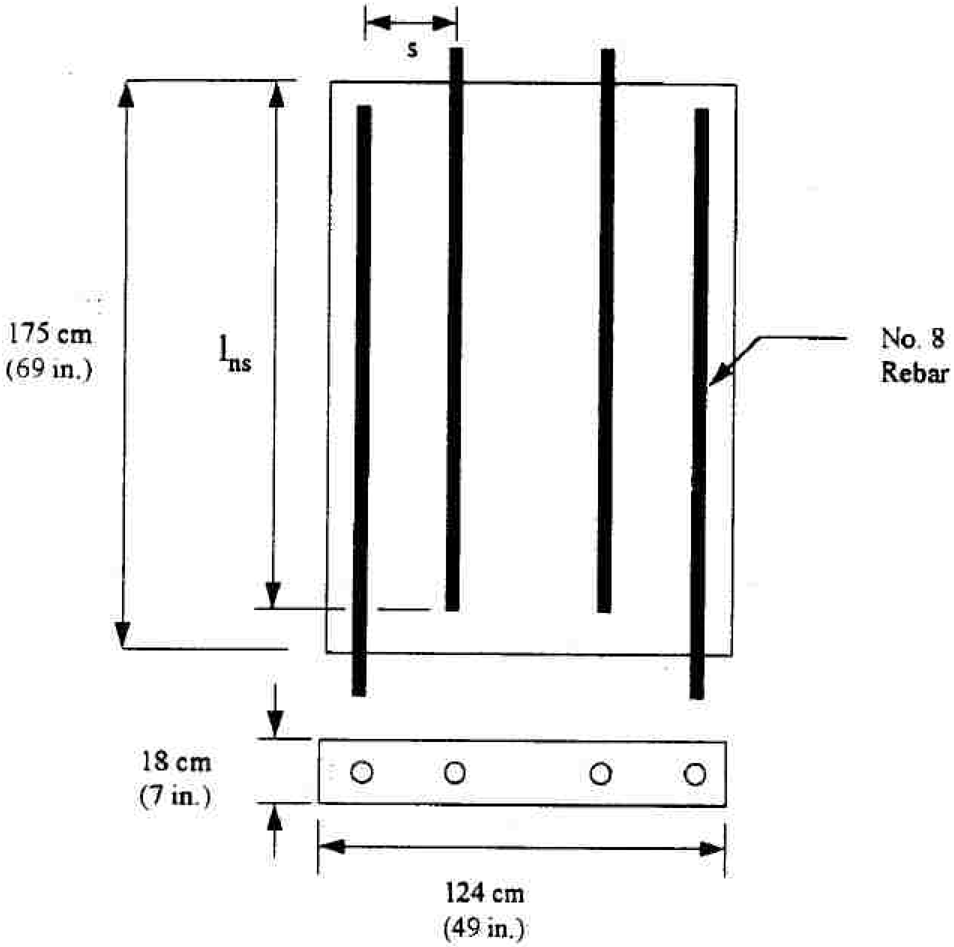

Figure 2-5. McLean panel specimen details (McLean et al. 1997)

Based on their test results, they proposed a similar two-dimensional strut-and-tie model to describe the behavior of noncontact lap splices in tension. Figure 2-6 illustrates a two-dimensional representation of the force transfer between non-contact longitudinal bars.

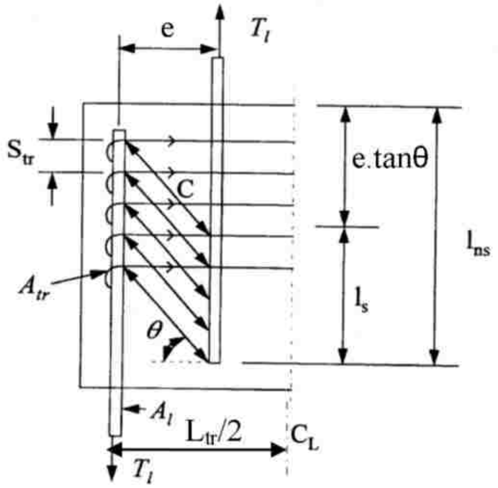

Figure 2-6. McLean two-dimensional model for non-contact lap splices (McLean et al. 1997)

According to this model, the transverse reinforcement is determined from Equation (2-3):

$$\frac{A_{tr}}{s_{tr}} = \frac{A_l f_{ul}}{f_{yt} l_s \tan\theta} \tag{2-3}$$

where,

A_{tr} = area of shaft transverse reinforcement or spiral (in.^{2})

A_l = total area of longitudinal column reinforcement (in.^{2})

f_{yt} = specified minimum yield strength of shaft transverse reinforcement (ksi)

f_{ul} = specified minimum tensile strength of column longitudinal reinforcement (ksi), 90 ksi for A615 and 80 ksi for A706

l_s = Class C tension lap splice length of the column longitudinal reinforcement (in.)

s_{tr} = spacing of shaft transverse reinforcement (in.)

θ = inclination angle of the strut (degree or rad)

Equation (2-3) indicates that a longer splice requires less transverse reinforcement. For the special case of the case of $\theta = 45°$, Equation 2-3 becomes:

$$\frac{A_{tr}}{s_{tr}} = \frac{A_l f_{ul}}{f_{yt} l_s} \tag{2-4}$$

This model of a non-contact splice is two-dimensional and would apply only to rectangular tied columns, not to circular columns confined by spirals.

McLean et al. tested one specimen (Specimen No. 12) in which 50% of the transverse reinforcement required by Equation (2-4) was placed only at the top region of the splice. This specimen failed by loss of bond of a longitudinal bar as a result of vertical splitting of concrete along the bar. They suggested that it is necessary to distribute the transverse reinforcement along the connection.

2.2.3 Discussion of Noncontact Models

Sagan’s and Mc Lean’s two-dimensional models were based on the test results of flat-panel specimens. More investigation is needed to apply this model to the geometry of a three-dimensional, noncontact lap splice in a column-shaft connection.

In column-to-shaft connections, the designer intends the plastic hinge to form in the column, above the interface of the column-shaft, whereas the enlarged shaft should be designed to work in the elastic range. Therefore, during an earthquake, the column reinforcement will be stressed until achieving tensile fracture while the strains in the shaft reinforcement are still in the elastic range of behavior. Thus, this situation is not similar tp the stress field in Sagan’s tests in which the reinforcement was stressed only until barely yielding.

Moreover, the models proposed by McLean et al. do not agree well with their test results. Their model implies that bond forces are uniformly distributed over the effective lap length, l_s. Thus, the required tensile member (i.e., transverse reinforcement) is also uniformly distributed along the effective splice length. However, the measured strains of the transverse bars, reproduced in Figure 2-7 and Figure 2-8, showed that the transverse strains are concentrated in the top of the specimens where the two inner bars were pulled upwards. At the bottom of the specimens, the strain in transverse bar was almost zero.

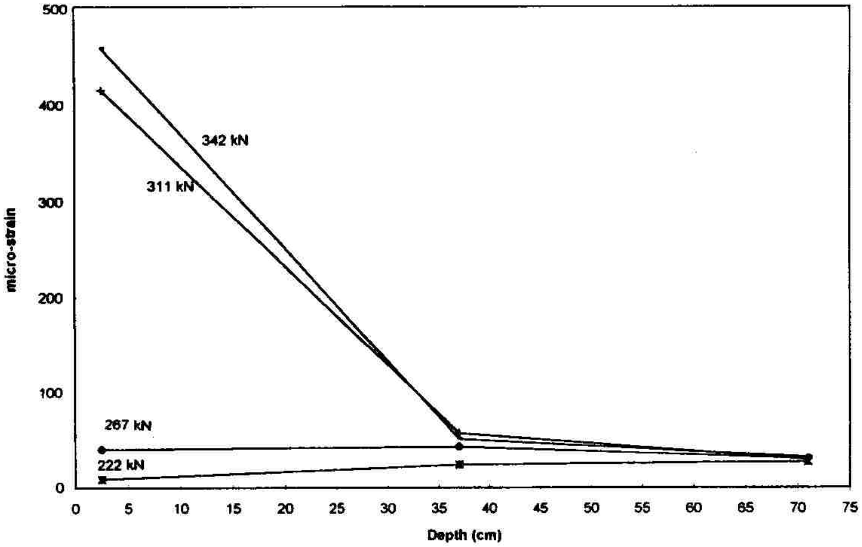

Figure 2-7. Transverse bar strains for an offset spacing of 6 in. (McLean et al. 1997)

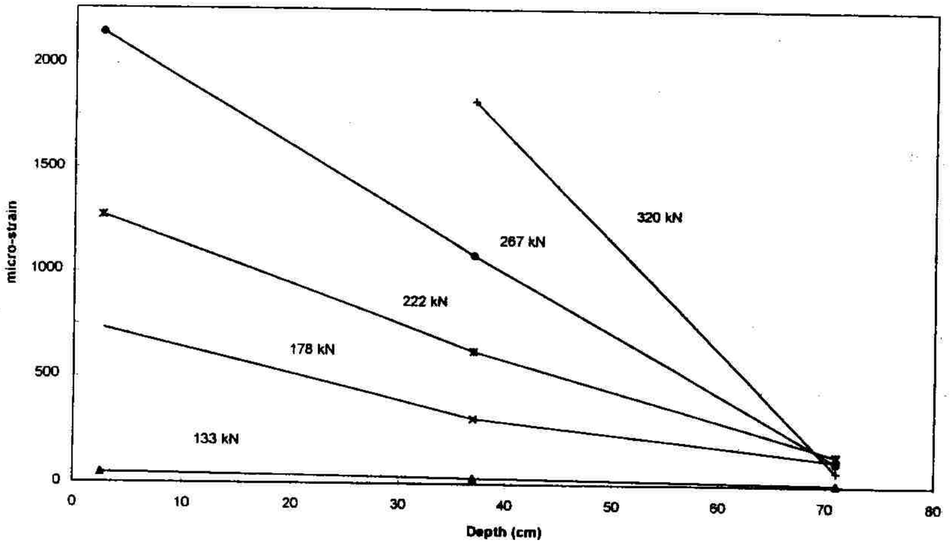

Figure 2-8. Transverse bar strains for an offset spacing of 15 in. (McLean et al. 1997)

The investigation of McLean et al. (1997)‘s test results demonstrates that the noncontact lap splice behavior and the proposed strut-and-tie model do not completely describe the behavior of column-shaft connection which is investigated in this report. For example, placing more transverse reinforcement at the top of the connection will have the better performance of connection. However, distribution of transverse reinforcement over the length of connection is necessary.

2.3 FORCE TRANSFER MECHANISM FOR THE COLUMN SOCKET CONNECTIONS

The modeling of the force-transfer mechanism of socket base column-to-foundation connections has been proposed as a rational method in the design for earthquake-resistant structures. Some models has been specified in specifications (DIN 1045 (1981), AIJ Recom. (1990)) and studied in some reports. In this section, these models are presented and evaluated for the design of column-shaft connections.

2.3.1 McLean et al. (1997) – 3-Dimensional Model

Based on their two-dimensional model proposed above (Sec. 2.2.2) McLean et al. (1997) proposed a three-dimensional model for circular columns (Figure 2-9). The model addresses loading in pure tension, rather than in bending.

The required spiral reinforcement in the transition region of the column-shaft connection, in order to fully develop the column reinforcing bars, is determined based on equilibrium of the proposed 3-dimensional model as:

$$\frac{A_{tr}}{s_{tr}} = \frac{A_l f_{ul}}{2\pi f_{yt} l_s \tan\theta} \tag{2-5}$$

They performed one column-shaft tension test, in which the transverse reinforcement (e.g. spirals) for both specimens was designed using Equation (2-5). In this test, no signs of distress were observed in the column-shaft region up through extensive yielding of that spliced bars. And the strains on the column bars decreased with depth while the strain on the shaft bars increased with depth as load was transferred from the column bars to the shaft bars. These profiles of strain versus depth were similar to those obtained for their panel test shown above.

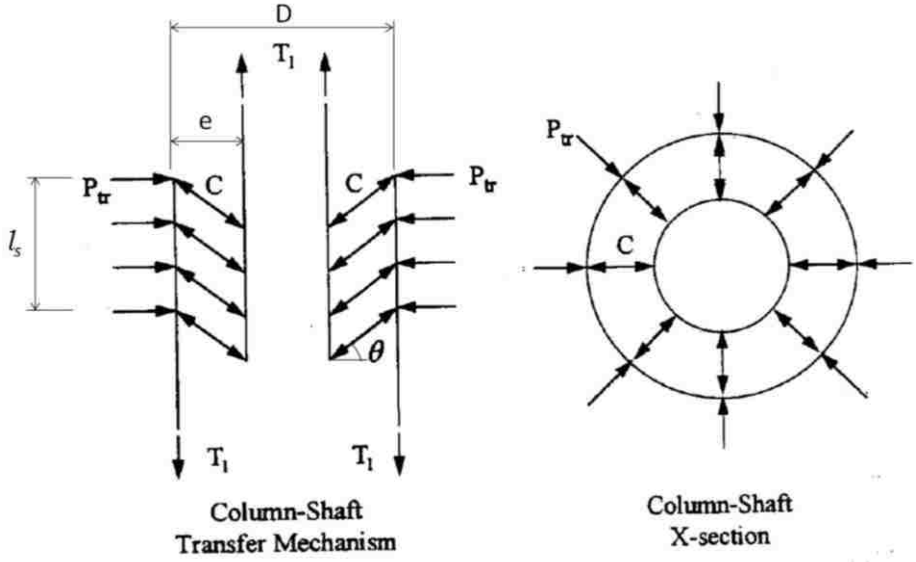

Figure 2-9. Proposed three-dimensional model for non-contact lap splices for circular column in pure tension (McLean et al. 1997)

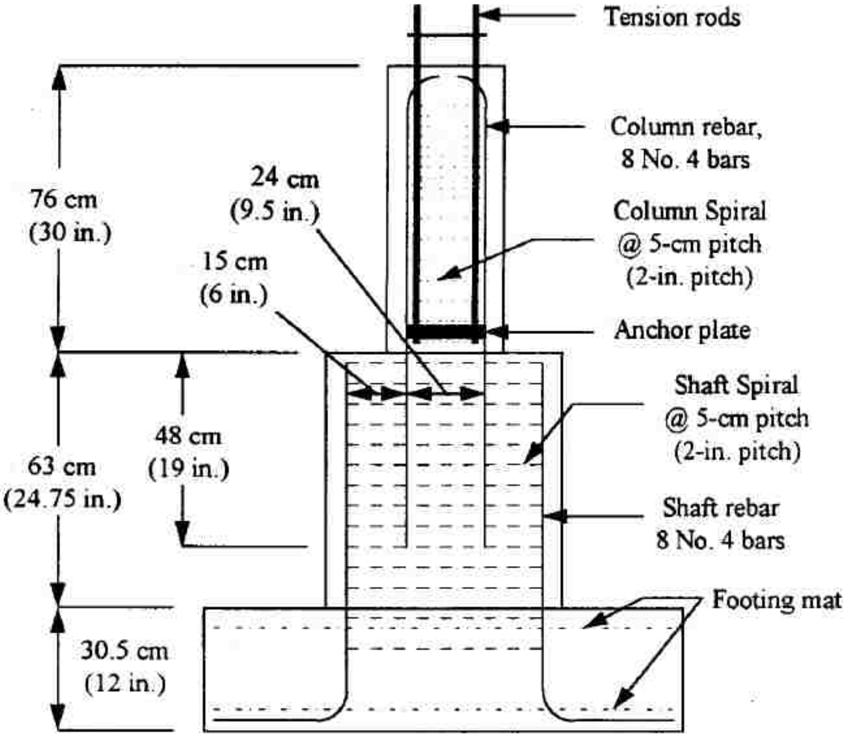

Figure 2-10. Column-shaft tension specimen details (McLean et al. 1997)

McLean and his colleagues also performed one column-shaft bending test (Figure 2-11), whose reinforcement was also proportioned to satisfy Equation 2-5. In the cyclic flexural test, cracks radiated outward from the column to the shaft and down the side of the shaft. However, there was no distress observed in the column-shaft connection. The load-deflection hysteresis curves obtained from the test (Figure 2-12) showed no loss of strength due to bar slip or concrete spalling.

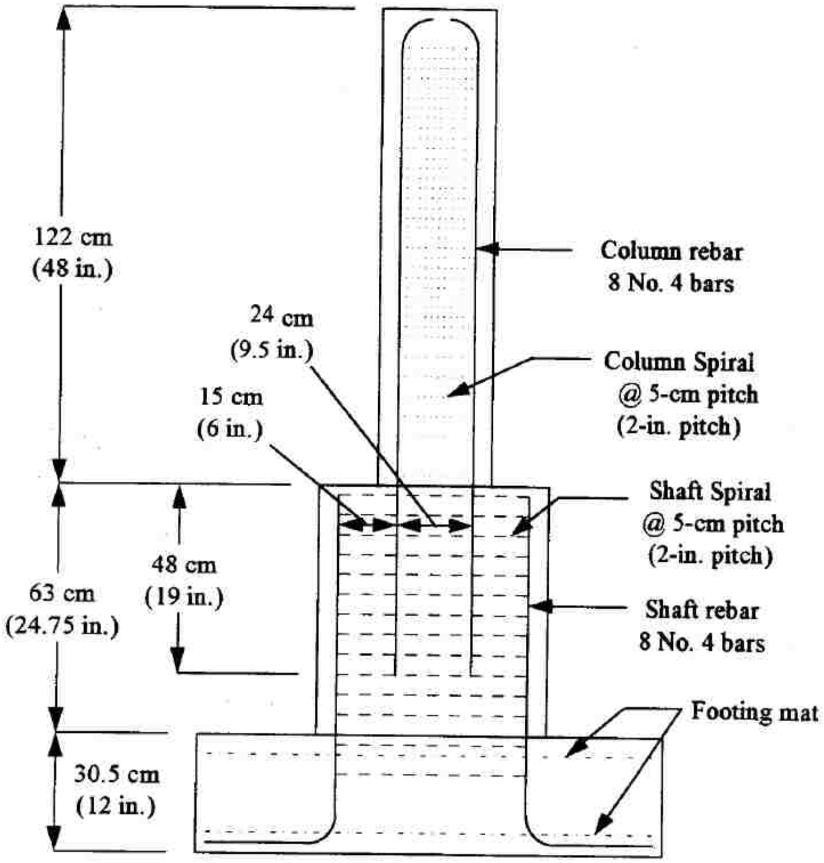

Figure 2-11. Column-shaft flexural specimen details (McLean et al. 1997)

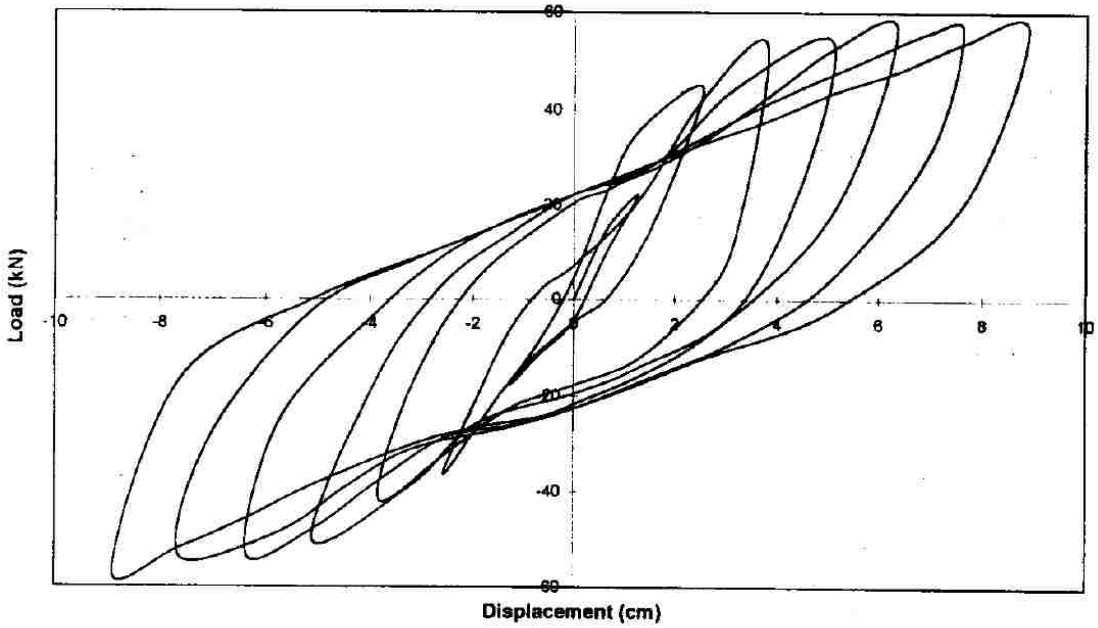

Figure 2-12. Load vs. displacement hysteresis curve for the column-shaft flexural specimen (McLean et al. 1997)

2.3.2 DIN-1045 (1981)(German Institute for Standardization)

In Germany, the methods of analysis and determining the required reinforcement of embedded column-to-base foundations are specified in DIN-1045 (1981). The concept underlying the DIN-1045 requirements is shown in Figure 2-13. These requirements are intended to apply to socket footings, which are used quite commonly in Europe for precast concrete building columns. The footings are typically narrower at the top than at the bottom, where they rest on the soil. That configuration differs from the cast-in-place socket footings used by Haraldsson et al. (2011)

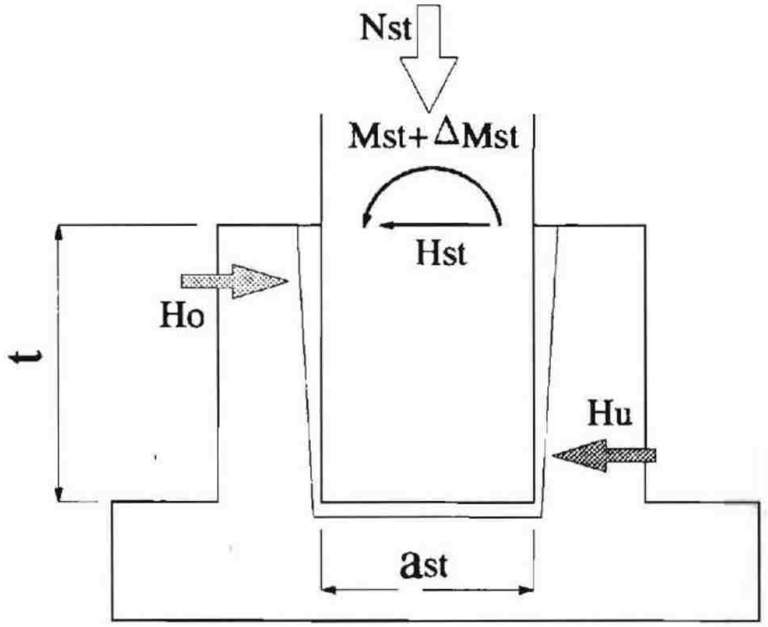

Figure 2-13. Concept of DIN-1045 (Osanai et al. 1996)

According to this concept, the column overturning moment and shear force are resisted by a couple of horizontal forces H_o and H_u at the top and bottom of the connection, respectively. The reaction force H_o is transmitted to the foundation with the transverse reinforcement, and it is determined for rough and smooth column surface cases as follows:

$$H_{o,R} = \frac{6}{5} . \frac{M_{st} + \Delta M_{st}}{t} + \frac{6}{5} H_{st} \qquad \text{for rough surface} \tag{2-6}$$

$$H_{o,S} = \frac{3}{2} . \frac{M_{st} + \Delta M_{st}}{t} + \frac{5}{4} H_{st} \qquad \text{for smooth surface} \tag{2-7}$$

Multiplying Eq. (2-6) by $\left(\frac{5}{6}t\right)$ and Eq. (2-7) by $\left(\frac{4}{6}t\right)$ results in the following two equations,

$$H_{o,R} . \left(\frac{5}{6}t\right) = (M_{st} + \Delta M_{st}) + H_{st} . t \qquad \text{for rough surface} \tag{2-8}$$

$$H_{o,S} . \left(\frac{4}{6}t\right) = (M_{st} + \Delta M_{st}) + H_{st} . \left(\frac{5}{6}t\right) \qquad \text{for smooth surface} \tag{2-9}$$

Both equations (2-8) and (2-9) are consistent with moment equilibrium taken at the middle of the column and along the line of action of H_u. These equations then imply that H_o acts at a distance of $(1/6\ t)$ from the column-shaft interface in both cases, and H_u acts at the bottom of column for rough surface case, and at $(1/6\ t)$ above the bottom of column for the smooth surface case.

Both equations are based on the assumption that the primary mode of transfer is by a couple consisting of horizontal forces. A couple consisting of two vertical forces is not explicitly considered, but it presumably accounts for the differences between equations (2-6) and (2-7). The reaction force of axial does not appear in these equations either. Such forces would not affect the moment equilibrium if the line of action of the upward vertical reaction was the same as that of the downward axial load. It might be that the axial load is assumed to be transferred to the centroid of the bottom section of column by bearing, or distributed over the vertical column surface by friction.

2.3.3 Osanai et al. (1996) Model

Osanai et al. (1996) believed that DIN-1045's equations of determining horizontal load at the top of footing were too conservative. They proposed a new model, which is a combination of two models. Model 1 is the case in which loads are resisted by a horizontal reaction force, C_{11}, and the axial reaction force, R. The loads in Model 2 are resisted by horizontal reaction forces. C_{12} and C_{22}, and friction forces, F_1 and F_2, along the column and the internal faces of the socket base, as shown in Figure 2-14.

For the formulation of the equilibrium equations, some hypotheses were adopted:

- The concrete tensile strength was ignored;
- The tensile forces in the foundation were taken only by foundation reinforcement;
- The vertical reaction was assumed to act only on the bottom face of the column.

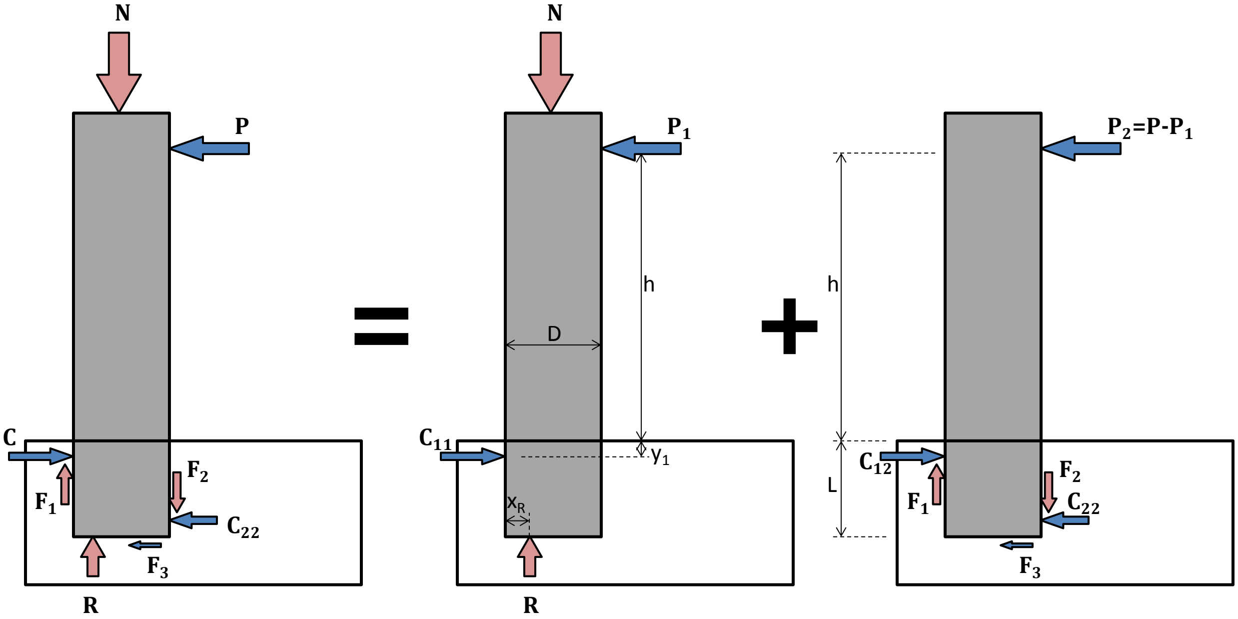

(a) Total model *(b) Model 1* *(c) Model 2*

Figure 2-14. Concept of Osanai et al. (1996)

Model 1:

First, the position of concrete compression resultant force at column critical section x_R is calculated with the assumption that plane sections remain plane. Figure 2-15 shows the assumed ultimate stresses distribution with the following notation:

C_c : compression force of concrete due to column axial force and overturning moment in column section;

C_s : compression force of column reinforcement due to column axial force and overturning moment in column section;

D : overall depth of column;

d_c : distance from extreme compression fiber to centroid of compression reinforcement;

d_t : distance from extreme tension fiber to centroid of tension reinforcement;

T_s : tensile force of column reinforcement due to column axial force and overturning moment in column section;

x_n : distance from extreme compression fiber to neutral axis;

x_R : distance from extreme compression fiber to point where C_c is acting.

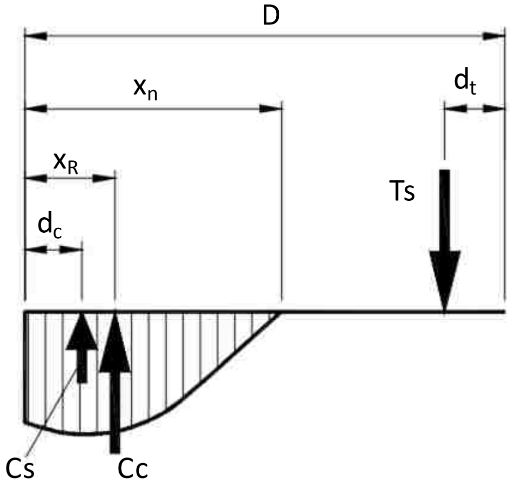

Figure 2-15. Stress distribution on the column section (Osanai et al. 1996)

Therefore, the lateral load carried by Model 1, P_1, and lateral reaction force C_{11} are calculated from the equilibrium condition as

$$C_{11} = P_1 = \frac{M_1}{h + y_1} \cong \frac{M_1}{h} = \left(\frac{D}{2} - x_R\right).\frac{N}{h} \tag{2-10}$$

where $N = R$, and y_1 is negligible compared with h.

Model 2:

The assumed connection stress distribution of Model 2 is shown in Figure 2-16. The force C_3 is the sum of the lateral reaction C_{22} and the friction force F_3.

$$C_3 = C_{22} + F_3 \tag{2-11}$$

$$L_3 = \frac{L_2}{2} = \frac{(L - 2y_1)}{6} \tag{2-12}$$

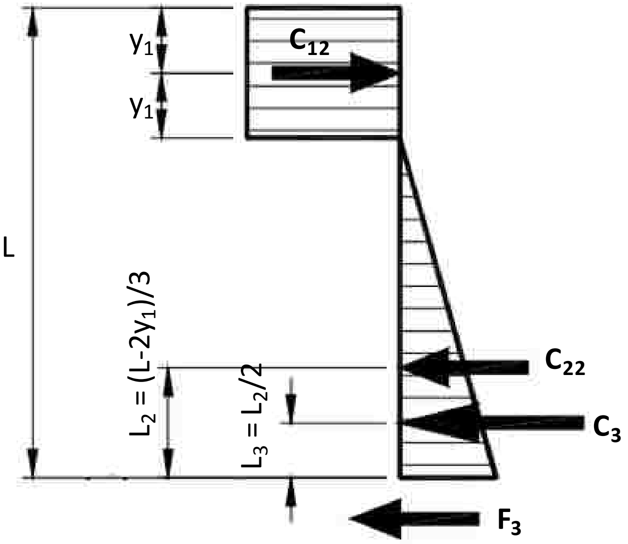

Figure 2-16. Stress distribution on the column embedded region of model 2 (Osanai et al. 1996)

From the equilibrium of forces and moment of Model 2, the equation for the reaction force C_{12} is obtained:

$$C_{12} = \frac{\left(\frac{5}{6}L + \frac{y_1}{3} + h\right).P_2}{\frac{5}{6}L - \frac{2}{3}y_1 + \mu.D} \tag{2-13}$$

where, μ is the friction coefficient among the column and the internal faces of the socket base. The reaction force C, which is transmitted to the foundation reinforcement, is given by the sum of equations (2-10) and (2-13):

$$C = C_{11} + C_{12} = \frac{\frac{\left(\frac{D}{2} - x_R\right)}{h}.(\mu D - y_1 - h).N + \left(\frac{5}{6}L + \frac{y_1}{3} + h\right).P}{\frac{5}{6}L - \frac{2}{3}y_1 + \mu.D} \tag{2-14}$$

Based on the strain responses of foundation reinforcement, Osanai et al. proposed using a friction coefficient μ equal to 0.5 when the embedded depth equals the column diameter, and equal to 1.0 when the embedded depth equals 1.25 times column diameter or more.

In general, the Osanai et al. model is quite similar to model of DIN 1045, except that the axial reaction force is assumed to act at the position of concrete compressive resultant force at column critical section, and place at the bottom of column as shown in Figure 2-14.

2.3.4 Schlaich and Schäfer (1991) Model

Schlaich and Schäfer (1991) proposed two detailed strut-and-tie models for a socket footing. In one model, the surfaces between the column and the walls of the socket are assumed to be rough, and in the other, they are assumed to be smooth as shown in Figure 2-17. In the smooth surface model, no friction can be carried across the vertical interface between column and socket, so the moments are resisted by a couple with horizontal forces, while in the rough surface model friction, is possible and the two vertical friction forces form the resisting couple.

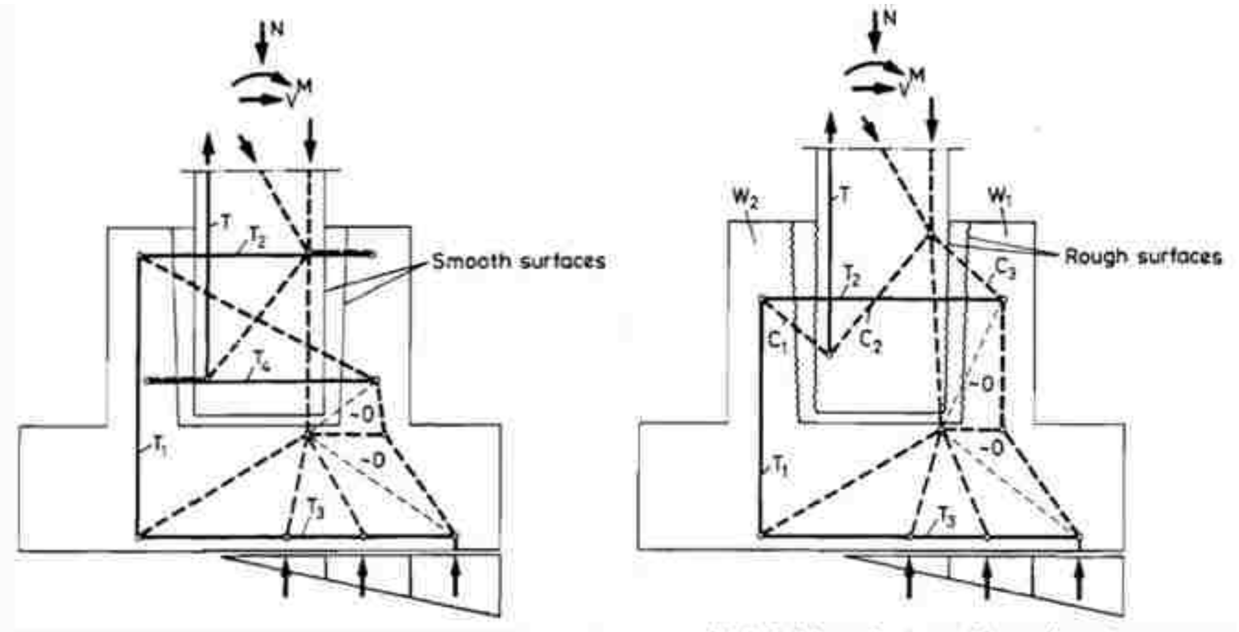

a)Model for a footing with smooth surfaces

b)Model for a footing with rough surfaces

Figure 2-17. STM models proposed by Schlaich and Schäfer (1991)

In general, Schlaich and Schäfer’s models are similar to Osanai’s, in that the overturning moment and shear force of the column are resisted by horizontal reactions, interface friction, and eccentric bottom reaction. However, the strut-and-tie models provide more detail on the locations and magnitudes of member forces, which are very useful for understanding the behavior of the connection, and help to design longitudinal and transverse reinforcement of the connection.

However, Schlaich and Schäfer’s models are 2-D, whereas the connection between a circular column and a drilled shaft consists of longitudinal reinforcement evenly distributed around the perimeter of column and shaft, so it is 3-D. The determination of nodes, struts and ties member is thus more complicated in that case. Furthermore, the forces at the bottom pass to the soil, so the distribution of struts and ties there may differ from those in a drilled shaft.

Hung Tran (2012) applied these two strut-and-tie models for column-shaft connections, but showed that these models are still too conservative and do not agree with the experimental data.Schlaich and Schäfer (1991) Model.

2.3.5 Murcia-Delso et al. (2013) Model

Murcia-Delso et al. presented an experimental and analytical investigation of connections between cast-in-place columns and shafts to determine the minimum required embedment length, and the transverse reinforcement required in the transition region. Experiments were performed to investigate bond stress under cyclic loads of large-diameter bars (No. 11, 14 and 18 bars). The results have been used to develop an interface element in a finite element program. In addition, for large-scale tests of column-shaft connection were conducted. Based on these tests, additional finite element analyses and new design recommendations have been proposed.

In order to fully develop the column reinforcing bars, the spacing, $s_{tr,max}$, of the transverse reinforcement in the transition region should be no more than that given by:

$$s_{tr,max} = \frac{2\pi A_{tr} f_{y,tr}}{N_{col} d_{b,col} \tau_u} \tag{2-15}$$

in which A_{tr} is the cross-sectional area of a transverse reinforcing bar, $f_{y,tr}$ is the nominal yielding stress of the transverse reinforcement, N_{col} is the number of column longitudinal bars, $d_{b,col}$ is the diameter of column longitudinal bars, and τ_u is the ultimate bond strength of the column longitudinal reinforcing bars, which can be taken to be 2.4 ksi for 5-ksi concrete.

2.4 DESIGN SPECIFICATIONS

2.4.1 AASHTO LRFD Specifications

According to AASHTO LRFD Specifications (2009), the column-drilled shaft connections should be designed to ensure that column reinforcing bars must be adequately spliced to the drilled shaft reinforcing as noncontact lap splices. Since the shaft longitudinal reinforcement is normally less than twice the column longitudinal reinforcement, a Class C splice is required (AASHTO [5.11.5.3.1-1]). Thus, the lap length should be $1.7l_d$. In addition, to account for the lack of contact, the splice length is increased by the distance between column and shaft reinforcing bars, e, (AASHTO [5.11.5.2.1]). Therefore, according to the specifications, the lap splice should be at least as long as:

$$l_{ns} = 1.7l_d + e \tag{2-16}$$

Also, the spacing between bars shall be no greater than one-fifth of the required lap splice length, or 6 in.

2.4.2 AASHTO Guide Specifications for LRFD Seismic Bridge Design.

The AASHTO Guide Specification requires the use of capacity design for designing columns, drilled shafts and their connections in Seismic Design Categories (SDCs) B, C, and D. Because columns are part of the primary energy dissipating system, the specification requires that the plastic hinge form in the column above the ground where it is easy to inspect and repair. The components connected to the plastic hinge region, such as the column, drilled shaft and column-shaft connection must be capacity protected. This protection is achieved by ensuring that the column-shaft connection is designed to remain elastic when the moments and shears in the ductile plastic hinge region of the columns reach their over-strength values. The overstrength moment of column is determined as

$$M_{po} = \lambda_{mo} M_p \tag{2-17}$$

where:

M_p = Plastic moment capacity for reinforced concrete column, determined using a moment-curvature section analysis, taking into account the expected material properties including strain-hardening effects of reinforcement.

λ_{mo} = overstrength factor, which is equal to 1.2 for ASTM A706 reinforcement

Based on the overstrength moment of column, the shaft is probably designed to work in elastic with the steel to resist it is carried up to the column-shaft interface. Therefore, even though the peak moment occurs below grade, the peak flexural demand/capacity ratio, which is what controls the failure location, most likely occurs just above the transition.

2.4.3 WSDOT Bridge Design Manual

The WSDOT Bridge Design Manual also provides requirements for minimum lateral confinement for single column-shaft foundation type for SDCs C and D. This requirement is based on noncontact lap splice report of McLean et al. (1997) with some modification.

The confinement reinforcement of the connection must be adequate to resist the internal tension forces that develop at noncontact lap splice zone of column-shaft connections. And as similar as Equation (2-5), the shaft lateral confinement reinforcement along the connection length shall be determined as:

$$\frac{A_{tr}}{s_{tr,max}} = \frac{k A_l f_{ul}}{2\pi f_{ytr} l_s} \tag{2-18}$$

where:

k = factor representing the ratio of column tensile reinforcement to total column reinforcement at the nominal resistance.

The ratio, k, is to be determined from column sectional analysis or, as a default, taken as k = 0.5.

2.4.4 Caltrans Seismic Design Criteria

In general, the Caltrans' requirements are similar to that of the AASHTO Guide Specification, except that the required values are more conservative.

For designing a column-shaft connection, the minimum embedment length must be $3D_{c,max}$, where $D_{c,max}$ is the larger cross-section dimension of the column, to ensure adequate column bar anchorage in case the plastic hinge damage penetrates into the shaft. Fifty percent of column confinement reinforcement placed in the plastic hinge zone, must extend into the shaft for the embedded portion of the column (spacing of hoops or pitch of spiral may be doubled). The shaft confinement reinforcement shall be provided for the top $3D_{c,max}$ of the shaft same as that provided in the column plastic hinge zone (i.e., identical transverse rebar and spacing/pitch), but the transverse reinforcement ratio should not be less than 0.5%.

It can be seen that Caltrans' requirements, in general, are more conservative than WSDOT's requirement and seem to be based upon practical, not analytical analyses.

CHAPTER 3.

DESIGN OF TEST SPECIMENS

Three drilled shaft-column connection specimens (DS-1, DS-2 and DS-3) were designed, constructed and tested at the University of Washington. The design of these specimens is described in this chapter.

The literature review in Chapter 2 showed that the force distribution in the connection region is not simple or obvious. Some methods were proposed to reproduce the behaviors and responses of the connection, and to guide designers. The connection designed with these methods differ both in the embedded length and the amount of transverse reinforcement (i.e. spirals). In the non-contact lap splice methods, transverse reinforcement is determined based on the tension force transfer mechanism from the column bars to the shaft bars. In the column socket-connection methods, transverse reinforcement is determined based on the interaction between column and the socket shaft foundation. The aim of the experiments was to determine the distribution of local forces in the connection region, which must be known to develop models and design recommendations.

3.1 OVERVIEW OF EXPERIMENTS

The three specimens each included three parts: a precast column, embedded in a cast-in-place transition, which in turn was anchored to the testing rig by a base (Figure 3-1). The bases and the columns were cast in the first batch. After few days, the precast columns were located and braced on top of the base, and the transition was cast. For all specimens, these three components had the following nominally identical geometries:

- PRECAST COLUMN: The cantilever-precast columns had a diameter of 20 in. and a shear span of 60 in., resulting in a shear span-to-depth ratio of 3. The total column length was 100 in., which included 28 in. embedded in the drilled shaft, and 12 in. extending above the centroid of the horizontally applied load.

- DRILLED SHAFT: The cast-in-place drilled shaft had a diameter of 30 in. for specimens DS-1 and DS-2, and 26 in. for Specimen DS-3. The shaft length was 31 in., which slightly exceeded the length of the transition region (28 in.)
- BASE: The drilled shaft was embedded in a 74”×48”×24” cast-in-place base to anchor the specimen to the base of the testing rig.

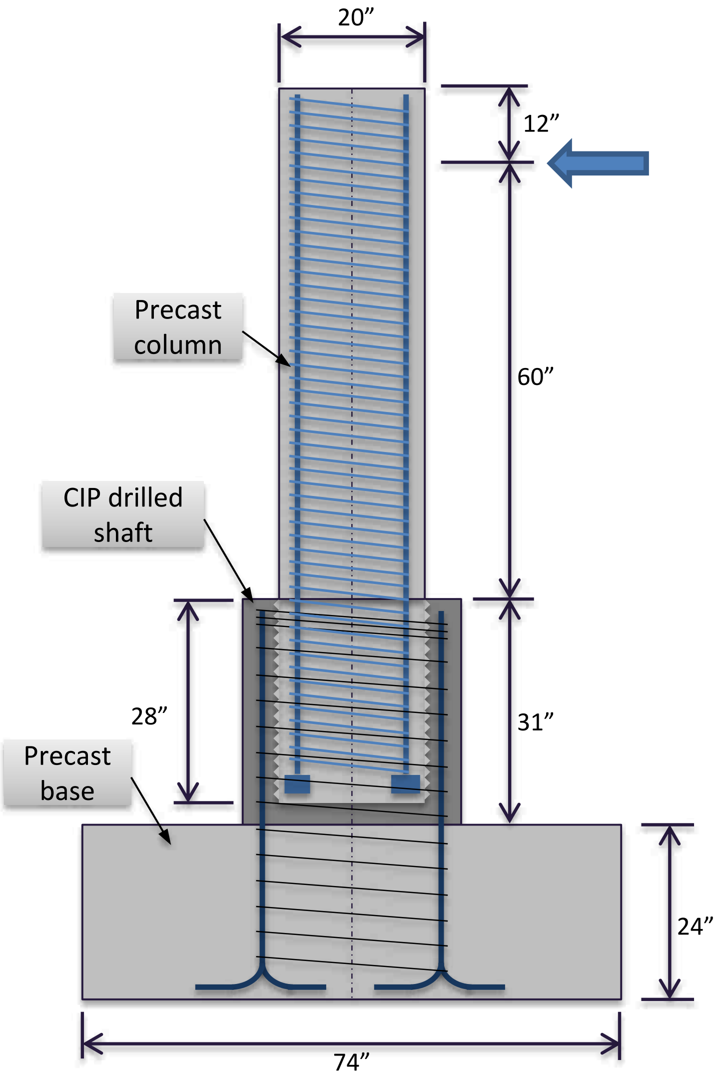

Figure 3-1. Column-shaft specimen

The columns are part of the primary energy dissipating system, so it is required that the plastic hinge form in the column. To easily inspect and repair, the plastic hinge position should be above the ground. The components connected to the plastic hinge region, such as the drilled shaft and column-shaft connection must be capacity protected.

In the first phase of this research, two specimens (DS-1 and DS-2) were designed to bracket the critical behavior and provide a lower bound and an upper bound on the capacity of the connection. The first specimen (DS-1) was designed such that its column would be weaker than the transition region, and the second specimen (DS-2) was designed such that the column would be stronger than the transition. DS-1 and DS-2 were designed based on the 2009 AASHTO LRFD Design Specifications, the AASHTO Guide Specifications for LRFD Seismic Design 2009, and the WSDOT Bridge Design Manual (2012).

The key dimensions and reinforcement of the test specimens are summarized in Table 3-1. The test specimen dimension and reinforcement in specimens DS-1 and DS-2 were scaled (1/3.6) from a real prototype. These two specimens had the same column diameter and height; column longitudinal and transverse reinforcement ratio; shaft diameter and longitudinal reinforcement. The only difference between these two specimens was that Specimen DS-2 contained only half the amount of spiral in the column-to-shaft transition region as was used in DS-1.

Specimen DS-3 was designed after evaluating the results of tests of specimens DS-1 and DS-2. The goal of Specimen DS-3 was to investigate the contribution to resistance of the hoop tension in the concrete, relative to the steel. Therefore, to minimize the effect of the hoop tension, Specimen DS-3 had the same column diameter as the other two, but it had a smaller shaft diameter, and more column and shaft reinforcement.

Table 3-1. Specimens' configuration

	DS-1	DS-2	DS-3
Column Diameter	20 in.	20 in.	20 in.
Clear Column Height	60 in.	60 in.	60 in.
Column Longitudinal Reinforcement Ratio	1.0 % (10#5)	1.0 % (10#5)	1.6 % (16#5)
Column Transverse Reinforcement	0.8 % (gage-3@1.25 in. pitch)	0.8 % (gage-3@1.25 in. pitch)	0.8 % (gage-3@1.25 in. pitch)
Shaft Diameter	30 in.	30 in.	26 in.
Shaft Height	30 in.	30 in.	30 in.
Transition Length	28 in.	28 in.	28 in.
Shaft Longitudinal Reinforcement Ratio	0.9 % (30 bundles of 2#3)	0.9 % (30 bundles of 2#3)	2.7 % (24 bundles of 3#4)
Shaft Transverse Reinforcement	0.14 % (bundle of 2 gage-9 @ 3.0 in. pitch)	0.07 % (1 gage-9 @ 3.0 in. pitch)	0.40 % (bundle of 3 gage-9 @ 1.5 in. pitch)
Lateral Reinforcement Efficiency Factor [k]	0.50	0.25	1.00

3.2 DESIGN OF TEST COLUMNS

The columns of these specimens were designed to be the same as previous column-spread footing tests done at the University of Washington (Haraldsson et al. 2011, and Janes et al. 2011). This column design was scaled down from a real prototype of a bridge in the Washington State. The same column design is also benefit in comparison between column's behavior of the two kinds of column-to-footing connection.

The test columns were designed to have a reinforcement ratio of 1% for specimens DS-1 and DS-2 and 1.6% for Specimen DS-3, which was provided using 10#5 bars and 16#5 bars respectively. The transverse reinforcement ratio was chosen as 0.82%, which is similar to the minimum requirement by AASHTO LRFD 5.10.11.4.1d, and also consistent with previous tests done at the University of Washington (Pang et al. 2008, Cohagen et al. 2008, Haraldsson et al. 2011, and Janes et al. 2011). This level of transverse reinforcement was provided by 3-gauge (0.244-in. diameter) spirals at a pitch of 1.25 in. All reinforcement was assumed to be ASTM A706, and the nominal concrete strength was assumed to be 6 ksi.

The flexural strength of the column in the specimens was estimated with moment-curvature analysis using an in–house program (Stanton 2012). For this analysis, the constant axial load applied in the column was assumed to be 10% the axial load capacity of column ($0.1\mathrm{A_g f'_c}$=159 kips). Steel properties were modeled according to AASHTO Guide Specifications, and the confined concrete properties were modeled using Kent and Park's model (Kent and Park 1971). However, the values of the confined concrete strength, the strain at peak stress and the ultimate compression strain were generated from the properties of the confinement reinforcement using Mander's recommendations (Mander et al. 1988; Priestley et al. 1996), rather than using the values recommended by Kent and Park. Details of moment-curvature analysis are reported in Chapter 6. Using the above moment-curvature program, the ultimate moment capacity of column cross section was $\mathrm{M_u} = 3530$ kip-in for DS-1 and DS-2 and was $M_u = 4165$ kip-in for DS-3.

The column had a circular cross-section, 20" in diameter, for most of its length. The bottom part of the column which was embedded in the shaft, the cross-section was octagonal. The 20" circle was inscribed within the octagon as shown in Figure 3-2. The outside surface was intentionally roughened using the saw-tooth pattern, scaled down to (1/3.6) of the dimensions of the prototype, which was 0.71 in. amplitude at 1.41 in. spacing. This saw-tooth detail was similar to the one required by the WSDOT BDM for the end forms for prestressed girders. The dimension of the saw-tooth detail satisfied the AASHTO LRFD requirement for surface-transferring shear-friction in term of minimum amplitude. All dimensions designed for the prototype were scaled down to the specimen dimensions.

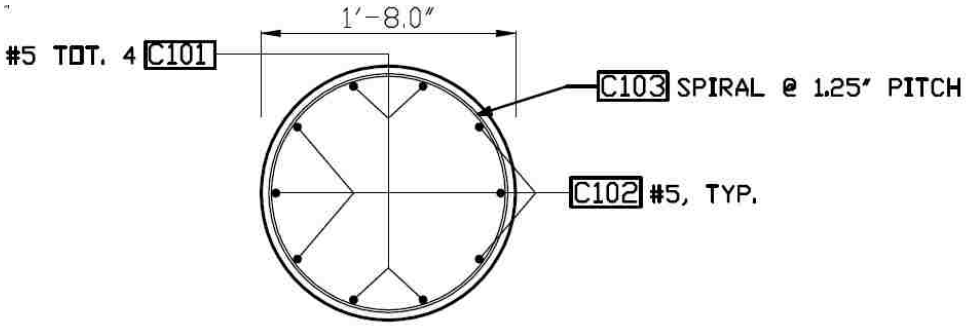

a). Column Section

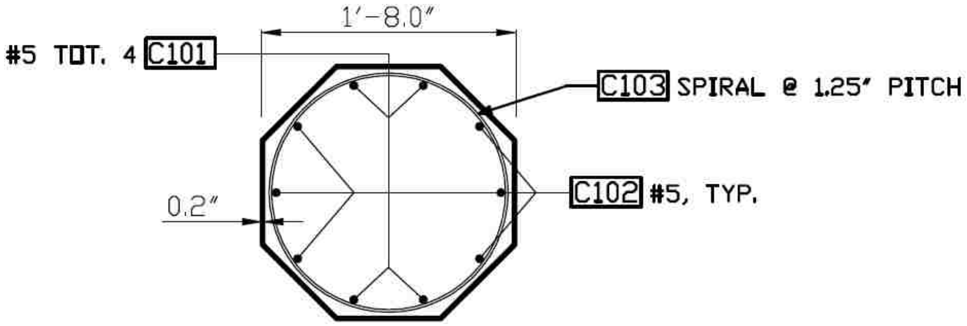

b). Column Embedment Section

Figure 3-2. Column cross sections (DS-1 and DS-2)

The ends of the longitudinal column reinforcement were terminated with rebar end anchors (Lenton Terminators). This kind of anchor not only helped to reduce the development length of longitudinal reinforcement, but also made the connection between precast column and cast-in-place drilled shaft more constructible.

The bottom of the shaft connected with a 74”×48”×24” cast-in-place footing to attach the specimen to the testing rig. The longitudinal bars of the drilled shaft were hooked at the bottom mat of footing as shown in Figure 3-3.

a). Column reinforcement b).Shaft-Footing reinforcement

c). Precast Column d). Column-Shaft connection

Figure 3-3. Specimen construction.

3.3 DESIGN OF TRANSITION REGION

The embedded length of the column in the drilled shaft (28 in.) was based on the scaled-down non-contact lap splice length of the shaft prototype according to WSDOT BDM 7.4.4. This length calculation was proposed by McLean et al. (1997). The embedded length was equal to $\mathrm{l_{ns}} = \mathrm{l}_s + \mathrm{e}$, as discussed in Chapter 2.

The shaft longitudinal reinforcement was designed to force the plastic hinge form in the column rather than in the shaft. To satisfy this requirement, the yielding moment of the shaft had to be larger than the maximum moment that could be developed at the base of the shaft (5353 kip-in. for specimens DS-1 and DS-2, and 6317 kip-in for Specimen DS-3) accounting for the over-strength moment and shear from the column above as given:

$$M_{sh} = \lambda_{mo} M_{p,col} + VL \tag{3-1}$$

where:

λ_{mo} = overstrength factor, which is equal to 1.2 for ASTM A706 reinforcement

L = length of the connection.

Calculations showed that using 30 bundles with 2#3 per bundle in specimen DS-1 and DS-2, and 24 bundles with 3#4 per bundle in Specimen DS-3 for the longitudinal shaft reinforcement in the test specimens would satisfy this requirement.

The confinement reinforcement of the connection (i.e., shaft spirals) must be adequate to resist the internal tension forces that develop within the noncontact lap splice zone of column-shaft connections. For DS-1, the shaft spirals were designed as non-contact lap splices based on Eq. (2-17) according to WSDOT BDM 7.4.4 and 7.8.2. This equation was proposed by WSDOT based on the noncontact lap splice report of McLean et al. (1997). Specimen DS-2 contained only half the amount of spiral in the column-to-shaft connection as was used in DS-1 to force failure into the connection. And in Specimen DS-3, spiral was designed based on McLean's equation (i.e. without using modification factor "k" as in Specimen DS-1).

CHAPTER 4.

EXPERIMENTAL PROGRAM

Quasi-static, cyclic tests were performed to evaluate the seismic performance of three column-to-drilled-shaft connections (DS-1, DS-2 and DS-3). In such testing, displacements are applied at a rate much lower than would be applied during an earthquake. This chapter describes the test setup, displacement history, instrumentation and data acquisition.

4.1 TEST SETUP

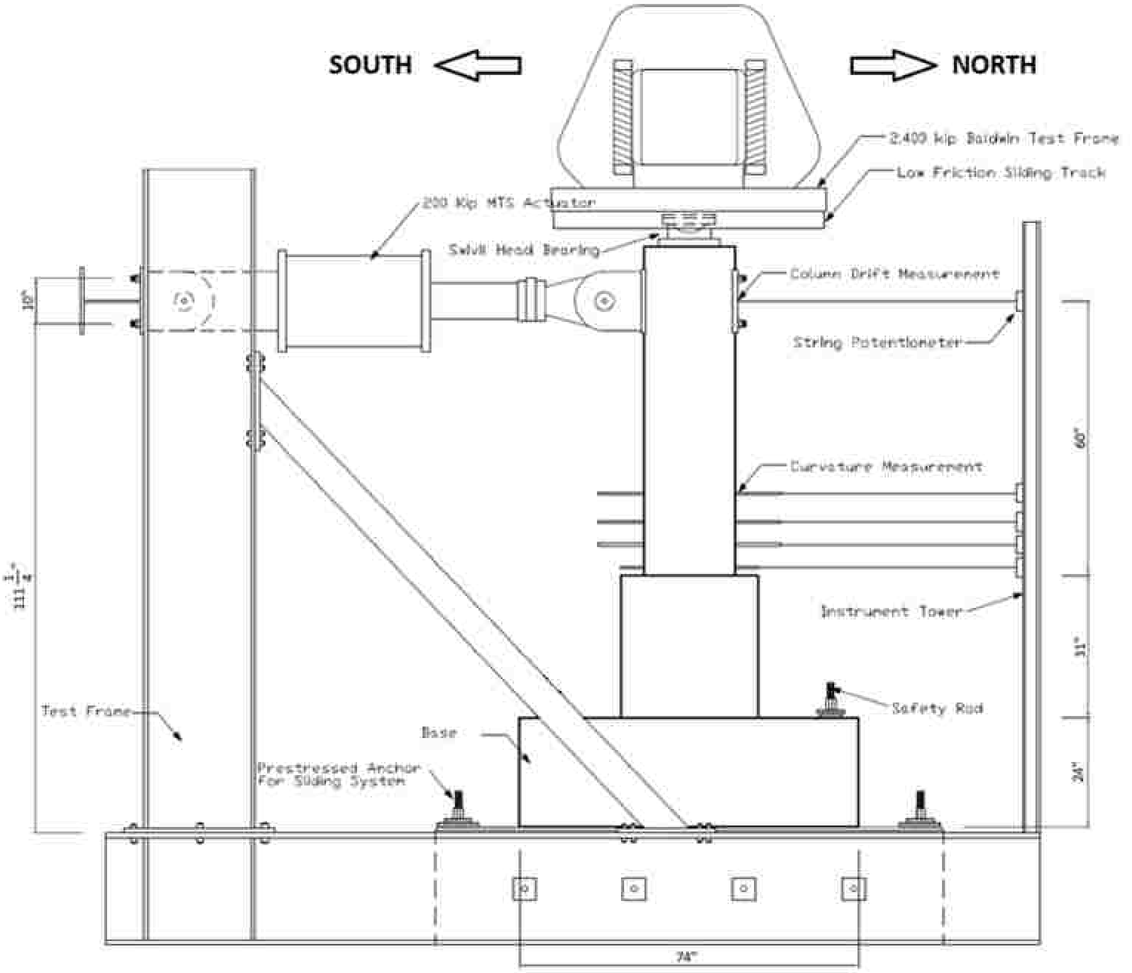

Figure 4-1. Test setup

The three specimens were tested by using the self-reacting rig shown in Figure 4-1. The lateral loads were applied to the column with a servo-controlled actuator with a capacity of 220 kips. The column axial load was provided by the 2.4-million lbs. Baldwin Universal Testing Machine.

4.2 INSTRUMENTATION

The axial load applied in the top of column was monitored by load cells in the Baldwin Testing Machine. The lateral load was monitored by a load cell in series with the MTS actuator. The deformations of the specimen were monitored by potentiometers, linear variable differential transformers (LVDTs), a research-grade motion capture system (Optotrak Certus brand), and strain gauges. The location of the external instruments are shown in Figure 4-2.

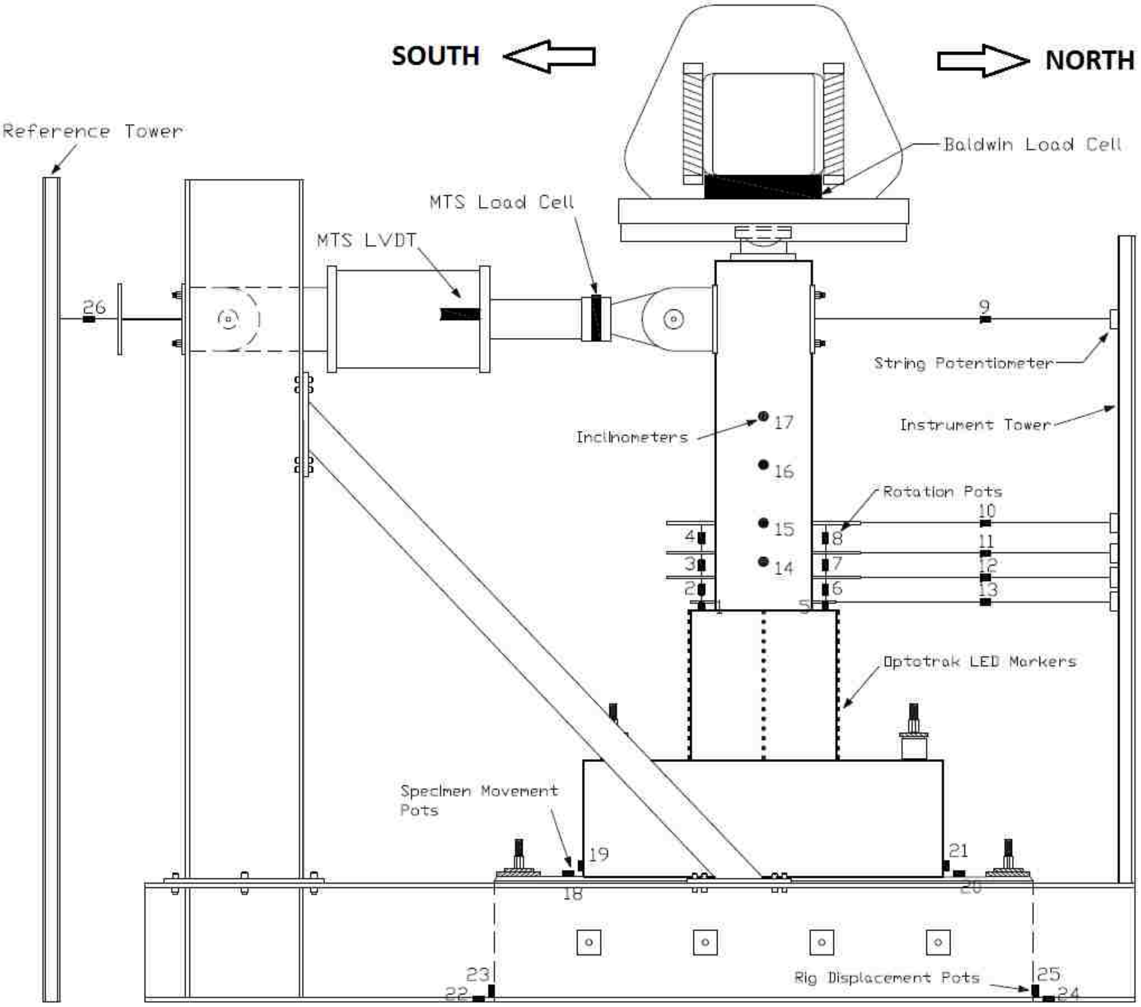

Figure 4-2. Locations of external instruments

Targets for the motion capture system were attached to the column and shaft surface in the north, west and south sides of the transition region to measure displacements (see Figure 4-2). Another four targets were attached close to the north curvature rods' positions to compare the data of string pots and the motion-capture system.

Strain gauges were attached to some key shaft and column longitudinal reinforcing bars, and in shaft spirals in the transition area of column and shaft as shown in Figure 4-3. The gages on the longitudinal bars and spiral were installed at the top, middle, and bottom of the transition region. The goal was to use the strain data to help to understand the behavioral mechanisms of the connection. All strain gauges were supplied by Texas Instruments, type FLA-6-11-5LT. These have a 6mm gauge length and are temperature-compensated to avoid any problems caused by the laboratory lights heating the strain gauge wires. Data from the motion capture system were recorded using NDI viewer with a 4Hz rate. All other data were recorded with a sampling rate 4Hz using LabVIEW (Laboratory Virtual Instrument Engineering Workbench) from National Instruments.

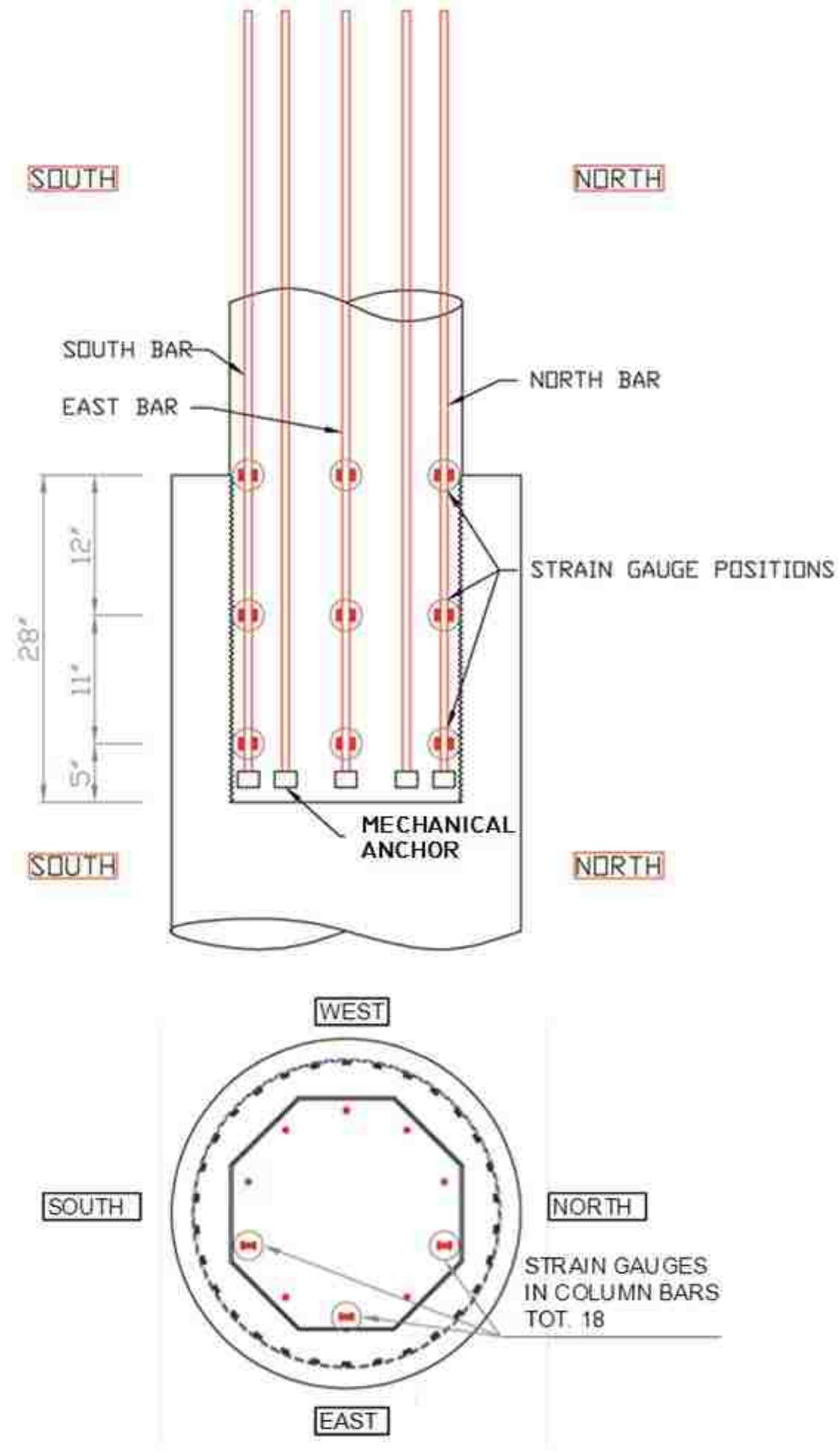

(a) Location of gauges in the column

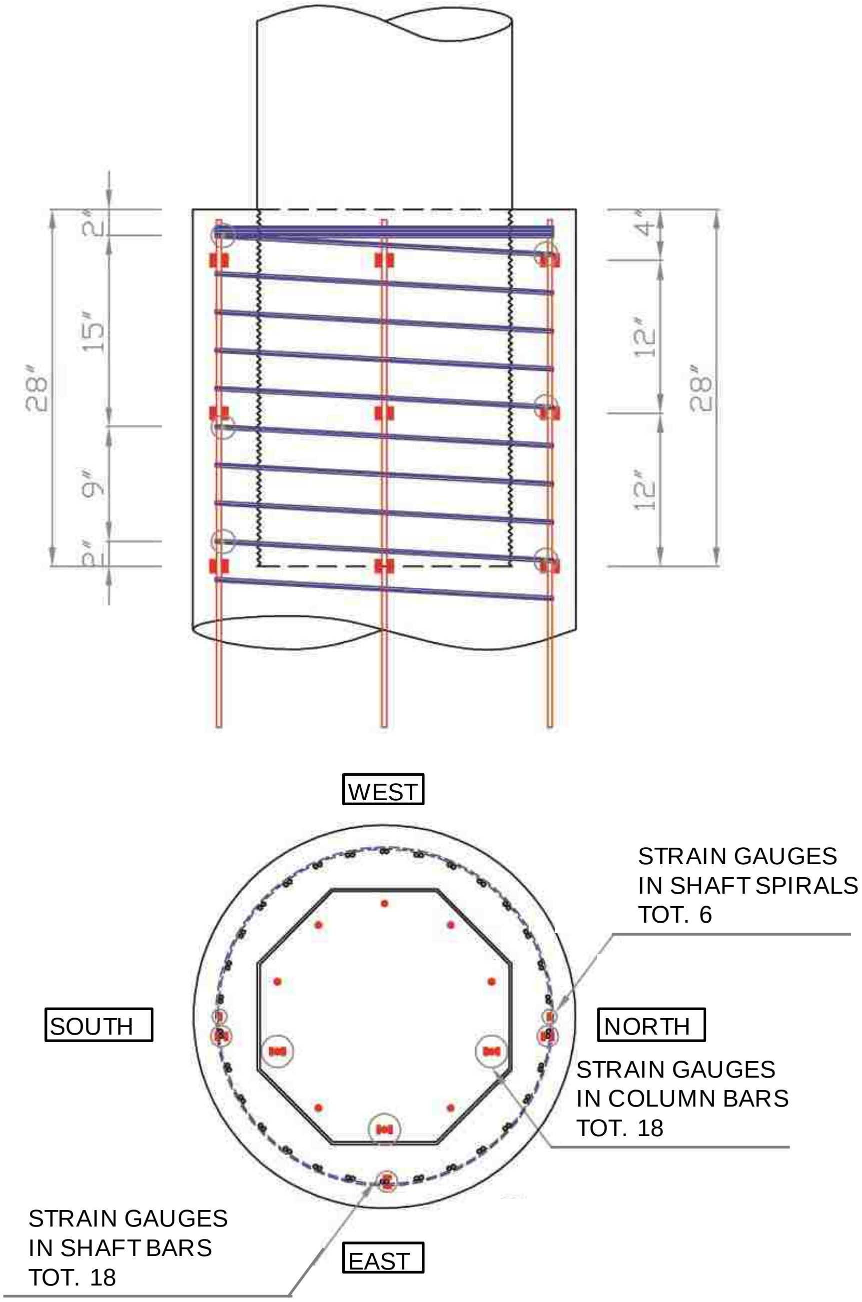

(b) Location of gauges on the shaft

Figure 4-3. Locations of strain gauges

4.3 DISPLACEMENT HISTORY

First, the column was loaded axially to 159 kips ($\approx 0.1A_g f_c'$), which represented, at lab scale, the expected dead weight on the column in a prototype bridge. This axial load was kept constant throughout the testing. Then, the specimens were subjected to displacement-controlled cyclic, lateral displacements. The displacement history was the same as applied in previous tests at the University of Washington (Pang et al. 2008, Cohagen et al. 2008, Haraldsson et al. 2011, Janes et al. 2011). This displacement history was a modification of a loading history for precast structural walls recommended in NEHRP 2004 (Building Seismic Safety Council).

The target displacement histories are provided in Figure 4-4, and consisted of sets of 4 cycles. Within each set, the peak amplitudes of the cycles were 1.2A, 1.4A, 1.4A, and 0.33A respectively, where A is the largest peak amplitude in the previous set. The small amplitude cycle (0.33A) at the end of the set was intended to evaluate the small-displacement stiffness in the specimen after the maximum peak amplitude cycle of each set. In all cycles, the actuator moved from zero displacement to the peak cycle displacement in 20 seconds. As in Haraldson's (2010) and Janes' (2011) report, the positive and negative peak displacement were called "peak" and "valley". The early cycles were chosen to be small enough to lie within the elastic range of behavior, and the largest target cycle (6.2 in. – 10.3% drift - displacement) was limited by the actuator stroke. In practice, the loading was stopped after fracturing of spirals or longitudinal bars.

During testing, the lateral displacement at the top of column was controlled by the LVDT attached in the lateral actuator (not by string potentiometer attached in the north of column). Therefore, the actual displacement at the top of column was slightly smaller than the target displacement, since the bending deformation of the crossbeam attached at the end of the lateral actuator. Another LVDT attached in the reference tower measured the bending deformation of the crossbeam (Figure 4-2). The measured data showed that the actual displacement (measured by string pot) was equal to the difference between lateral actuator displacement and crossbeam bending deformation. The difference between target and actual displacement was small and did not affect the purpose of testing.

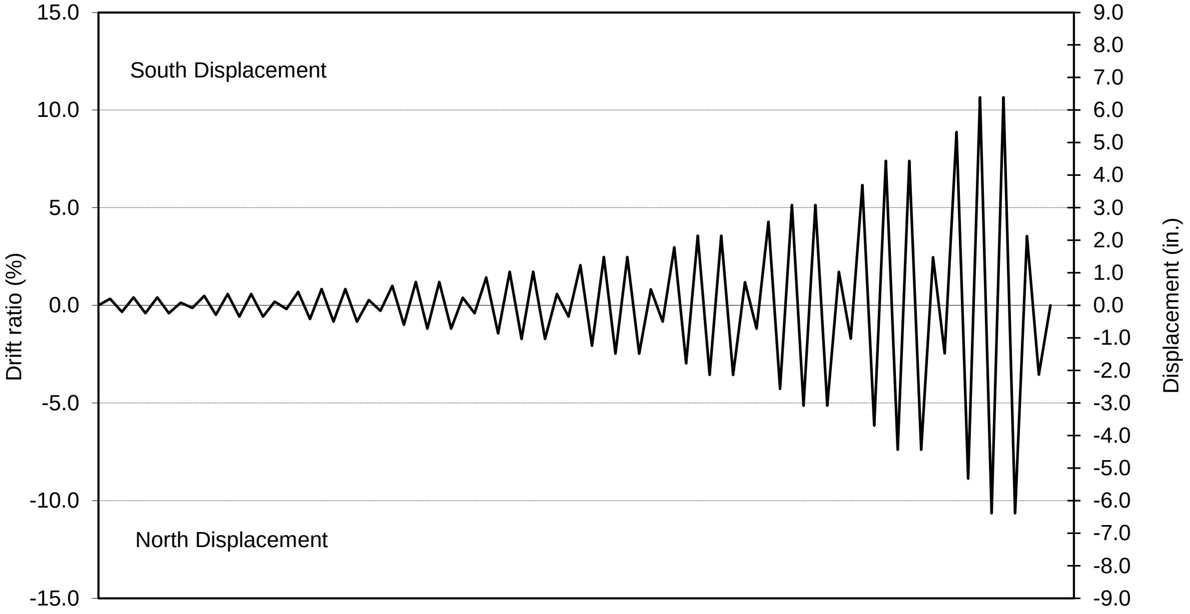

Figure 4-4. Lateral loading displacement history

CHAPTER 5.

EXPERIMENTAL RESULTS

5.1 DAMAGE PROGRESSION

In the first two load cycles of each set, the loading was interrupted at extreme displacements (“peak” and “valley”) to allow inspection of cracks, and again at zero displacement to measure the width of the widest residual crack. In the second two cycles of each set, the loading was continuous with no interruptions and no cracks were inspected or marked.

Specimens DS-1 and DS-2 were both subjected to a total of 38 cycles (up to cycle 10-2), and Specimen DS-3 was subjected to 40 cycles (up to cycle 10-4). The details of the damage progression for specimens DS-1, DS-2, and DS-3 are shown in Table 5-1. In the table, the drift ratio refers to the lateral displacement at the actuator level divided by the vertical distance from the actuator centerline to the top of the shaft.

In the initial cycles, up to about 0.7% drift ratio, the cracks in all specimens were fine and closed almost completely at zero displacement between cycles. At about 0.7% drift ratio, the longitudinal steel in the column yielded and the first significant horizontal cracks appeared. Those cracks did not close completely when the load dropped to zero.

After the longitudinal column reinforcement yielded, the behaviors of the three specimens started to differ significantly. In DS-1 and DS-3, the damage was concentrated in the columns, and the specimen eventually failed by fracture of the longitudinal steel in the plastic hinge region of the column, in what might be described as a typical column flexural failure. First, significant spalling occurred in the column (at about 3.6% drift ratio). Then, the longitudinal bars buckled, causing a kink in the spiral steel, which initiated its fracture. After the spiral fractured, the longitudinal bars straightened, re-buckled with each load cycle and eventually fractured due to the low-cycle fatigue caused by the alternate bending and straightening. The longitudinal steel in the shaft never yielded, and the transverse steel in the shaft yielded but never fractured.

Table 5-1. Comparison of specimens' drift ratios for the major damage states

	DS-1	**DS-2**	**DS-3**
0.7% drift ratio			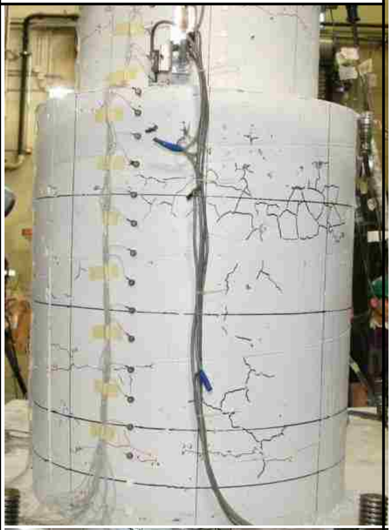
4.3% drift ratio			
10.3% drift ratio			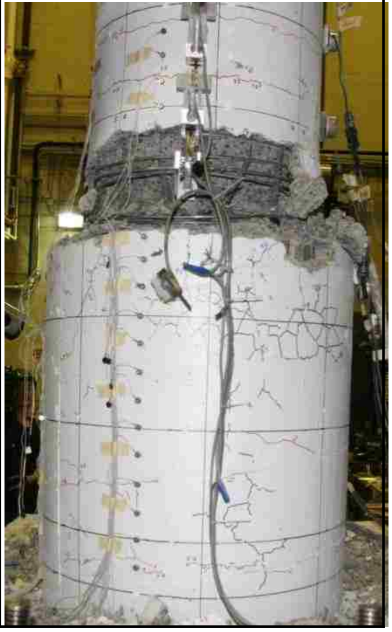

In Specimen DS-2, the amount of spiral steel in the shaft was only half that in Specimen DS-1. It is therefore not surprising that, the transverse shaft reinforcement for this specimen yielded earlier than in DS-1, and subsequently fractured. The behavior of Specimen DS-2 was characterized by very large cracks opening in the shaft, which suffered extensive deformations as a result. Failure was initiated by fracture of the spiral steel in the shaft, starting at the top and progressing downwards. The damage to the shaft caused the load to drop even though the drift was increasing. The longitudinal bars in the column did not buckle, and it was observed that the spirals in the column never fractured.

Vertical shear sliding at the curved interface between the precast column and cast-in-place shaft was an important behavioral mechanism. No instruments measured this displacement, so visual observations provided the only available evidence, and they could be made primarily only after the test was complete. After testing, in specimens DS-1 and DS-3, the damage to the shaft existed mainly in the small region of top cover concrete above the ends of the vertical bars (Figure 5-1). In the remainder of the shaft, the column was still held firmly by friction and no relative motion between the two was visible. However, in Specimen DS-2 the shaft had been pried open by the lateral movements of the column so much that the spiral steel in it had yielded and fractured, and the column could be lifted freely out of the shaft with no resistance (Figure 5-1). The radial separation between the column and the shaft allowed free slip between the two.

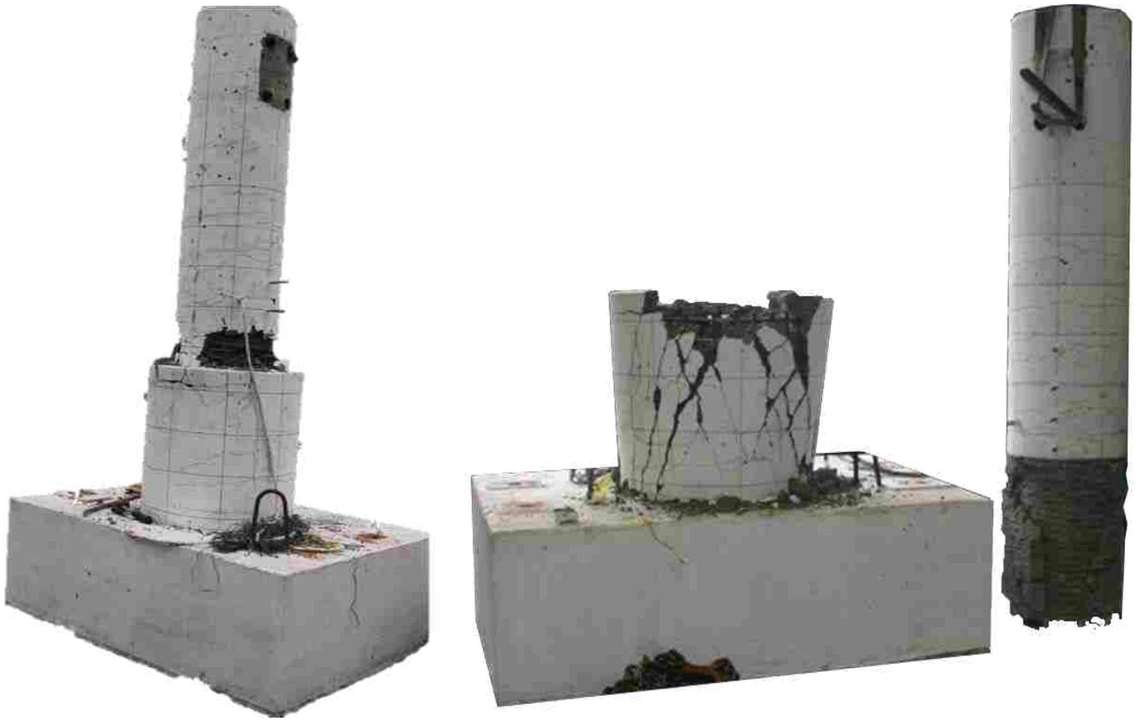

DS-1 DS-2

Figure 5-1. Specimens after testing

5.2 MEASURED RESPONSE

5.2.1 Moment-Drift Response

The moment-drift response was similar to the load-displacement response, but it differs slightly, because the moment includes components from both the vertical and lateral loads, whereas the load-displacement response includes only the horizontal load.

The moment at the base of column (i.e. the top of the shaft) is given by (Figure 5-2):

$$M_c = h_1.V - F_{fric}.h_2 + (\Delta_2 - \Delta_3).P \tag{5-1}$$

where:

M_c = the column moment at the base.

h_1 = height from the column-shaft interface to the line of action of the lateral load.

h_2 = is the height from the interface to the top of column where the axial load, P, is applied by the Baldwin Universal Testing Machine.

V = applied lateral load.

F_{fric} = the friction force between the bearing and the sliding channel, and the greased steel-to-steel spherical element on bearing.

Δ_1 = the lateral displacement at the location of the lateral load.

Δ_2 = the lateral displacement at the top of the column.

Δ_3 = the lateral displacement at the top of the transition, was taken approximately as lateral displacement at the first curvature rod (2 inches above the top of transition).

In the absence of a measured value for Δ_2, it was approximated by assuming that the column rotated as a rigid body about its base, in which case:

$$(\mathit{\Delta}_2 - \mathit{\Delta}_3) \approx (\mathit{\Delta}_1 - \mathit{\Delta}_3).\frac{h_2}{h_1} \tag{5-2}$$

and

$$M_c = h_1.V - F_{fric}.h_2 + (\mathit{\Delta}_1 - \mathit{\Delta}_3).\frac{h_2}{h_1}.P \tag{5-3}$$

It should be noted that the vertical load, P, contributed about one third of the total moment at the maximum drift, and less than that at smaller drifts. Thus, any relative error in the approximation of Δ_2 creates a smaller relative error in the moment calculation.

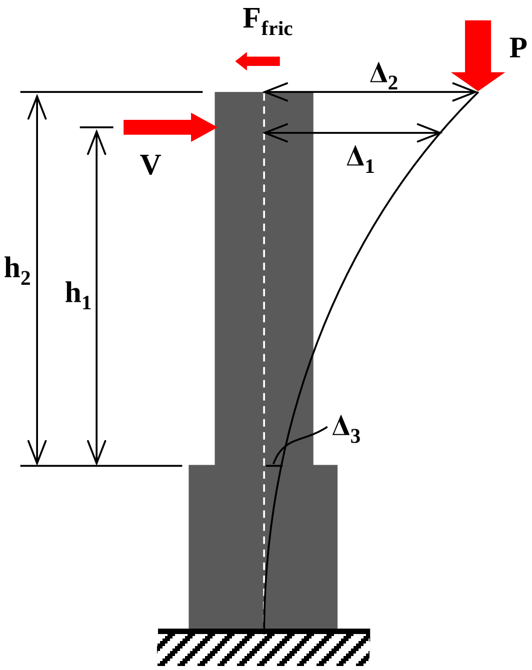

Figure 5-2. Displacements and forces on test specimen

Figure 5-3 shows the moment vs. drift ratio response of the test specimens DS-1, DS-2, and DS-3. In specimens DS-1 and DS-3, failure occurred by plastic hinging in the column while the connection region in the foundation remained largely undamaged. Their cyclic responses were similar to those of column-to-spread footing connection specimens performed at the University of Washington. However, in Specimen DS-2, failure occurred in the connection region after some damage had first occurred in the column. That difference is not apparent from the plotted responses of the specimens.

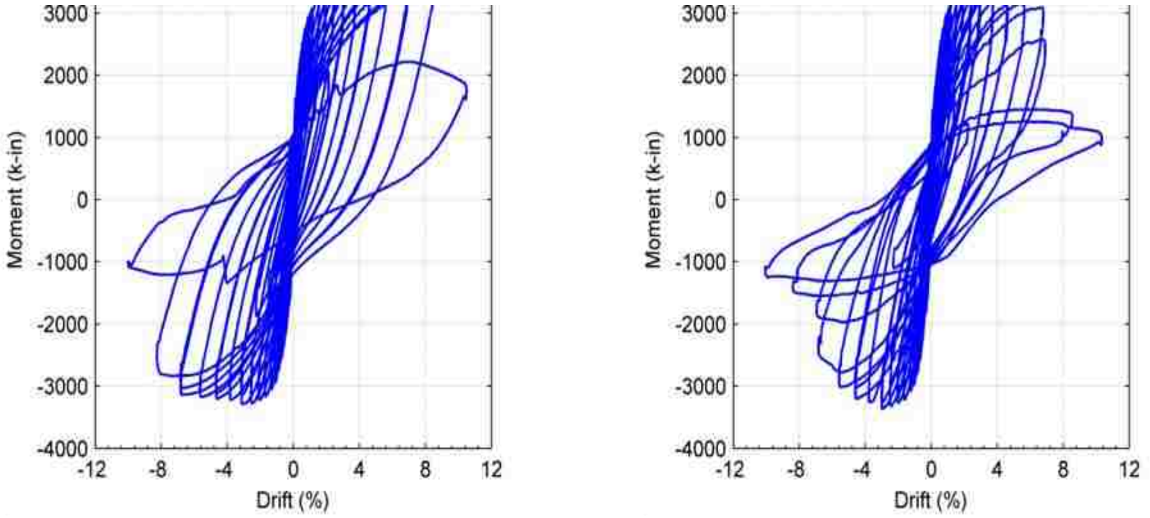

a). Specimen DS-1

b). Specimen DS-2

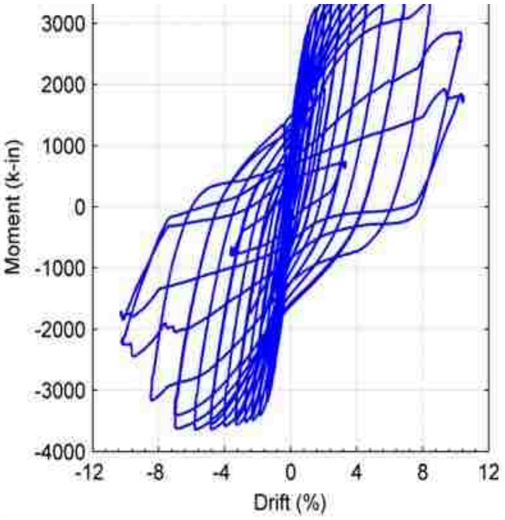

c). Specimen DS-3

Figure 5-3. Moment vs. drift ratio responses

5.2.2 Distribution of Deformation

In the test specimens, the horizontal displacement at the top of the column depended on the deformations of the individual elements. To simplify discussion, those deformations are broken down into the following components, which are illustrated in Figure 5-4:

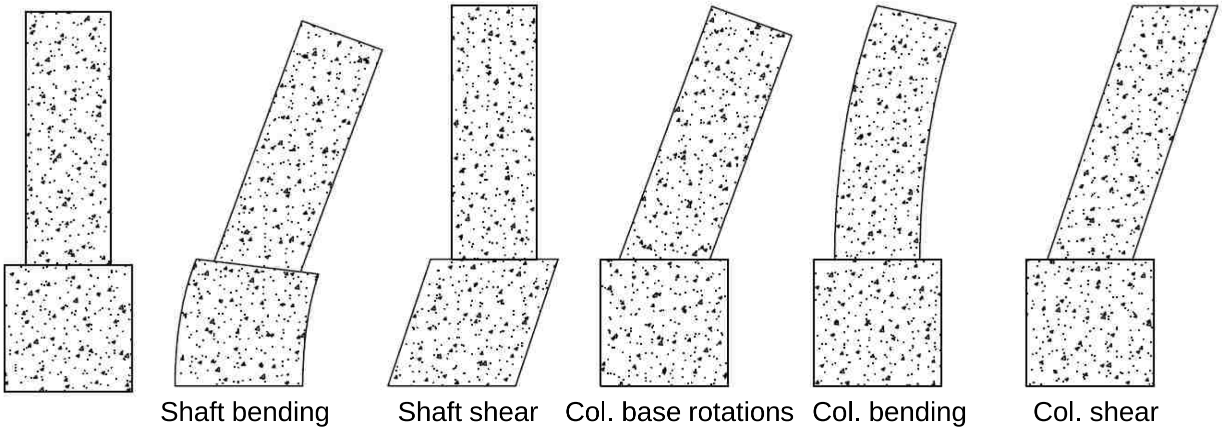

Figure 5-4. Displacement types

1. *Shaft bending deformations*. These are the curvatures of the shaft, and depend on the elongation of one vertical face and the shortening of the opposite one. Curvature was measured by the three "Optotrak" markers attached to the shaft at the same level, using the motion capture system. At each level, one "Optotrak" marker was attached on each of the North, South, and West sides of the shaft. The rotations of the shaft were taken as the rotation of the plane defined by these three points. Then, the average curvature of segment was calculated by dividing the difference of rotation at adjacent level to segment's height.
2. *Shaft shear deformations*. These deformations consist of pure shear deformations of the shaft. They were obtained as the difference between the total lateral displacements and bending displacements of the shaft. The total displacements were obtained from the horizontal displacements measured by the motion capture system (and verified by the string potentiometers). The bending displacements were obtained by integrating the rotations obtained from (1) above.
3. *Column base rotations*. The column can rotate as a rigid body, due to damage in the transition region of the shaft. These rotations were obtained from the bottom couple of potentiometer attached to the column (for Specimen DS-1), and from the group of three "Optotrak" markers attached to the bottom of column (2 in. above the interface) for specimen DS-2 and DS-3.

4. *Column bending deformations*. These deformation consist of the curvatures of the column. Rotations were measured at discrete locations up the column and average curvature was computed from the difference between rotations at adjacent locations. The rotations were obtained using the inclinometers, curvature rods instruments in three specimens, and they were also compared with rotations calculated by "Optotrak" data, in Specimen DS-2.
5. *Column shear deformations*. These consist of the pure shear deformations of the column. They were very small in both cases, and were estimated from subtracting the total displacement to the displacement of components (1), (2), (3), and (4). This value would include error in this computation.

The method of measuring rotation of specimens using groups of three Optotrak marker was compared with the results of inclinometers to evaluate the accuracy of this method. The comparison is shown in Figure 5-5 and Figure 5-6 for Specimen DS-2. The comparison showed that the results of method using Optotrak were similar to inclinometers' results. The maximum error was about 0.5 degree for large cycles.

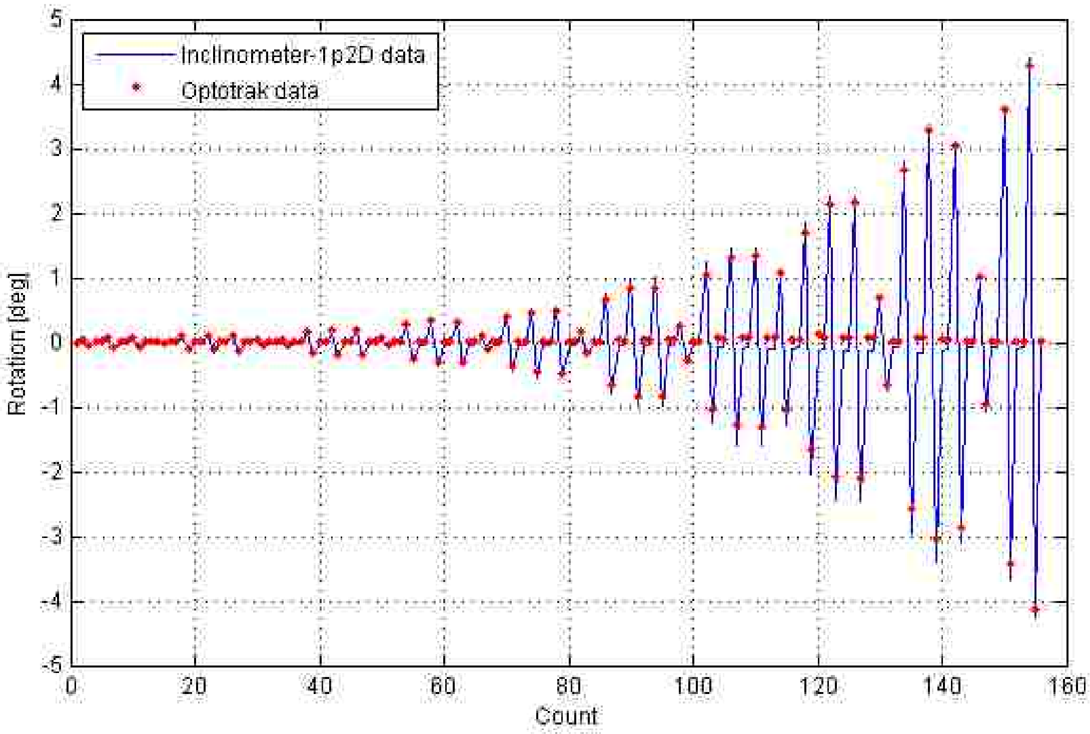

Figure 5-5. Rotation comparison at 10" above the interface (Specimen DS-2)

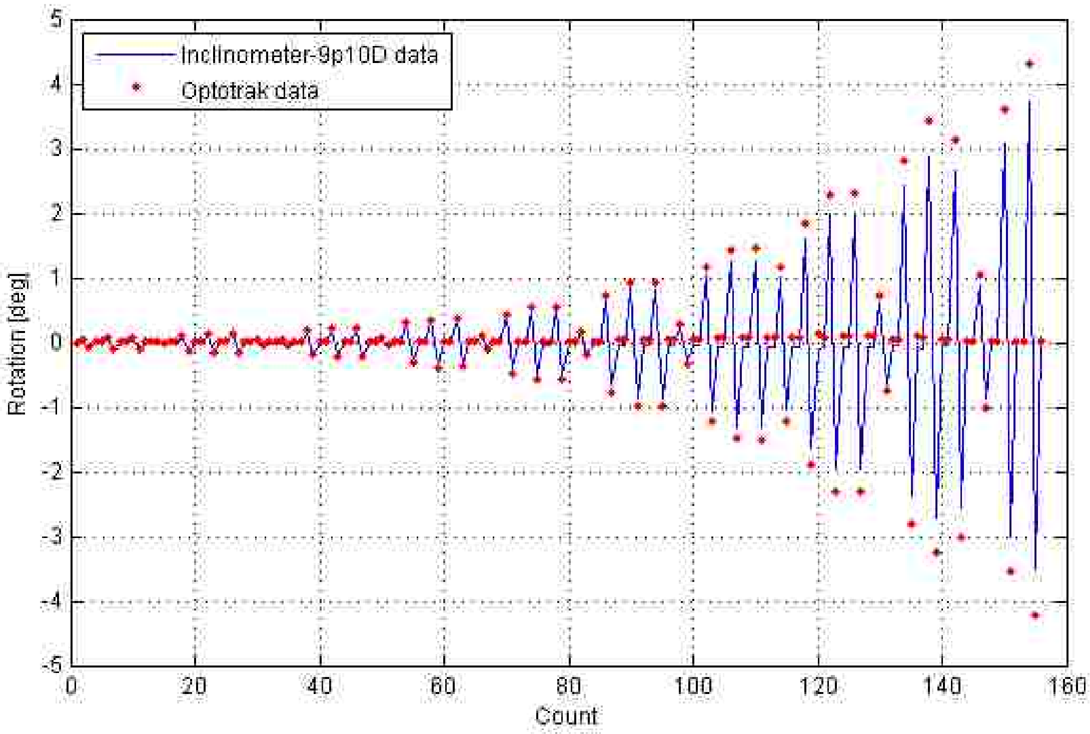

Figure 5-6. Rotation comparison at 18" above the interface (Specimen DS-2)

The displacement contribution for three specimens are plot in Figure 5-7. The combination contribution of shaft bending and shear deformation is shown as blue color, column bas rotation as green color, and column bending as red color. Ideally, the displacement of all contribution is equal as (i.e. 100%) total displacement. So the difference between combination values and 100% are contribution of column shear deformation and errors, where the contribution of column shear deformation is believed to be small.

The column base rotation could not be measured after 4% drift in Specimen DS-1 since the potentiometer in the North side was broken, and after 6% drift in Specimen DS-3 since the concrete spalling removed the LED markers.

The response of Specimen DS-2 shows that the contribution of column bending deformation reduced gradually, while the contribution of column base rotation kept increasing, and reached about 60% at 7% drift ratio. However, in specimen DS-1 and DS-3, the contribution of column bending deformation for the lateral displacement at the top kept constant at about 40% at small drift ratio, and dominated specimens' behavior at large drift ratio. Since the shaft diameters were larger in specimens DS-1 and DS-2 than in Specimen DS-3, so the shafts were stiffer, and the contributions of shaft deformation in specimens DS-1 and DS-2 were smaller than in Specimen DS-3.

The displacement profiles of the shaft and column at key displacement levels are plotted for specimens DS-1, DS-2, and DS-3 in Figure 5-8, Figure 5-9, and Figure 5-10 respectively. The vertical axis represents distance above the base of the shaft, while the horizontal axis is the displacement in inches. Note that the shaft was 30 inches high, and the height of the column, measured from the top of the shaft to the loading point, was 60 inches.

Profiles are given for the peak displacement in each cycle set, up to 3.0% drift. Separate curves are given for the positive and negative directions. For each load level, two curves are presented. The solid line represents the total displacement, while the dotted line represents the sum of the displacements due to components 1, 2 and 3 (shaft bending, shaft shear and column base rotation). Components 1 and 2 may be thought of as shaft contributions to the overall displacement. Component 3, column base rotation, may be thought as column boundary condition contributions which is nearly zero in the column-spread footing socket connection of Haraldsson et al.

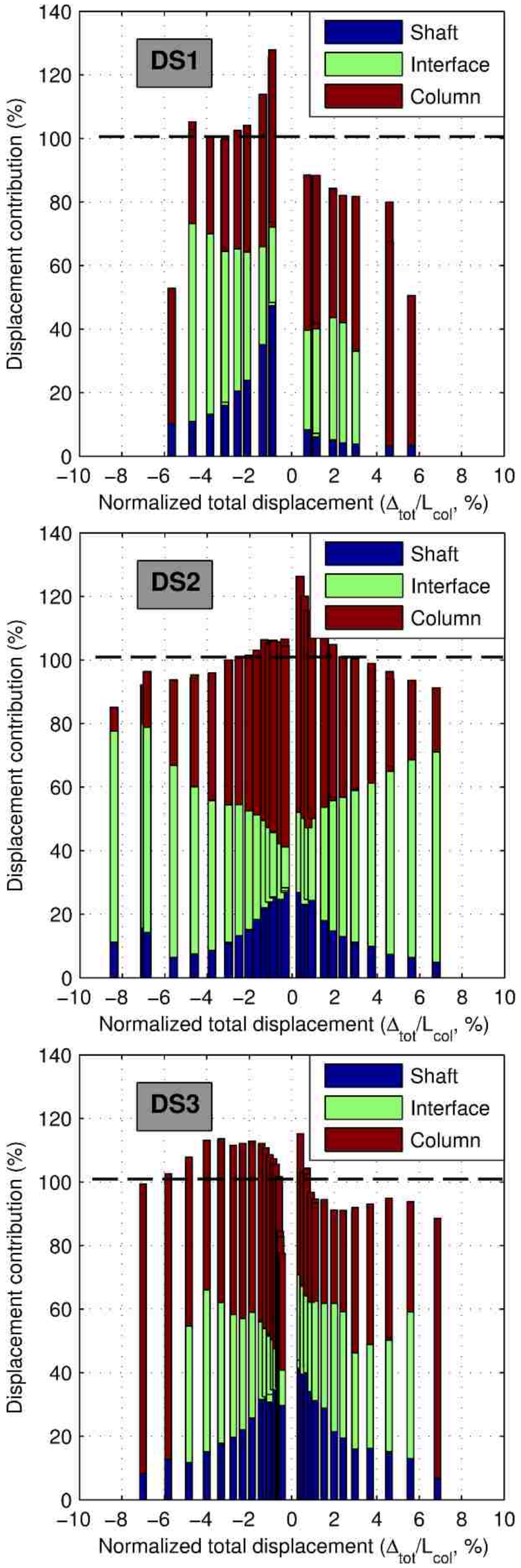

Figure 5-7. Displacement contribution

(2011). The difference between the dashed and solid lines for any load level therefore represent the displacement due to column bending and shear, or in other words the column contributions to the total displacement. The column shear component was in all cases small compared with the column bending component.

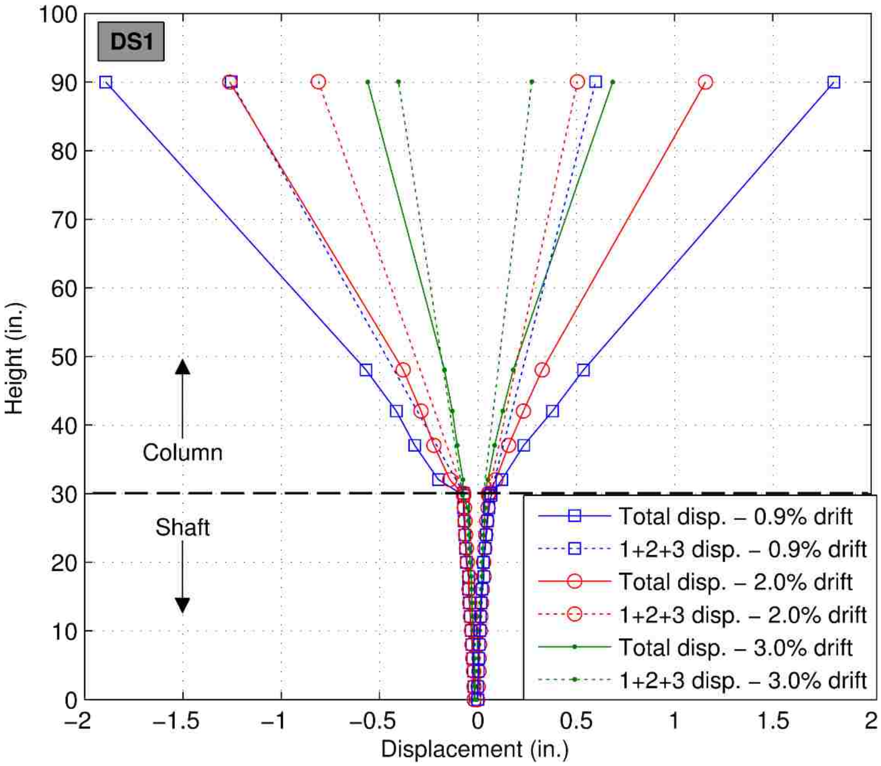

Figure 5-8. Displacement profile – DS-1

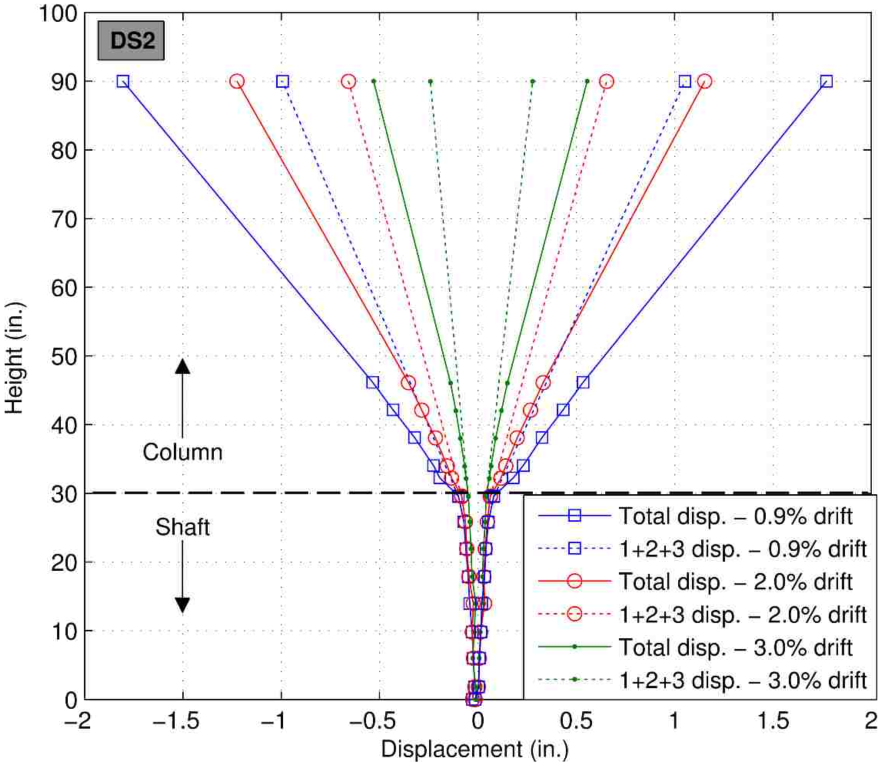

Figure 5-9. Displacement profile – DS-2

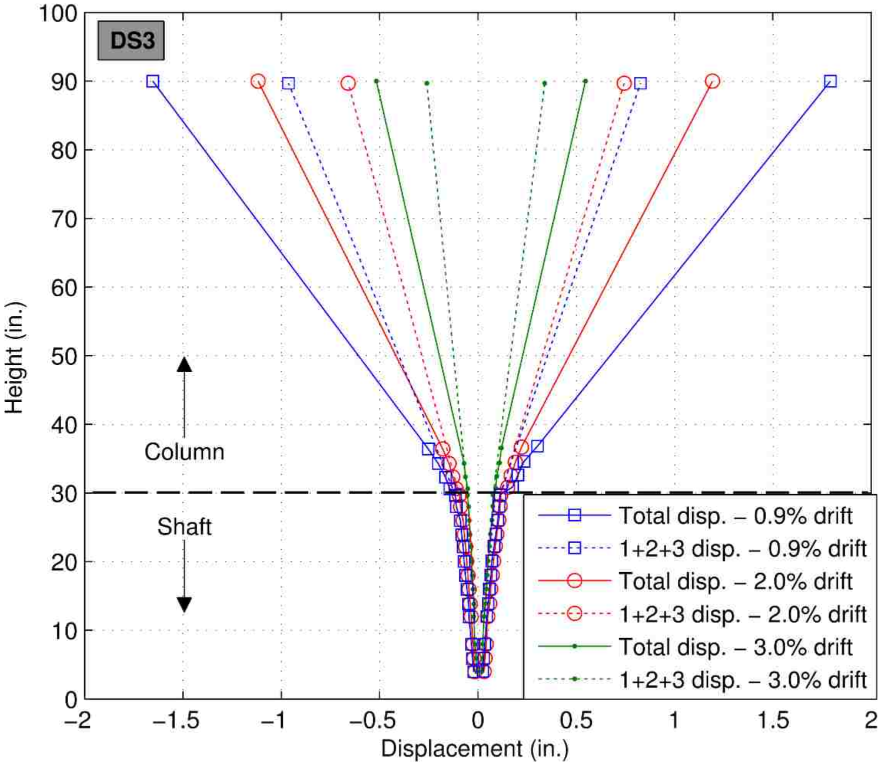

Figure 5-10. Displacement profile – DS-3

5.2.3 Strains in Column Reinforcing Bars

The longitudinal reinforcing bars in the column were gauged as described in Figure 5-11 and Figure 5-12. Because they were configured symmetrically, only the East reinforcing bars were gauged. In all specimens, gauges were attached on the reinforcing bars in pairs at three locations: 0 in., 12 in. and 23 in. below the interface of the shaft and column.

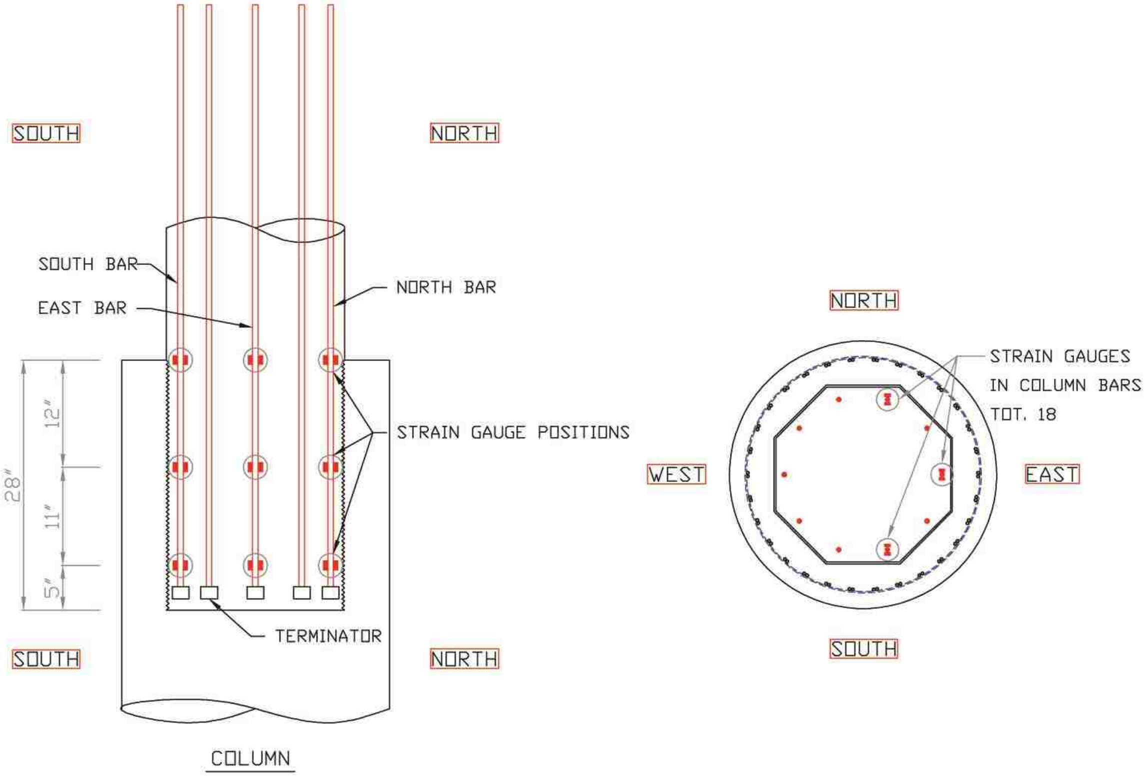

Figure 5-11. Column strain gauge positions – DS-1 and DS-2

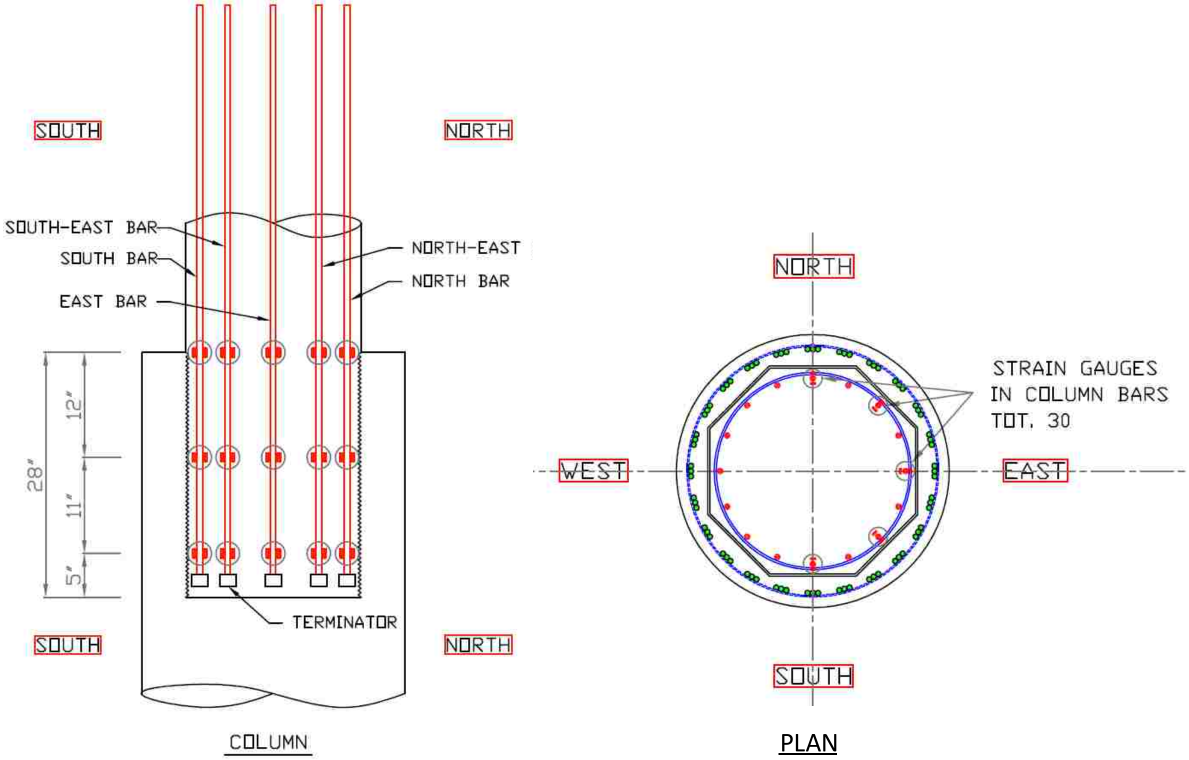

Figure 5-12. Column strain gauge positions – DS-3

Figure 5-13, Figure 5-14, and Figure 5-15 show the axial strain distributions (obtained by averaging the readings from each pair of gauges) over the height of the North, South and East reinforcing bars at various drifts for specimen DS-1, DS-2 and DS-3 respectively. The strains were plotted up to 3% drift. Both specimens show similar strains profiles before yielding in the reinforcing bars. The plots show that the reinforcing bars in North and South experienced alternate tension and compression as they were loaded cyclically, and they started to yield in tension at the column-shaft interface at 0.7% drift. The East reinforcing bars were located at the mid-depth of the column, so they experienced almost equal tension strains when the column was displaced to the North and South. They started to yield in tension at 1.2% drift.

At a location 12 in. below the interface, the bars started to yield at 2.0% drift in the North and South reinforcing bars, and at 3.0% drift in the East reinforcing bars in all specimens. After 3.0% drift, the tension strains began to exceed the measurement range of the data acquisition system, which was from -0.011 to +0.011 in/in. For real strains outside this range, the recorded value was

+/- 0.011 in/in. When the real strain came back within the readable range, the correct value was again recorded.

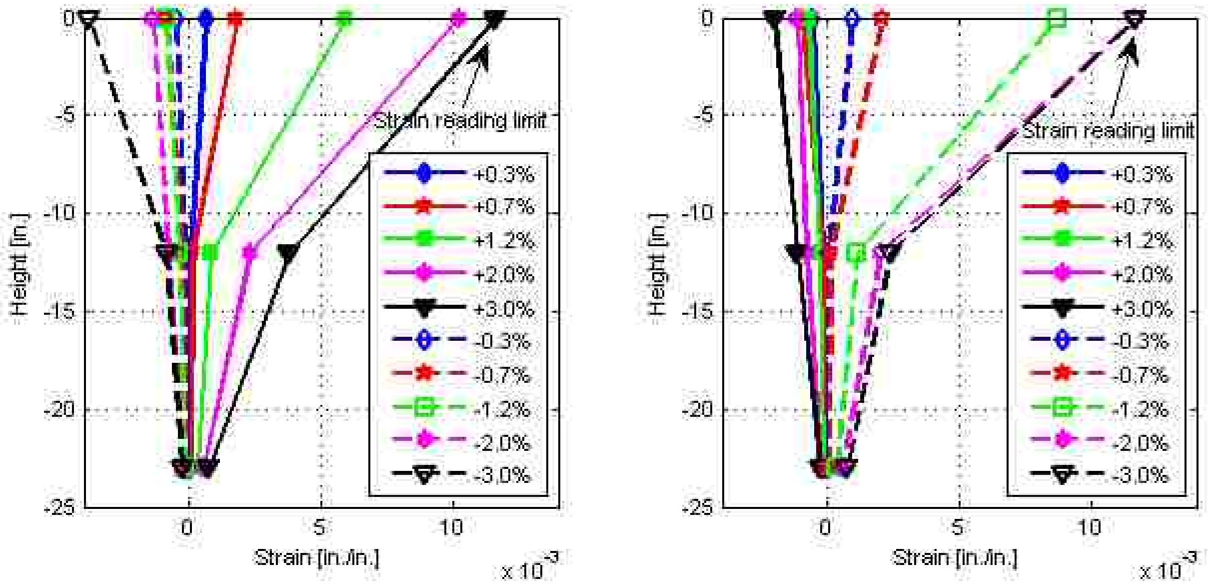

a). DS-1 - North reinforcing bar of column. b). DS-1 - South reinforcing bar of column.

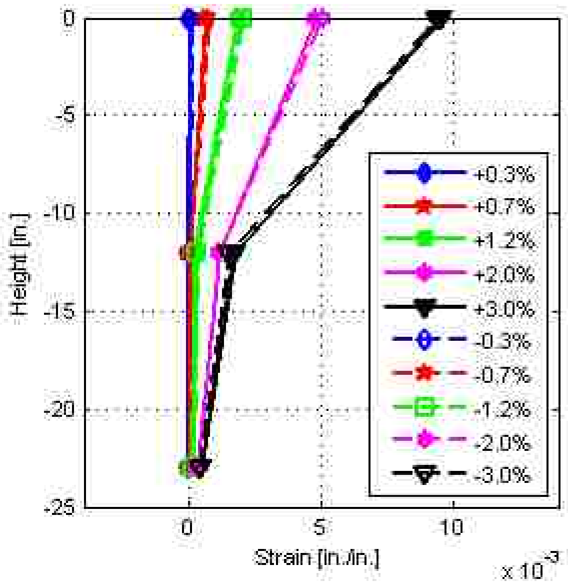

c). DS-1 - East reinforcing bar of column.

Figure 5-13. Strain profiles in reinforcing bars of the column (until 3% drift) – DS-1

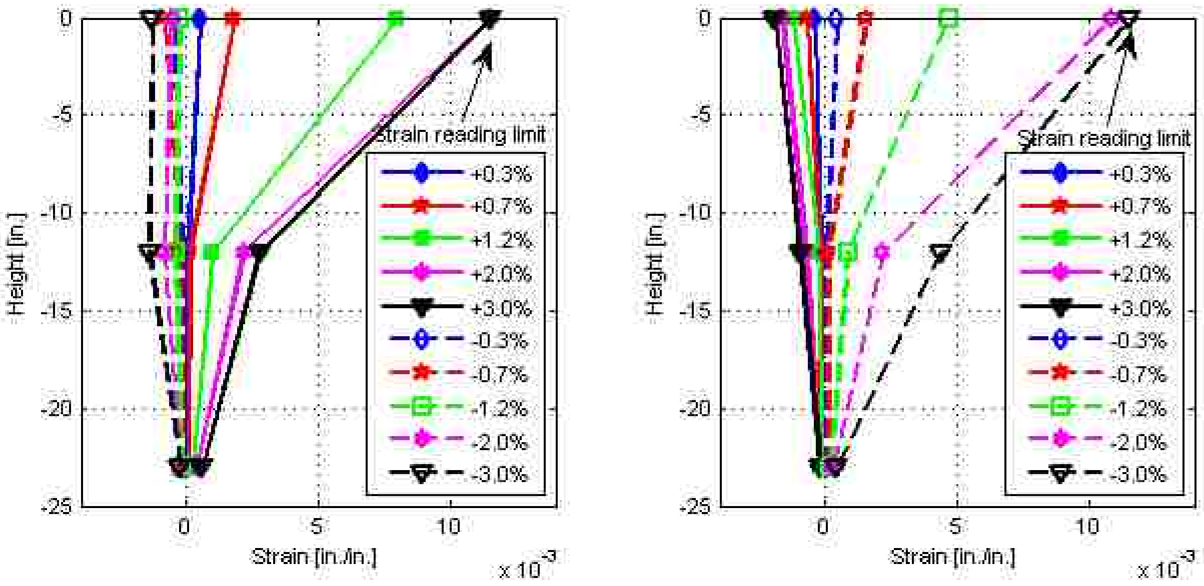

a). DS-2 - North reinforcing bar of column.   b). DS-2 - South reinforcing bar of column.

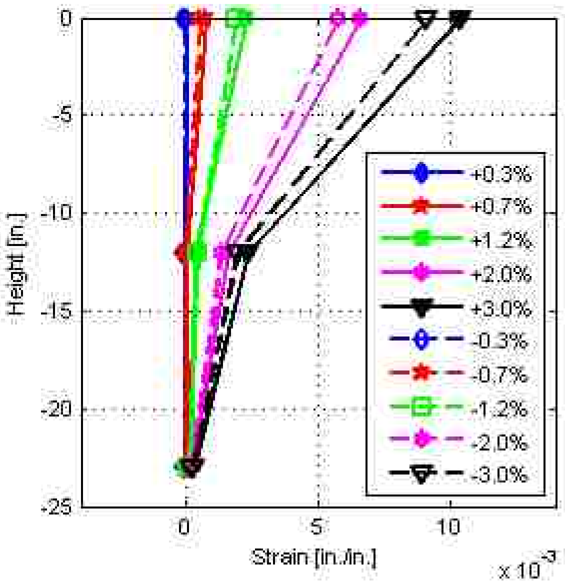

c). DS-2 - East reinforcing bar of column.

Figure 5-14. Strain profiles in reinforcing bars of the column (until 3% drift) – DS-2

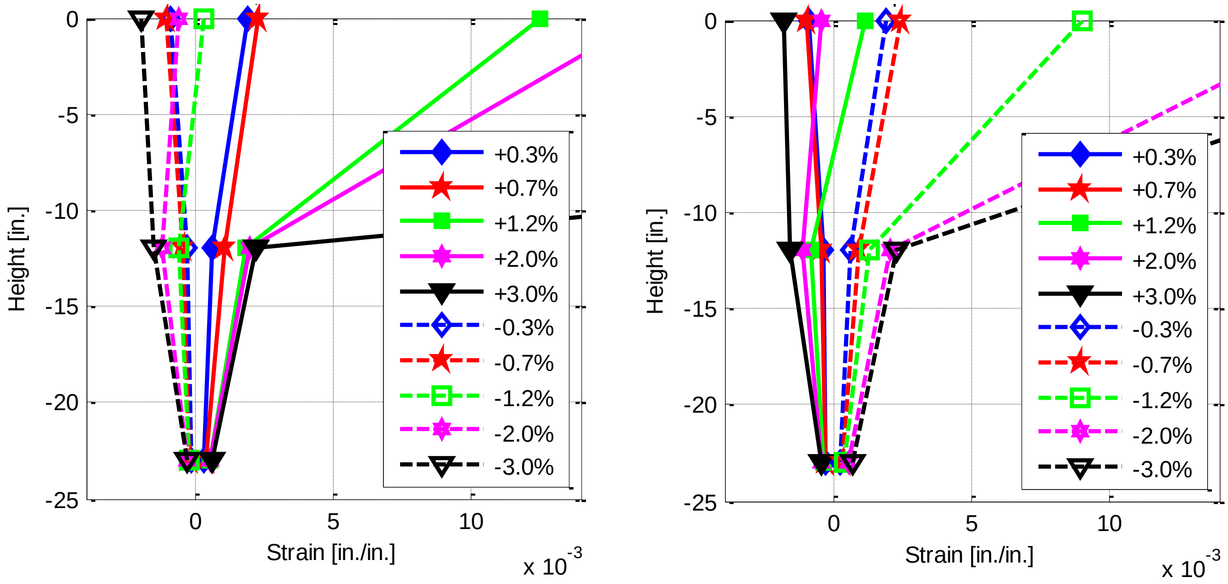

a). DS-3 - North reinforcing bar of column.
b). DS-3 - South reinforcing bar of column.

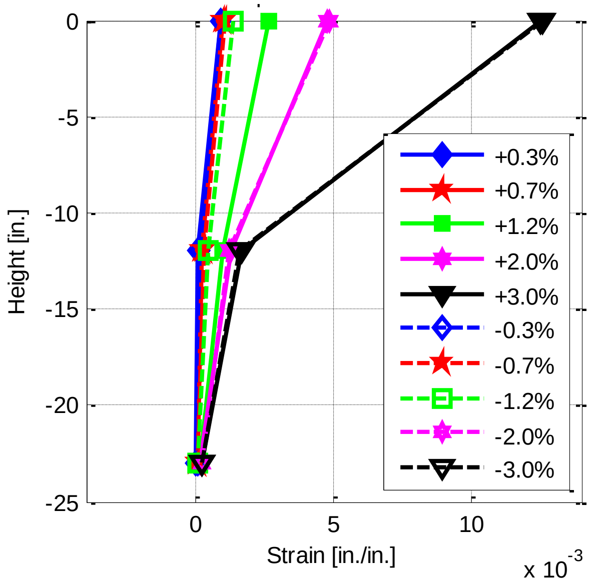

c). DS-3 - East reinforcing bar of column.

Figure 5-15. Strain profiles in reinforcing bars of the column (until 3% drift) – DS-3

The axial strains distributions after 3% drift are plotted in Figure 5-16, Figure 5-17, and Figure 5-18. For the reasons given above, the recorded values are limited to the range +/- 0.11 in/in. They were plotted up to 8.4% drift when the spiral in the column broke. At the next cycle, 10% drift, the reinforcing bars in the column broke. so no strain is presented.

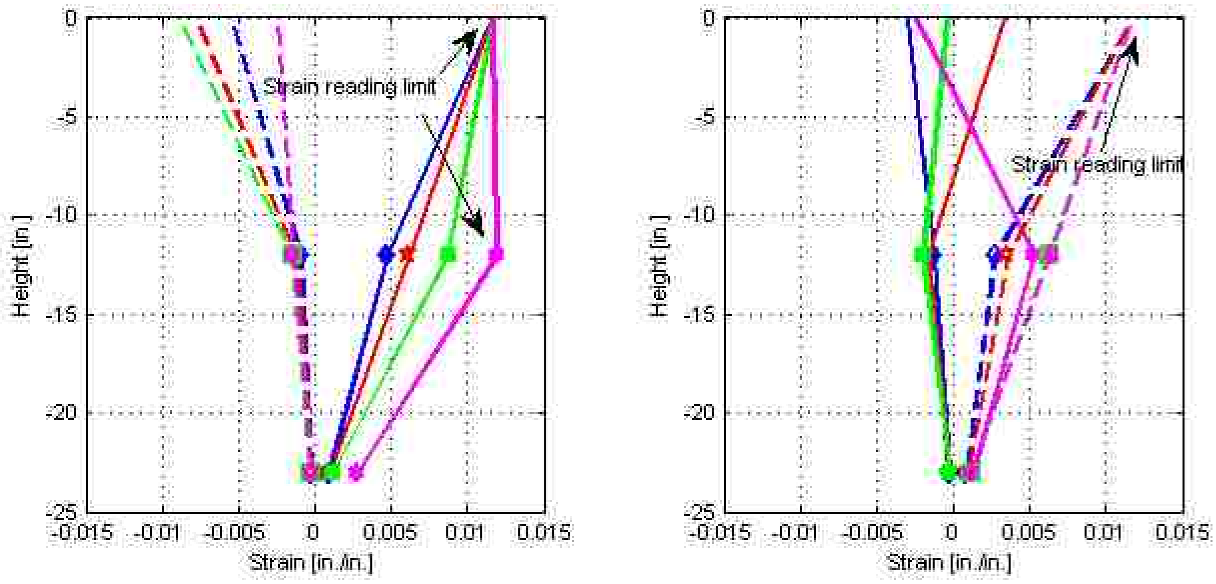

a). DS-1 - North reinforcing bar of column.

b). DS-1 - South reinforcing bar of column.

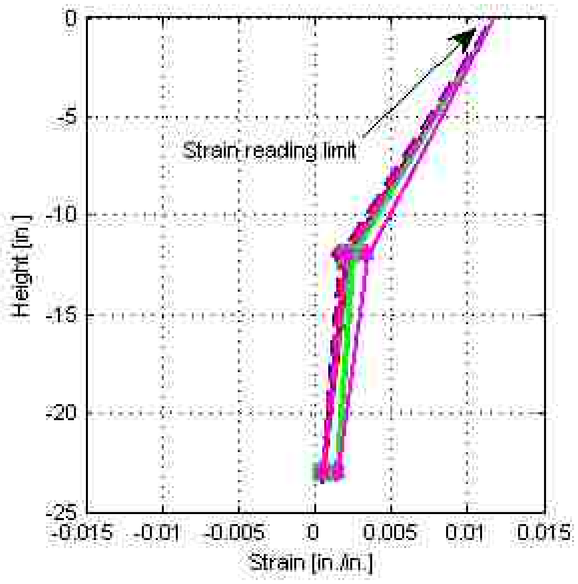

c). DS-1 - East reinforcing bar of column.

Figure 5-16. Strain profiles in reinforcing bars of column (after 3% drift) – DS-1

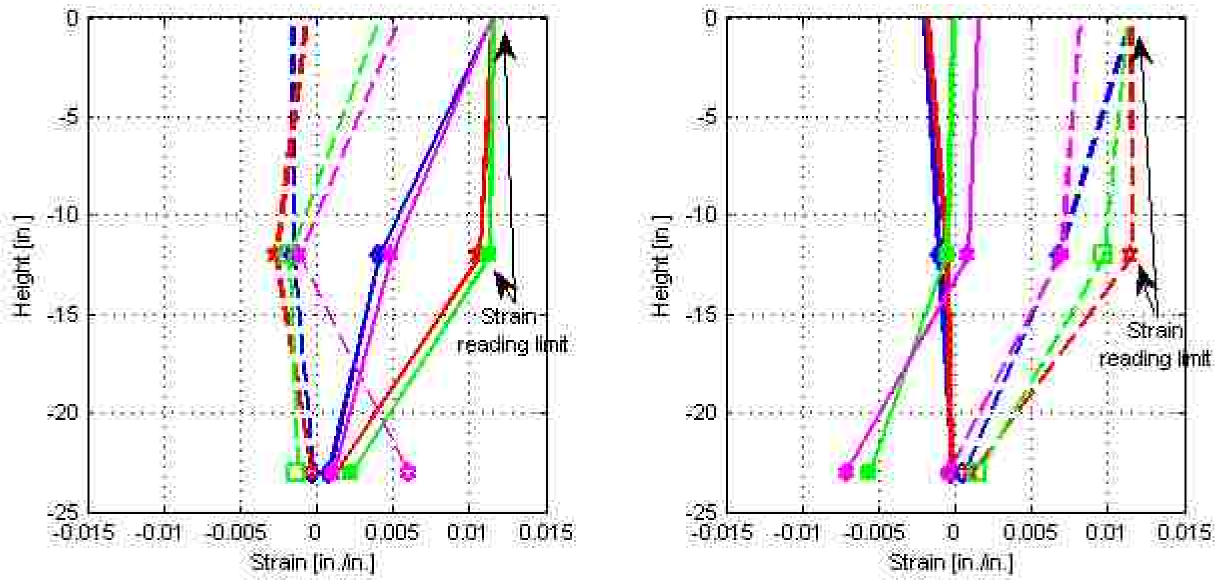

a). DS-2 - North reinforcing bar of column.

b). DS-2 - South reinforcing bar of column.

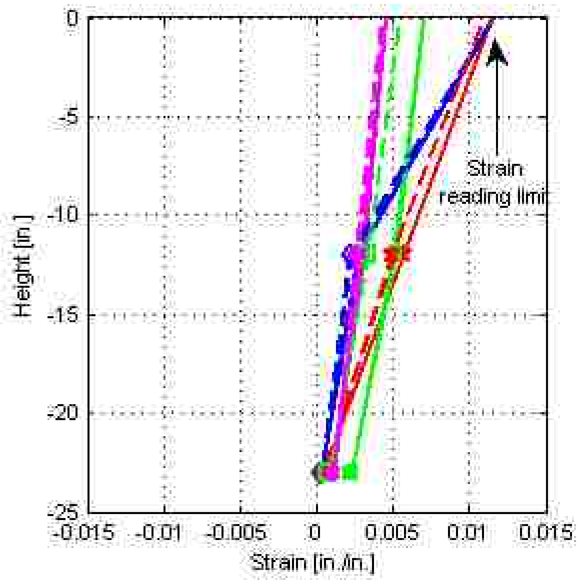

c). DS-2 - East reinforcing bar of column.

Figure 5-17. Strain profiles in reinforcing bars of column (after 3% drift) – DS-2

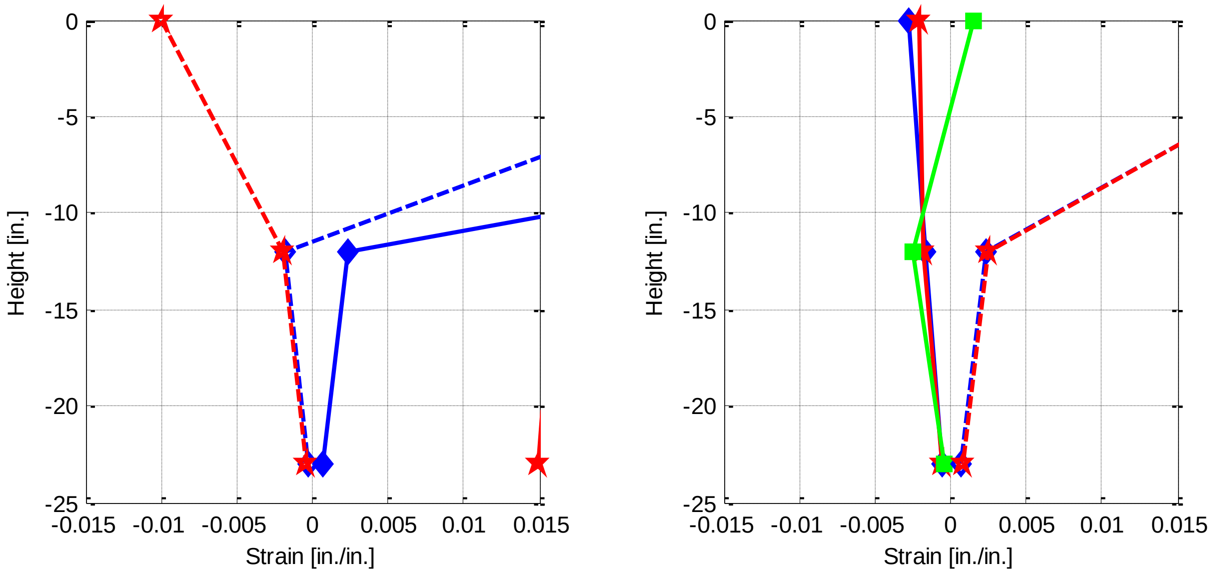

a). DS-3 - North reinforcing bar of column.

b). DS-3 - South reinforcing bar of column.

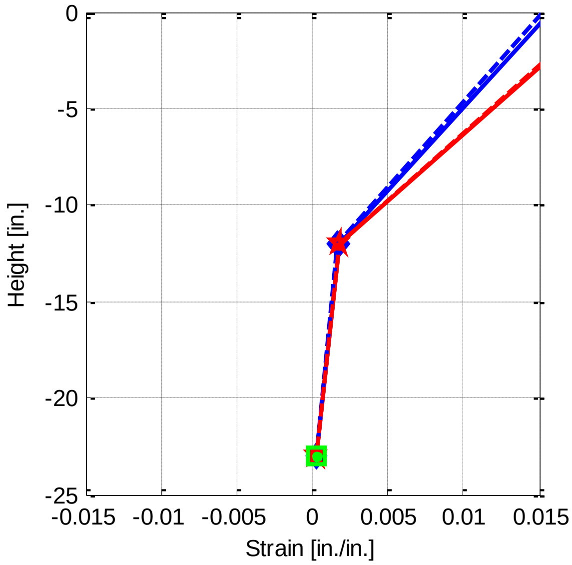

c). DS-3 - East reinforcing bar of column.

Figure 5-18. Strain profiles in reinforcing bars of column (after 3% drift) – DS-3

The plots show that after 3% drift, the strain distributions of specimens differed. Consider first the bar strains at the interface. In both the North and South bars in specimen DS-2 and in the South bar of specimens DS-1 and DS-3, the bar experienced only modest compression strains (no more than -0.003 in./in.). This suggests that the concrete in the region was reasonably intact and was still carrying most of the compression force. By contrast, the North bar experienced large compressive strains (to -0.009 in./in.) at 6.9% drift for DS-1 and (to -0.010 in./in.) at 4.6% drift for DS-3 because the concrete had suffered significant damage and most of the force was being carried by the bars as seen in Table 5-1. However, by 8.4% drift the column spiral had fractured and the bars had buckled, so the load they resisted and the strain they displayed were reduced.

At the bottom of the column, the bars in all cases never reached yield in tension. This suggests that the anchorage of the bars was being provided at least partly by bond. However, because the tension strain was close to yield, the anchor heads were clearly necessary. In Specimen DS-2, the South bars exhibited high compression strains at drifts of 6.9% and above. These are believed to be caused by the column rocking on its edges after the resistance of the shaft had largely been lost. This can be seen in figures of damages at the bottom of column of specimen DS-2 after testing in the Appendix C.

The strain distributions in the East bars were also different between specimens DS-1, DS-2 and DS-3. In specimens DS-1 and DS-3, the strains distribution were non-linear, suggesting that the moment decayed rapidly with depth. However, in specimen DS-2, after 4.6% drift, the strain distribution was linear. It is also noticeable that the strains decreased after 4.6% drift. This is explained by the drop in load then, caused by the damage to the transition region of the shaft.

5.2.4 Strains in Shaft Reinforcing Bars

The longitudinal reinforcing bars in the shaft were gauged as shown in Figure 5-19. The symmetry of the shaft and column was utilized, thus, only the East bars were gauged. In both specimens, gauges were attached on the reinforcing bars in pairs at three locations: 4 in., 16 in., and 28 in. below the shaft-column interface.

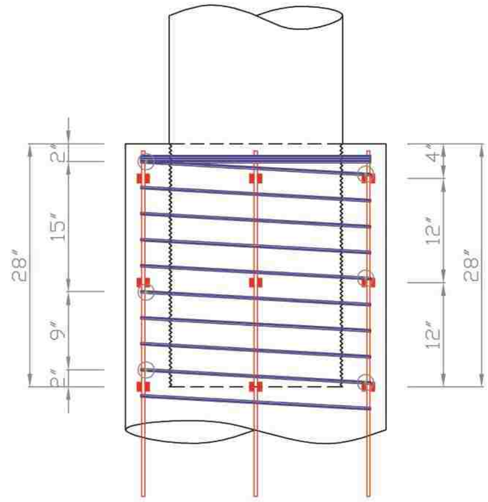

SHAFT

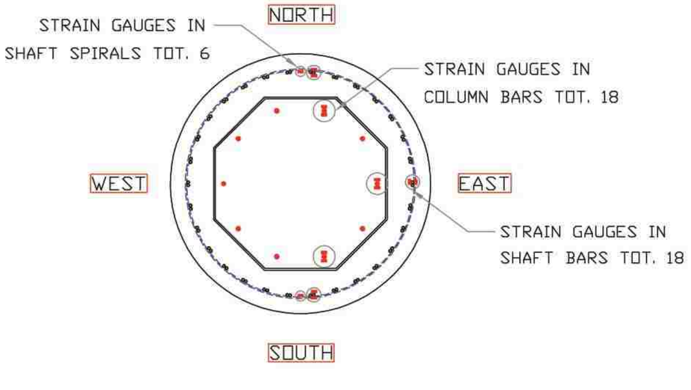

PLAN – DS1 & DS2

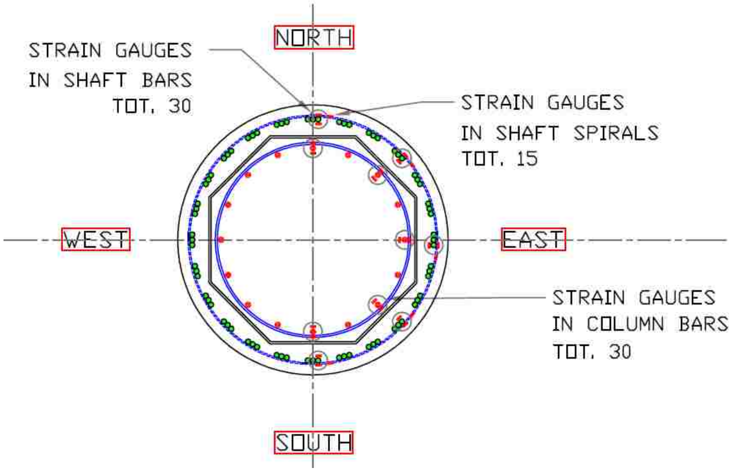

PLAN – DS3

Figure 5-19. Strain gauge positions in the shaft

The strain distributions (the average of each pair of gauge readings) over the height of the North, South and East of shaft bars at various drifts for specimen DS-1, DS-2 and DS-3 are shown in Figure 5-20, Figure 5-21, and Figure 5-22 respectively. The strains were plotted up to 3.0% drift. All specimens show similar strain profiles. Until 0.7% drift, tension strains at the top position (4in. below the interface) were small in all specimens. The compression strains were higher, about 200με. However, after 0.7% drift, the top of the shaft cracked vertically and diagonally, so the tension strain in the bars increased as explained above. The tensile strain distribution of the North and South shaft reinforcing bars were nearly linear in all specimens. It suggested that the bond stresses of the shaft tensile bars were nearly constant.

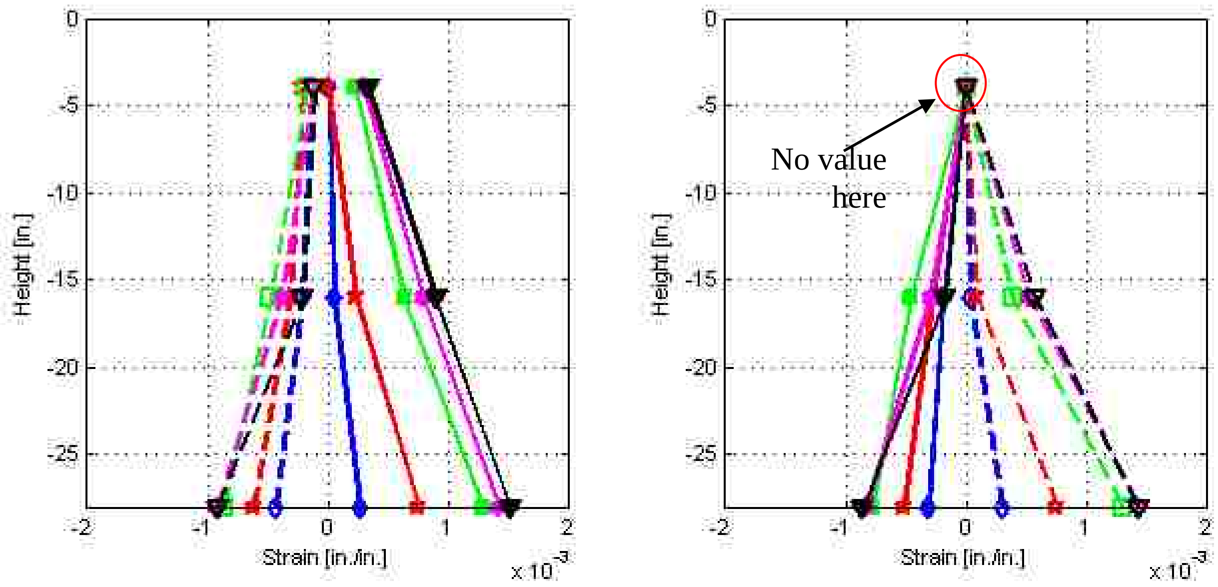

a). DS-1 - North reinforcing bar of shaft.

b). DS-1 - South reinforcing bar of shaft.

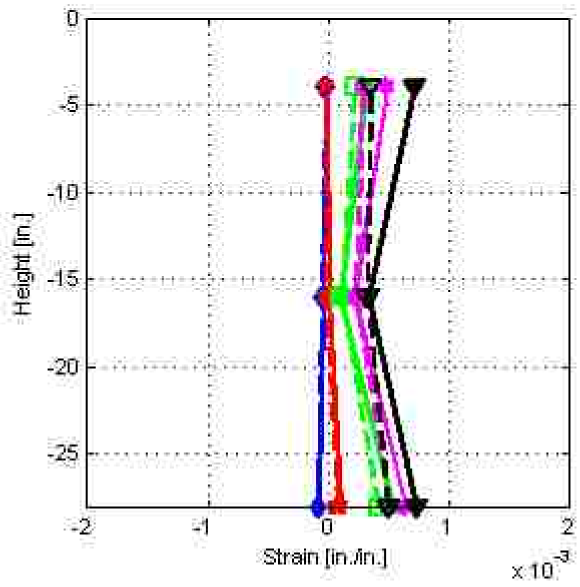

c). DS-1 - East reinforcing bar of shaft.

Figure 5-20. Strain profiles in the shaft reinforcing bars – DS-1

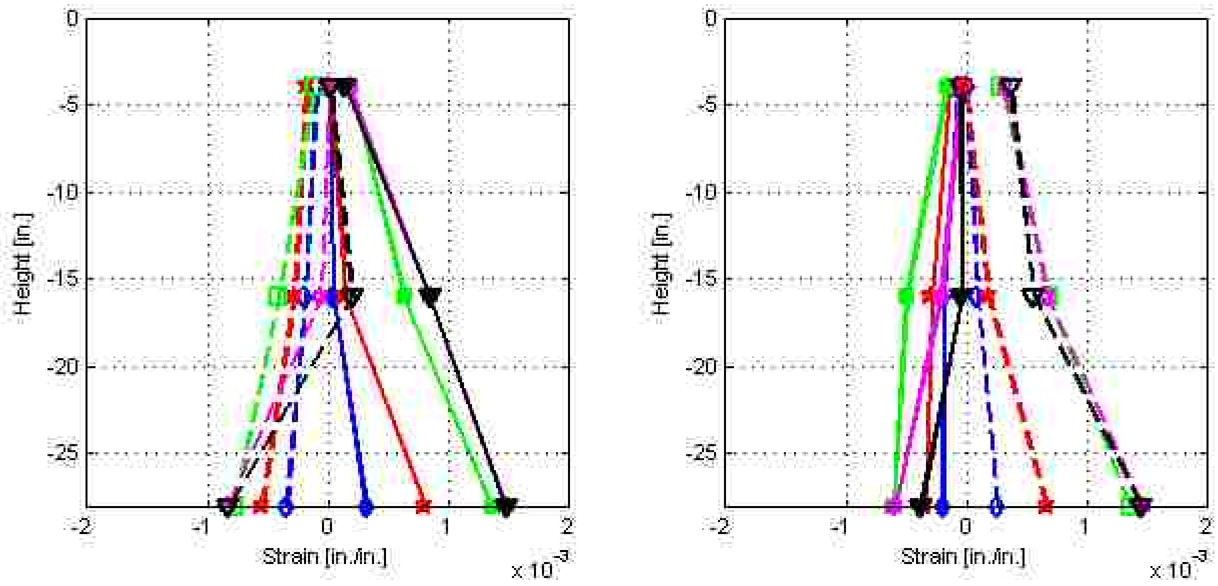

a). DS-2 - North reinforcing bar of shaft.

b). DS-2 - South reinforcing bar of shaft.

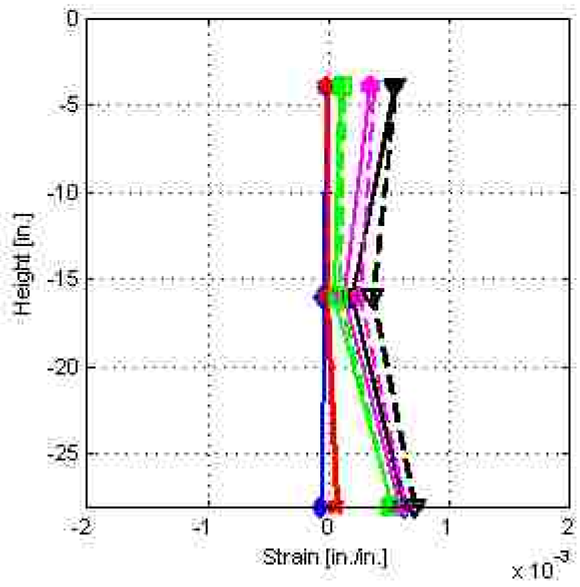

c). DS-2 - East reinforcing bar of shaft.

Figure 5-21. Strain profiles in the shaft reinforcing bars – DS-2

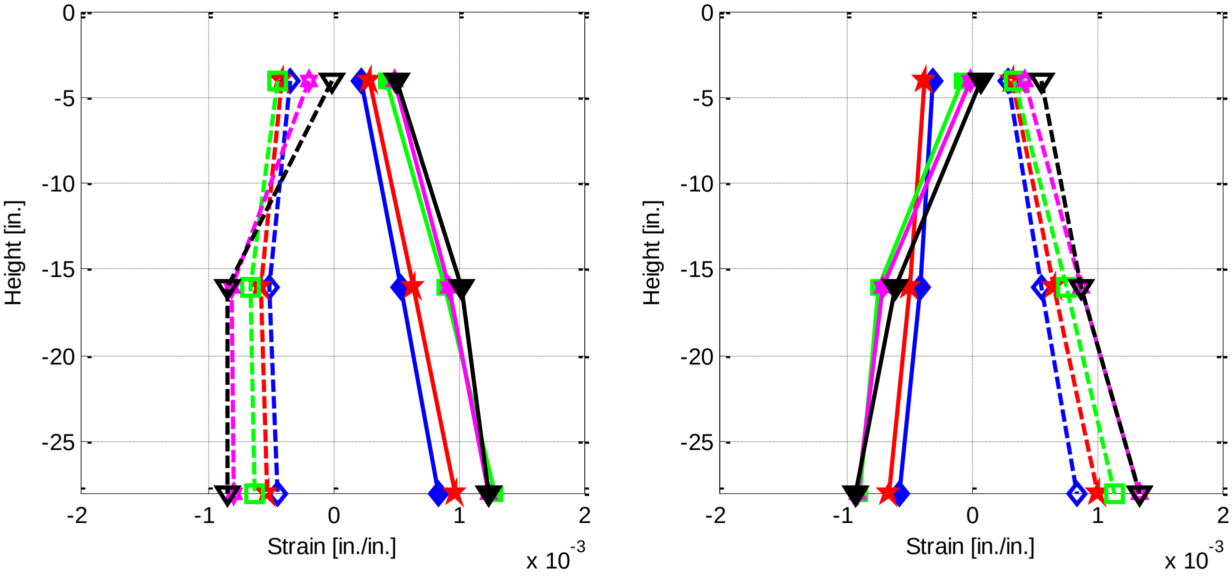

a). DS-3 - North reinforcing bar of shaft.

b). DS-3 - South reinforcing bar of shaft.

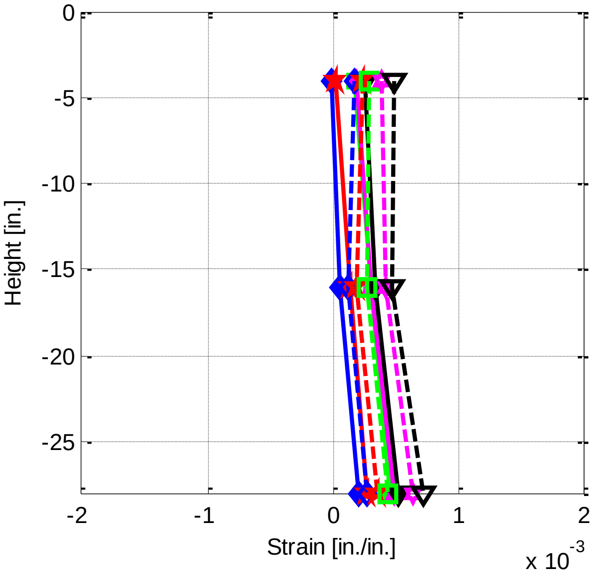

c). DS-3 - East reinforcing bar of shaft.

Figure 5-22. Strain profiles in the shaft reinforcing bars – DS-3

5.2.5 Strains in Shaft Spirals

The shaft spirals were gauged as described in Figure 5-19. In all specimens, gauges were attached on the spirals at three levels close to those of the gauges on the vertical bars, 4 in., 16 in. and 28 in. below the interface of the shaft and column. Because of the symmetry of the column longitudinal bars, at each level, only the East and South sides were gauged in specimens DS-1 and DS-2, and the North, Northeast, East, Southeast and South sides were gauged in Specimen DS-3. At each place, only 1 strain gauge was used.

The strains in the shaft spiral at the East and South sides are shown in Figure 5-23. Because all three gauges on the South side of Specimen DS-1 were broken before testing, only the spiral strains on the East side in DS-1 were plotted.

The overall trends were:

- In all specimens, the strains in the spiral were tensile regardless of the direction of loading.
- In all specimens, the strains were much larger at the top of the shaft than in the middle or bottom.
- The spiral in specimens DS-1 and DS-3 just reached the yield point. However, in Specimen DS-2, the spiral first yielded at the top at 3% drift and fractured at 6.9% drift.
- The strain was larger at the South gauge than at the East gauge, at any drift ratio, in specimens DS-2 and DS-3. That comparison was not possible in Specimen DS-1 because no data were available from the South gauges.

The fact that the strains in Specimen DS-2 were higher than those in specimens DS-1 and DS-3 is consistent with the lower spiral steel ratio in Specimen DS-2 and the observed damage.

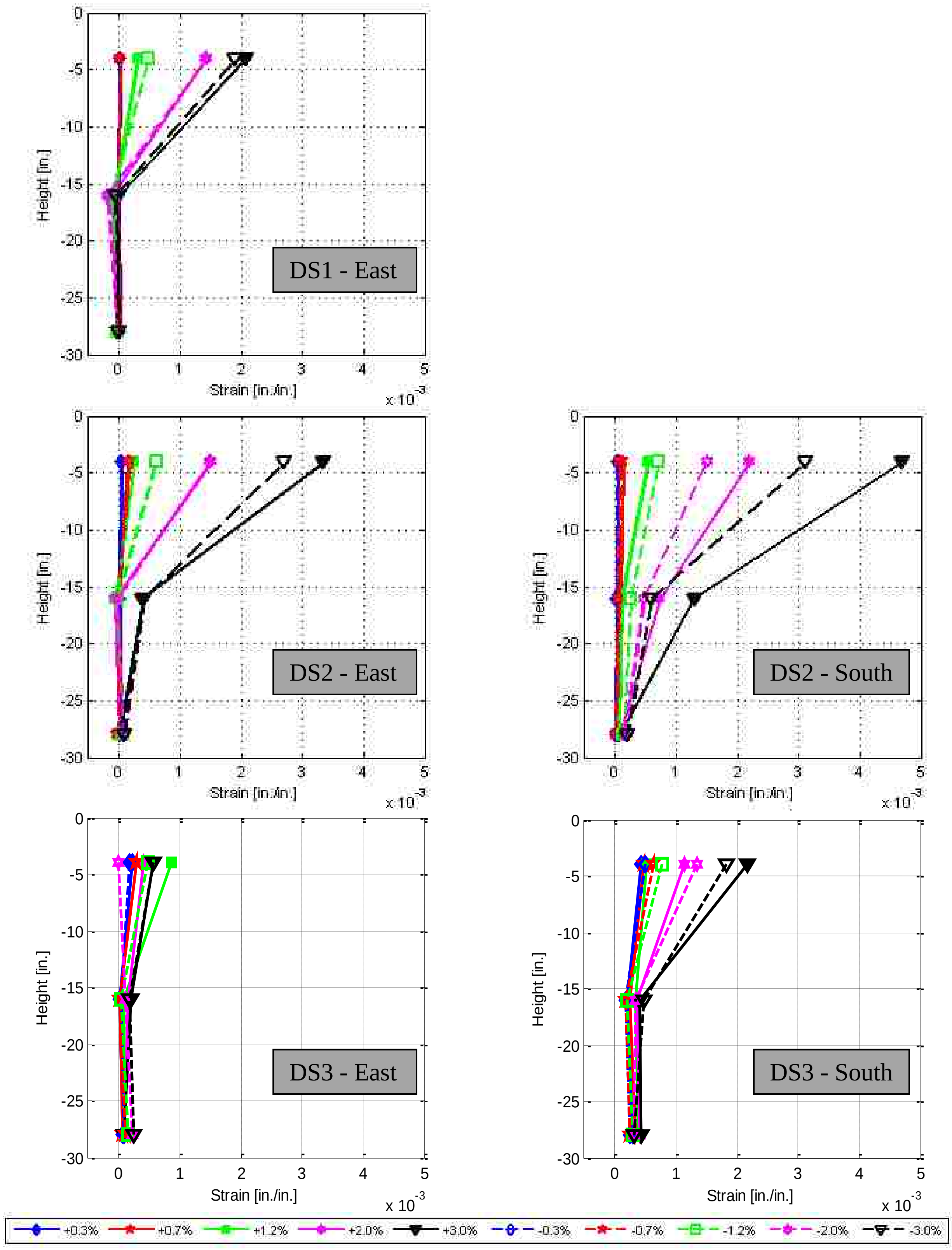

Figure 5-23. Strain in shaft spirals

As illustrated in figures, up to 3.0% drift, in specimen DS-1 and DS-3, tension strain increased at the top position after each cycle and reach 0.002 at 3.0% drift. Whereas, at the middle position, strain were small and increased a little until 3.0% drift. At the bottom position, strain were nearly zero. However, spiral strain in Specimen DS-2 were different. All strain value were in tension at 3.0% drift. At the top position, the strain were in tension and increased after each cycle like in specimens DS-1 and DS-3. But the value were higher. The max strain on East side was about 3.4e-3 and on South side was 4.7e-3. At middle position, until 2.0% drift, strain was nearly zero on East side and increased to 0.4e-3 at 3.0% drift. On the South side, strains increased in tension after each cycle and reached 1.25e-3 at 3.0% drift. At the bottom position, max strains were about 0.2e-3.

The strain distribution in the shaft spiral is one of the most important results of the tests. First, it rejects the assumption of uniform strain distribution as proposed by non-contact lap splice methods. The better understand of the lateral strain distribution also helps designer placing spiral in a more suitable and more economical way (i.e. more spiral at the top part of the connection and less spiral at the bottom part). Finally, it provides data help to understand clearly the force transfer mechanism in the connection, a way to evaluate the capacity of the connection, and a potential way to design it, which is discussed in the next two chapters.

CHAPTER 6.

DEVELOPMENT OF STRUT-AND-TIE MODEL

6.1 INTRODUCTION

In this chapter a strut-and-tie model is developed to proportion the transverse reinforcement for the transition region between the column and the drilled shaft.

First, the forces acting at the connection boundaries for the seismic loading are estimated (Section 6.2). This estimate is done using sectional analysis of the elements that adjoin the transition region, namely the column and the shaft. These sectional analyses allow the designer to identify the longitudinal force resultants and their locations within the cross-sections.

Next, a strut-and-tie model of the transition region is developed to resist the forces from the sectional analyses acting at the boundaries (Section 6.3). The elements of the strut-and-tie model transfer the forces internally between their points of application on the boundary. The computed forces in the model elements are evaluated by comparing them with values derived from the experiments (Section 6.4), and the lateral capacity of the system is evaluated in terms of the capacities of the struts and ties.

6.2 DETERMINATION OF FORCES ACTING ON THE BOUNDARY OF THE TRANSITION REGION

To determine the appropriate flexural tension and compression resultant forces, and their locations at the boundaries of the transition regions, moment-curvature analyses were performed for both the column and shaft cross-sections. At high drift ratios, a plastic hinge may form at the bottom of the column, if some other element has not failed before. Within the plastic hinge, the validity of moment curvature analysis, which assumes that plain sections remain plane, may be questioned. However, it was found here that the moments and the steel strains predicted by the cross-sectional analysis were close to those measured in the laboratory tests, so they were judged to be sufficiently accurate to predict the forces at the boundaries of the strut-and-tie model.

6.2.1 Methodology for Flexural Analyses

Moment-curvature analyses were conducted using an in–house University of Washington program (Stanton 2010). Two sets of analyses were conducted, corresponding to two sets of assumptions about the material properties.

The concrete model used in the analyses was based on the one proposed by Kent and Park (1971) and is illustrated in Figure 6-1b. In this figure, the tension stresses and tension strains are positive. The stress-strain relationship in compression consists of a parabolic rising curve, followed by a linear falling segment, then a constant stress extending to infinite strain. In the program, the initial parabolic curve was replaced by a cubic, which allows the user to specify E_{c0}, ε_{c0} and f'_c independently. It defaults to the original parabolic curve if E_{c0} is chosen to be $f'_c/(2\varepsilon_{co})$. The values of the confined concrete strength, $f_{cc} = 8\,ksi$, and the ultimate compression strain, $\varepsilon_{cu} = 0.009$, were generated from the properties of the confinement reinforcement using Mander's formula (Mander et al. 1988; Priestley et al. 1996), rather than using the values recommended by Kent and Park. A linear stress-strain relation is assumed in tension up to the tensile strength, $f_r = 0.24\sqrt{f'_c(ksi)}\ \ or\ \ 7.5\sqrt{f'_c(psi)}$.

The steel model in the program contained three regions: elastic, a yield plateau, and a curved strain-hardening region. In the first set of analyses the expected steel reinforcement properties were used in accordance with the *AASHTO Guide Specifications for LRFD Seismic Bridge Design (2009)*. These recommendations ($f_y = 68\,ksi; \varepsilon_{sh} = 0.015; f_u = 95\,ksi$) are based on data collected by Caltrans. The steel properties in the second set of analyses were based on the measured reinforcement properties for these tests. For specimens DS-1 and DS-2, they were as follows: $f_y = 68\,ksi; \varepsilon_{sh} = 0.0027; f_u = 106\,ksi$. For Specimen DS-3, they were: $f_y = 62\,ksi; \varepsilon_{sh} = 0.015; f_u = 86\,ksi$).

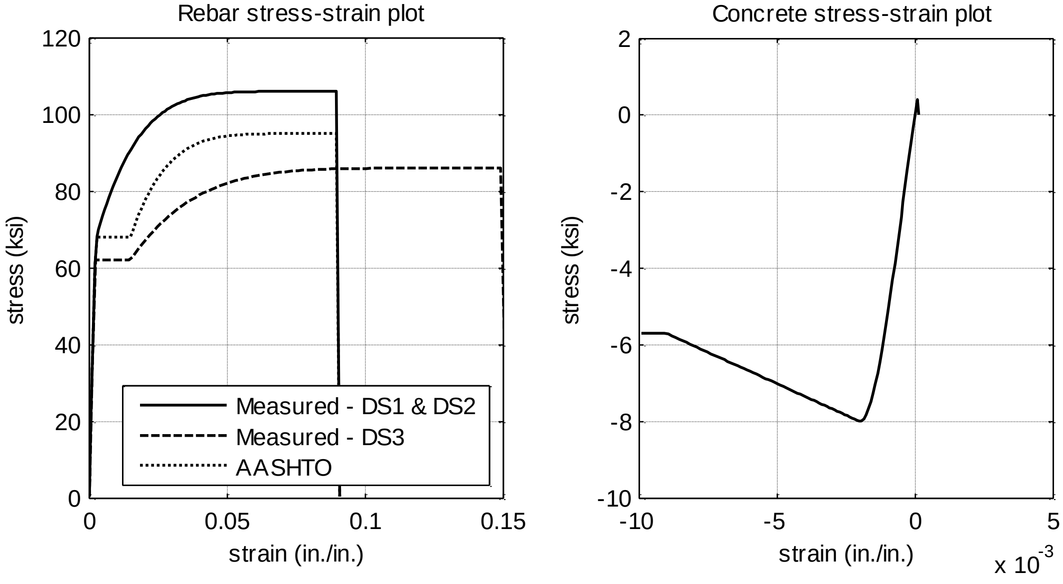

(a) (b)

Figure 6-1. Assumed material stress-strain relationships

6.2.2 Moment-Curvature Results for Columns

The calculated moment-curvature relationships for the columns are shown in Figure 6-2. The flexural strengths predicted by the analyses and measured values are listed in Table 6-1.

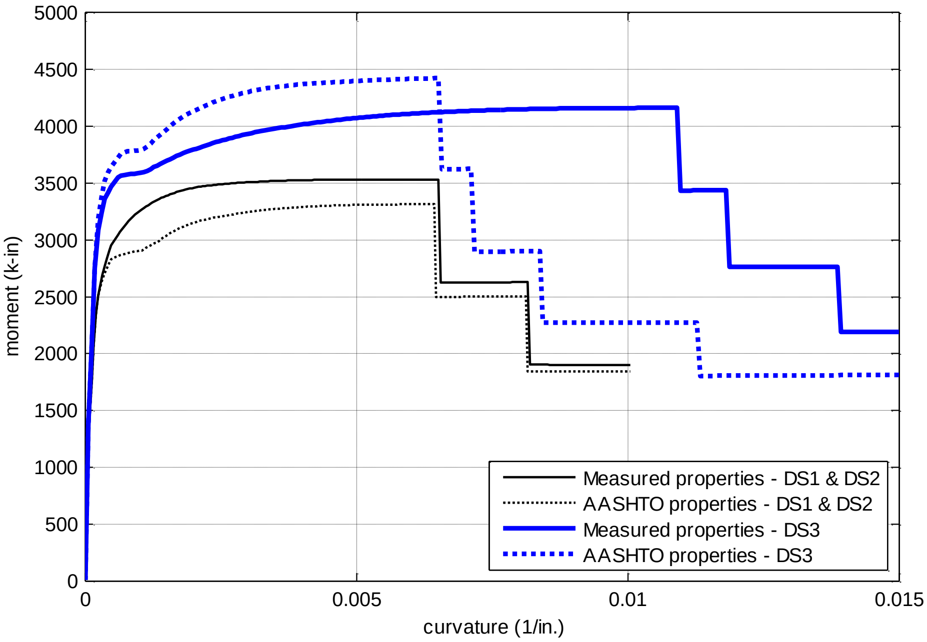

Figure 6-2. Moment-curvature analyses of columns

Table 6-1. Comparision of peak column moment

Specimen	**Moment calculated using expected properties [kip-in.]**	**Moment calculated using measured properties [kip-in.]**	**Measured moment [kip-in.]**	**Ratio of measured to predicted moment using measured properties**
DS1	3315	3530	3476	0.98
DS2	3315	3530	3393	0.96
DS3	4423	4165	3622	0.87

For specimens DS-1 and DS-2 the moments predicted by both analyses give values within 2-4% of the measured peak moment. These results suggest that the differences in the longitudinal reinforcement properties did not have much effect on the flexural strength of the column. Both analyses resulted in the ultimate flexural strength occurring at a curvature of 0.0065 rad/in.

However, at lower drift ratios, when the curvature lay between about 0.0005 and 0.002 rad/in., the moments predicted by the two analyses differ significantly. This difference occurs because, at those curvatures, the reinforcement in the analysis of expected properties reaches the yield plateau region, whereas, the reinforcement in the analysis using the measured properties enters the strain-hardening region. Thus, the tension force in the reinforcement in the measured properties analysis is larger than in the expected properties analysis, and so is the moment.

Later, when the reinforcement strain reaches the fracture point, the stresses and the moment strengths predicted by the two analyses are similar. In the test of Specimen DS-2, the column did not fail, so the measured peak column moment recorded in the table is the maximum measured value but is not the flexural strength.

Specimen DS-3 contained much more reinforcement than specimens DS-1 and DS-2, and its predicted strengths from the two analyses were correspondingly higher, as shown in Table 6-1 and Figure 6-2. The higher column strength was intended to increase the demands on failure in the transition region. Nonetheless, the failure occurred in the column, and at a measured moment that was lower than that predicted by either analysis.

The comparison between the moment-curvature curves calculated using measured material properties and the measured moment-curvature curves for specimens DS-1, DS-2 and DS-3 are shown in Figure 6-3, Figure 6-4 and Figure 6-5 respectively. The measured moment was calculated by using the measured axial load, horizontal load and displacement at the top of column and at the column-shaft interface. The column curvature was calculated by using the extreme column reinforcement strains, which measured with strain gauges, at the column-shaft interface divided by the distance between the bars. Since, the strain gauge range was limited, larger values of curvature could not be measured using this method.

The comparisons showed that the predicted values were in good agreement with the measured value for the range of curvatures for which strains could be measured reliably. The reason for this discrepancy in the maximum moment (Table 6-1) is not certain, but it appears to be related to the modeling of column at large curvatures, because the calculated and measured moment-curvature responses are similar for curvatures up to and including the yield plateau.

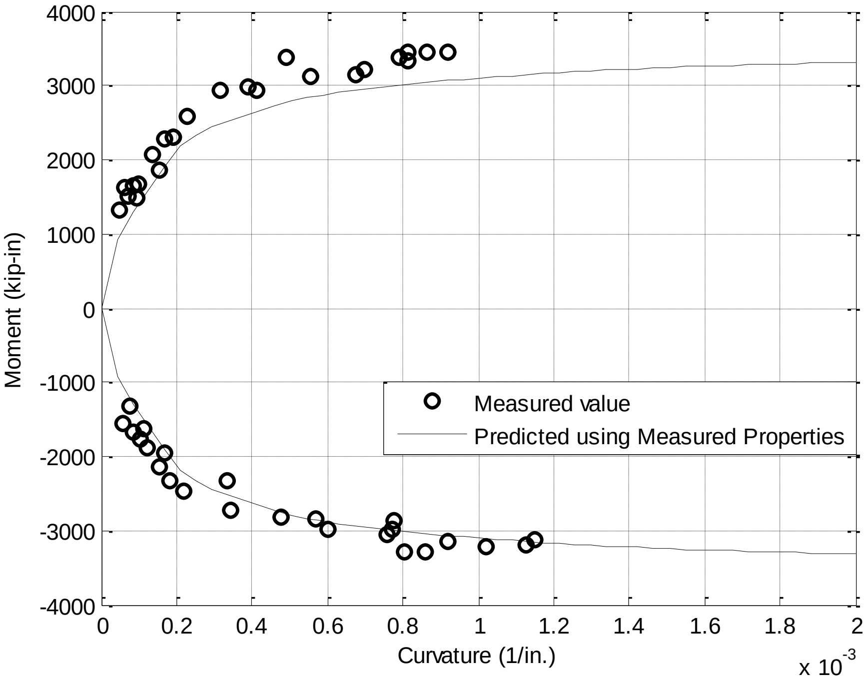

Figure 6-3. Column moment vs. curvature – DS-1

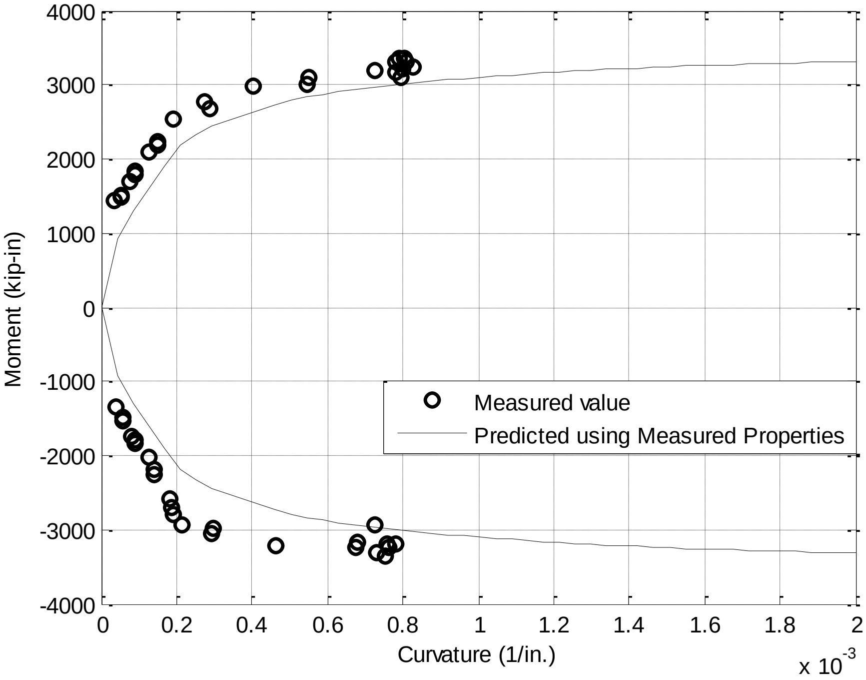

Figure 6-4. Column moment vs. curvature – DS-2

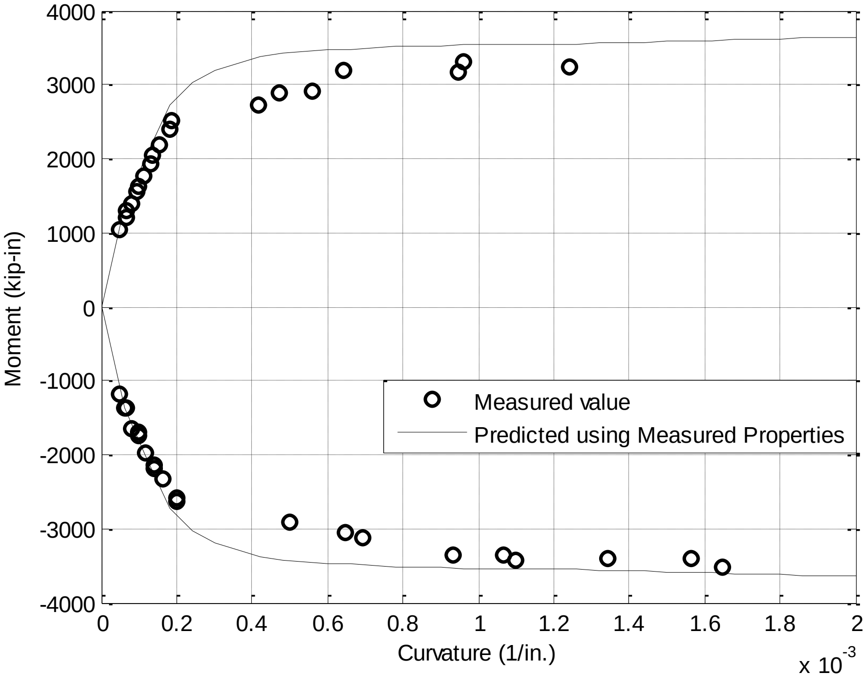

Figure 6-5. Column moment vs. curvature – DS-3

Figure 6-6, Figure 6-7, and Figure 6-8 show plots of moment vs. strain in the extreme tensile reinforcement for specimens DS-1 DS-2, and DS-3 respectively. They give the measured values and the values predicted by the moment-curvature analyses. The curves were plotted up to the peak strain measured in the tests, of about 0.011. At larger strains, the gages continue to read but, the data acquisition system saturated. All curves included two regions: an elastic region and a curved post-yield region.

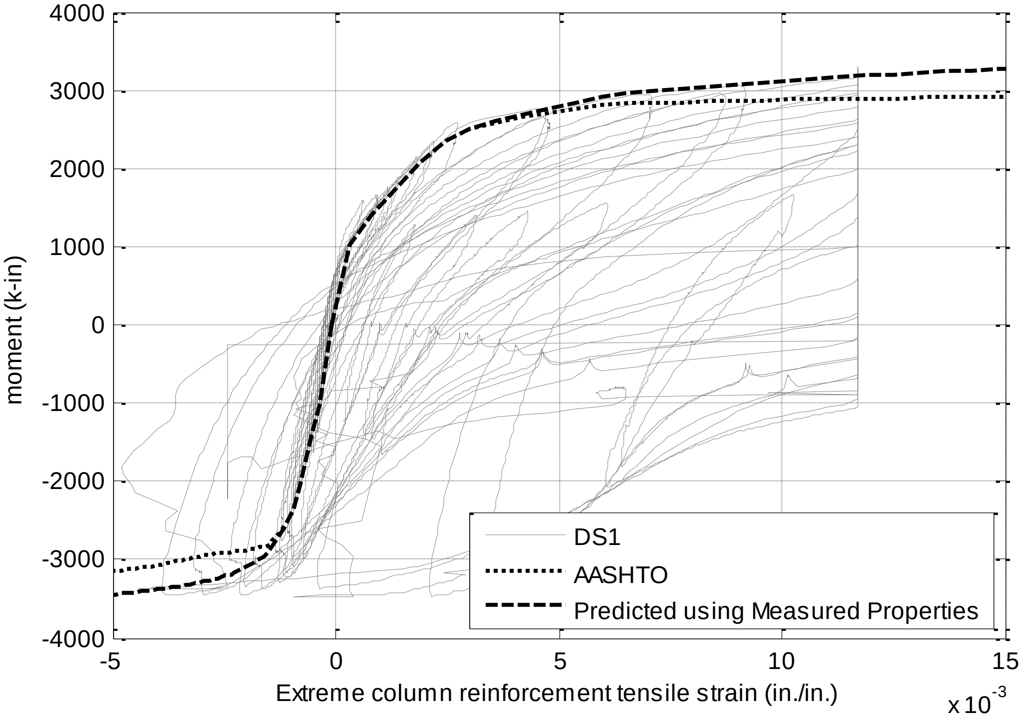

Figure 6-6. Moment-extreme reinforcement tensile strain relationship for DS-1 column

The measured moments for a given strain in both specimens DS-1 and DS-2 are remarkably similar to the ones predicted by the analysis that used measured reinforcement properties. The moments in the post-yield region in the analysis that used expected reinforcement properties are smaller than the measured ones. At a strain of 0.0115, the measured moment is approximately 10% higher than the one predicted using the AASHTO recommended properties. The cause of the discrepancy, as mentioned above, is because of the yield plateau region of the expected steel model. In the confined concrete model, the strain at peak stress, ϵ_{cc} is taken as 0.002 instead of 0.0034 as in Mander's formula. If Mander's formula were used here, the predicted moments in the yield region in the two analyses would be approximately 10% and 20% smaller than the measured one.

Figure 6-8 shows the moment plotted against strain for Specimen DS-3. As discussed above, the measured moments are significantly smaller than the predicted ones for large strains.

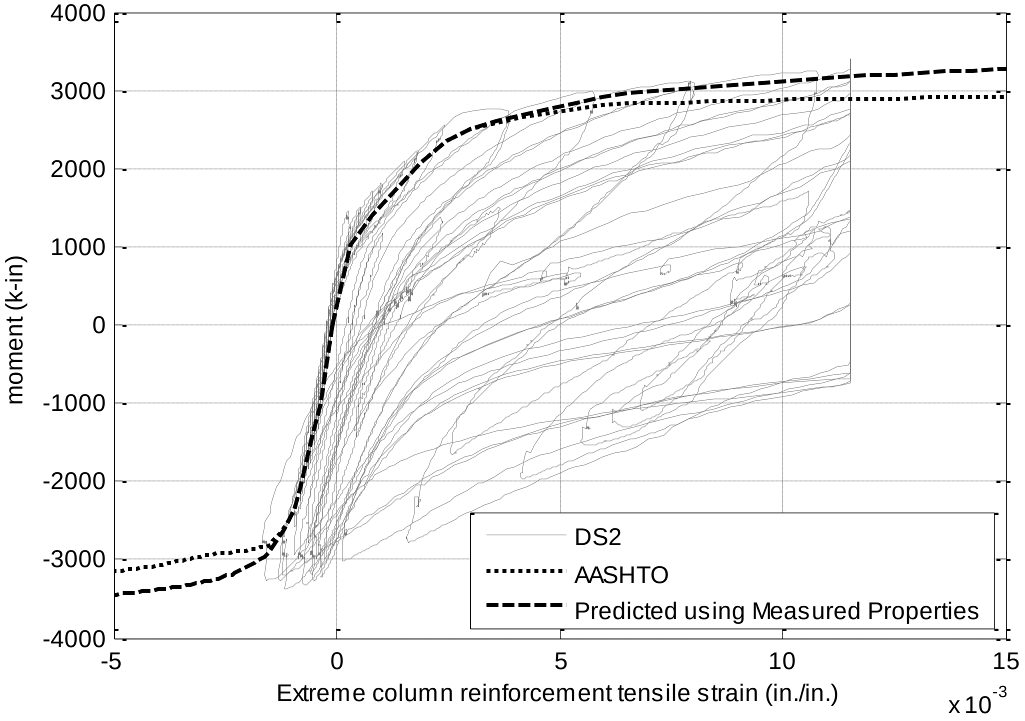

Figure 6-7. Moment-extreme reinforcement tensile strain relationship for DS-2 column

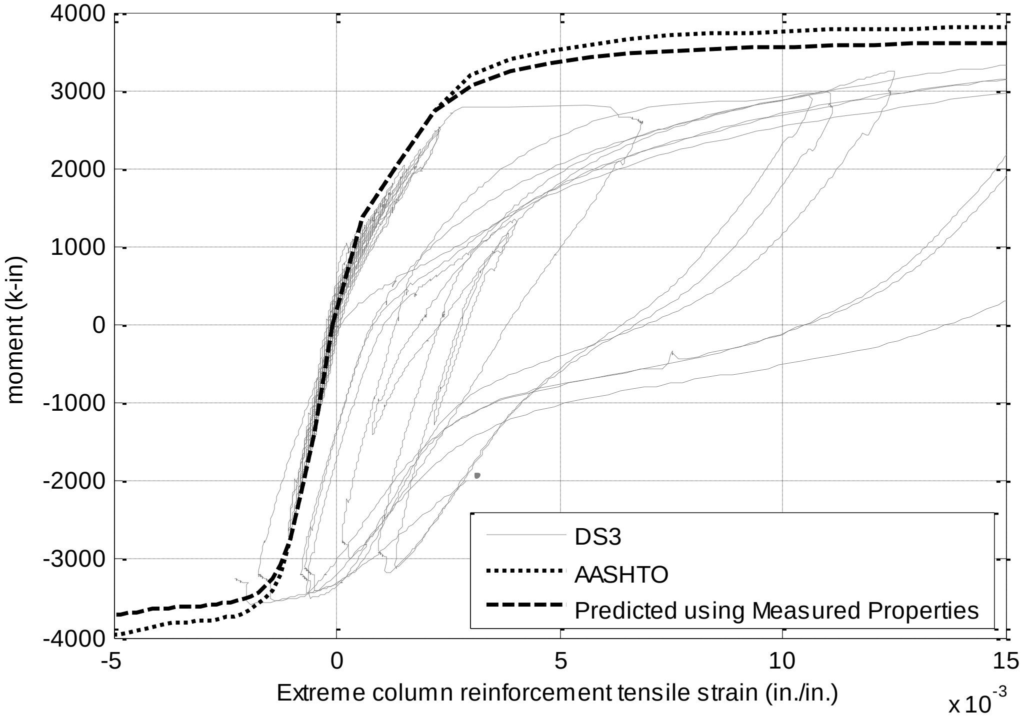

Figure 6-8. Moment-extreme reinforcement tensile strain relationship for DS-3 column

6.2.3 Moment-Curvature Results for Shafts

The shaft longitudinal reinforcement strains were smaller than 0.002 throughout the testing, so the shaft remained elastic. Figure 6-9, Figure 6-10 and Figure 6-11 shows the relationship between moment at the base of the shaft and the tensile strain in the extreme longitudinal reinforcement in the shaft at the bottom of connection of specimens DS-1, DS-2 and DS-3 respectively. The figures include measured data and moments predicted using measured material properties and strains at the bottom of the shaft. The analysis is comparable to the second analysis for the column, using the measured material properties, and the geometry of the shaft rather than the column. Note that the jump in the predicted curve at about 2400 in-kips for DS-1 and DS-2, and at about 1900 in-kips for DS-3 indicates first cracking.

The predicted moment-extreme reinforcement tensile strain relationships for shaft are in good agreement with the measured value of specimens DS-1, DS-2 and DS-3. They confirm that the stress state at the boundary of the connection can be predicted reliably with flexural analysis.

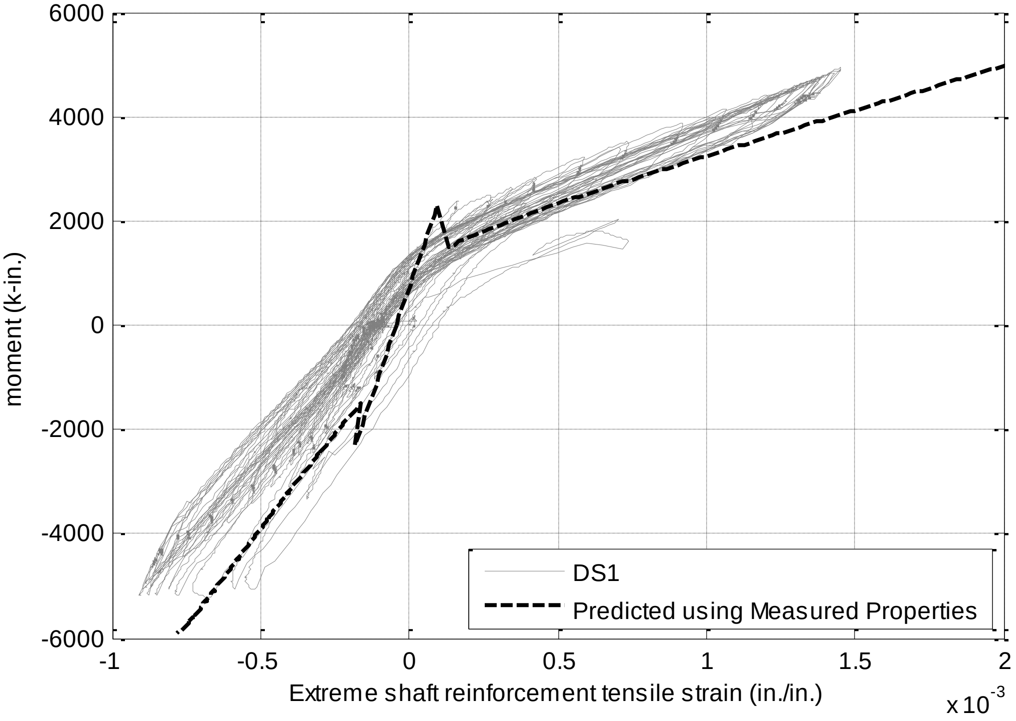

Figure 6-9. Moment-extreme reinforcement tensile strain relationship for DS-1 shaft

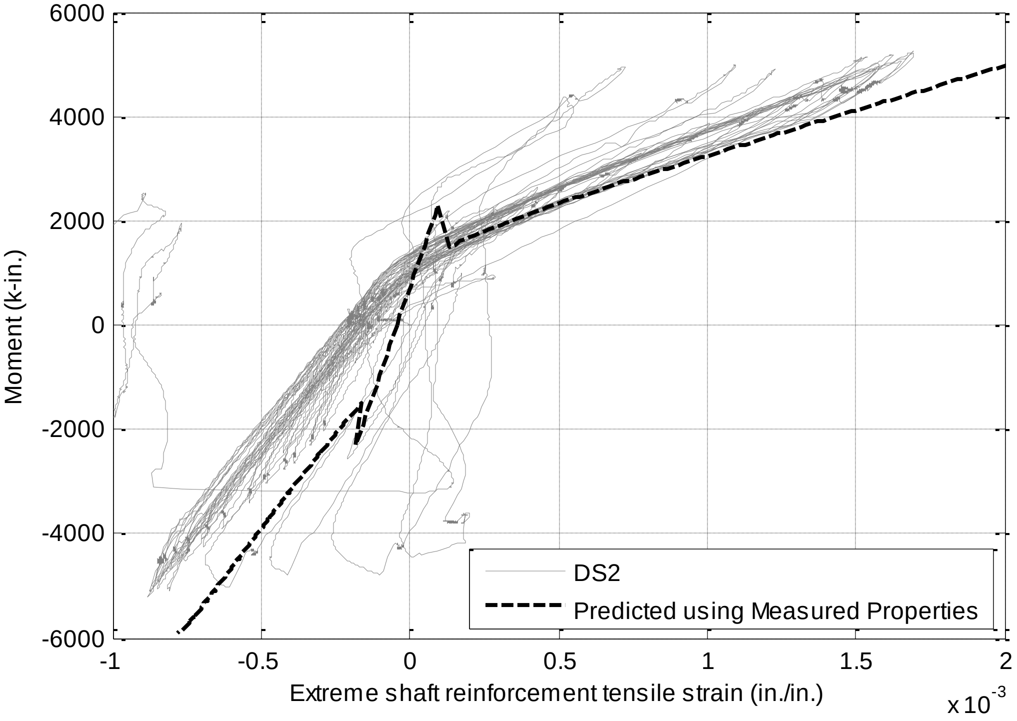

Figure 6-10. Moment-extreme reinforcement tensile strain relationship for DS-2 shaft

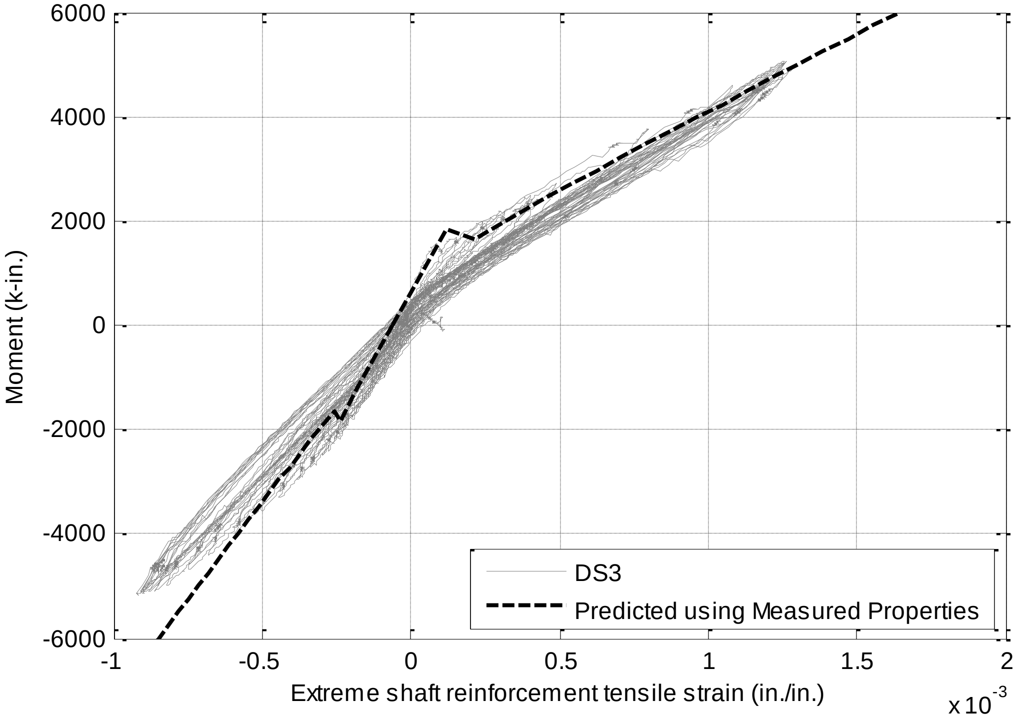

Figure 6-11. Moment-extreme reinforcement tensile strain relationship for DS-3 shaft

6.2.4 Magnitudes of Flexural Tension Resultant Forces

To create a strut-and-tie model, it is necessary to estimate the force resultants and their locations at the model boundaries. The calculated and measured column flexural tension resultant forces for the column-shaft interface are compared in Figure 6-12, Figure 6-13, and Figure 6-14 for specimens DS-1, DS-2 and DS-3 respectively. Similarly, Figure 6-15, Figure 6-16, and Figure 6-17 show the calculated and measured column flexural tension resultant forces for the bottom of the transition region. The measured values were calculated based on the readings from the strain gages attached to the relevant reinforcement, and from the measured properties of the reinforcement. The measured and predicted values are similar for all three tests.

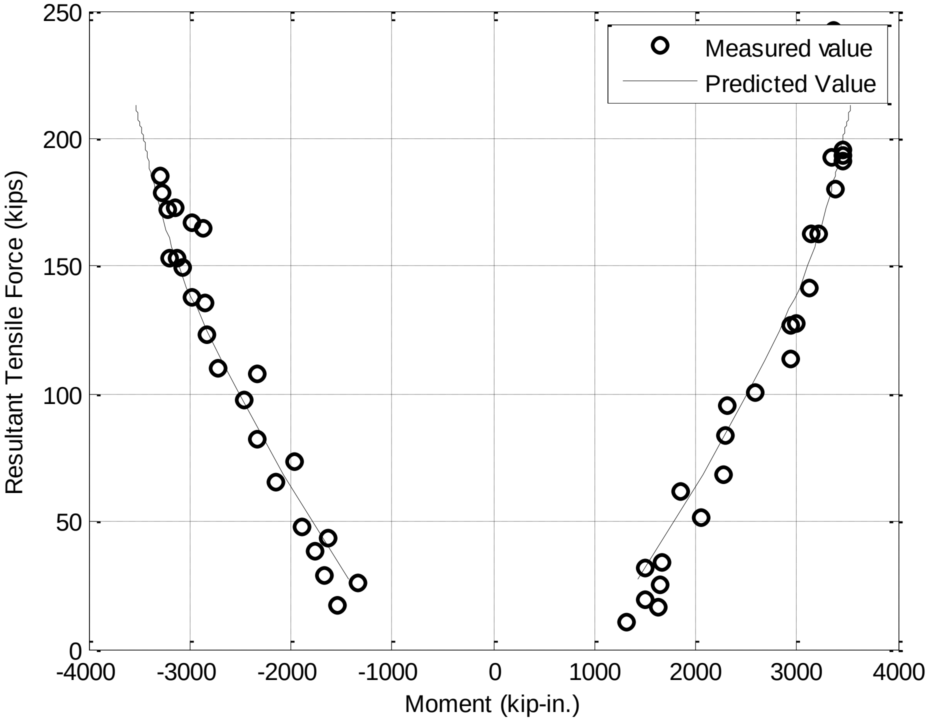

Figure 6-12. Flexural tensile resultant force at the column-shaft interface – DS-1

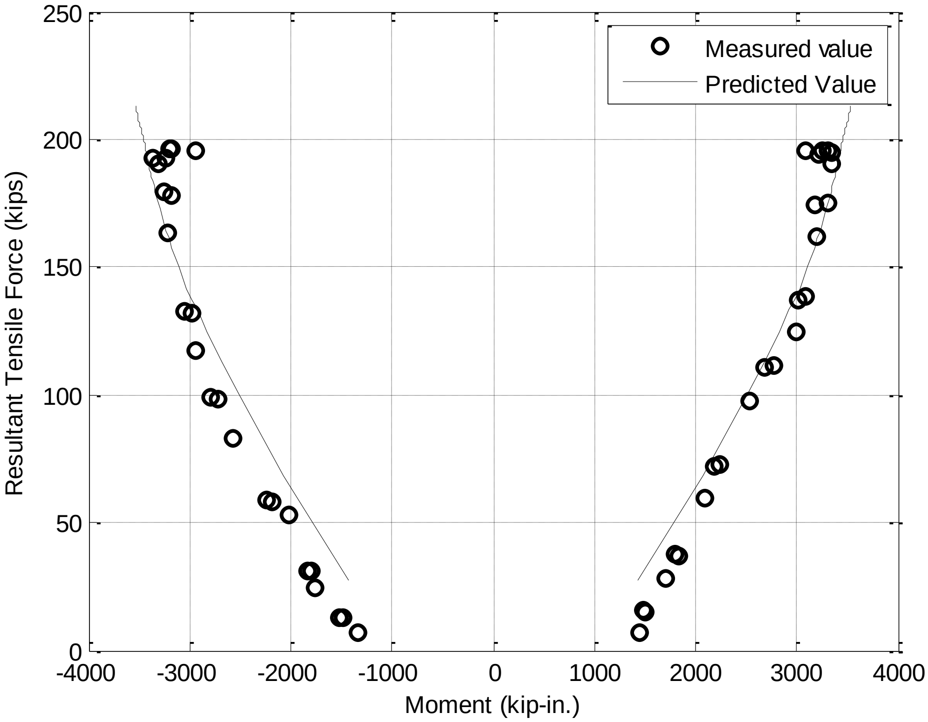

Figure 6-13. Flexural tensile resultant force at the column-shaft interface – DS-2

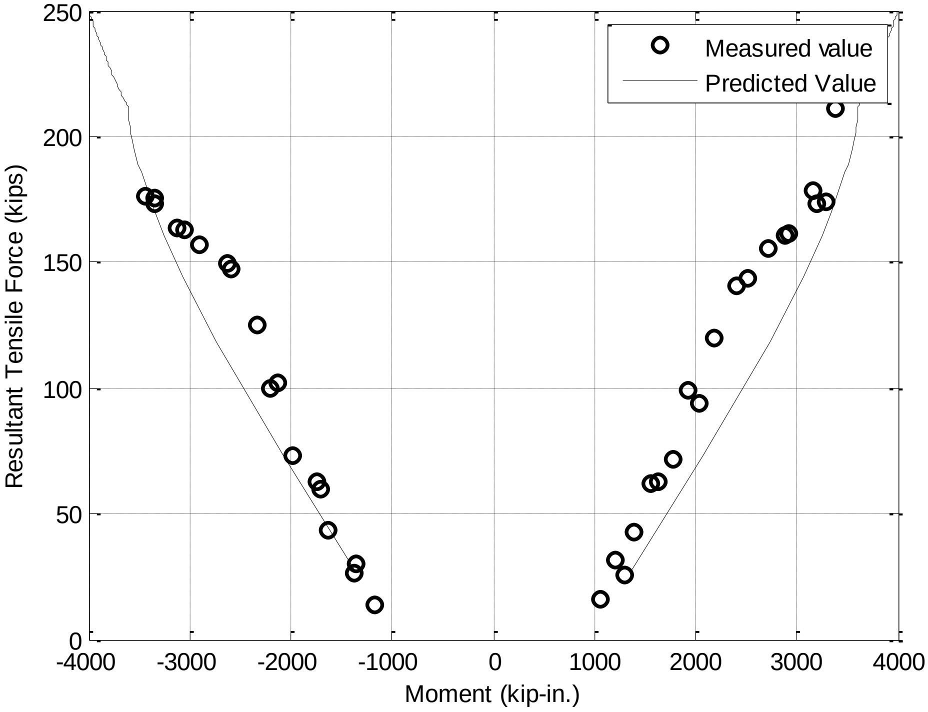

Figure 6-14. Flexural tensile resultant force at the column-shaft interface – DS-3

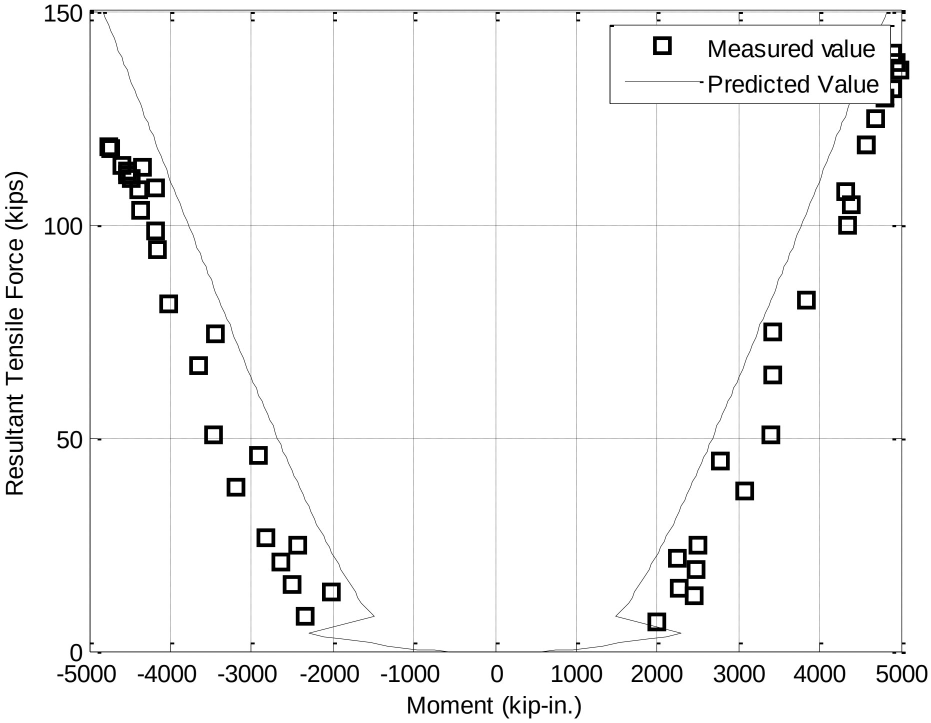

Figure 6-15. Flexural tensile resultant force of shaft at the bottom of connection – DS-1

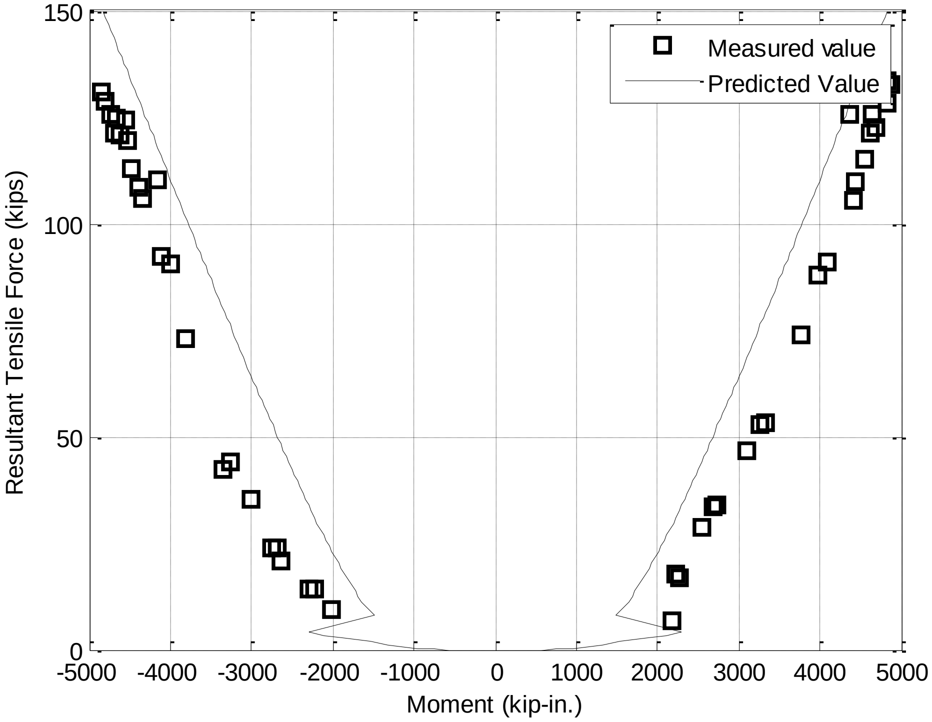

Figure 6-16. Flexural tensile resultant force of shaft at the bottom of connection – DS-2

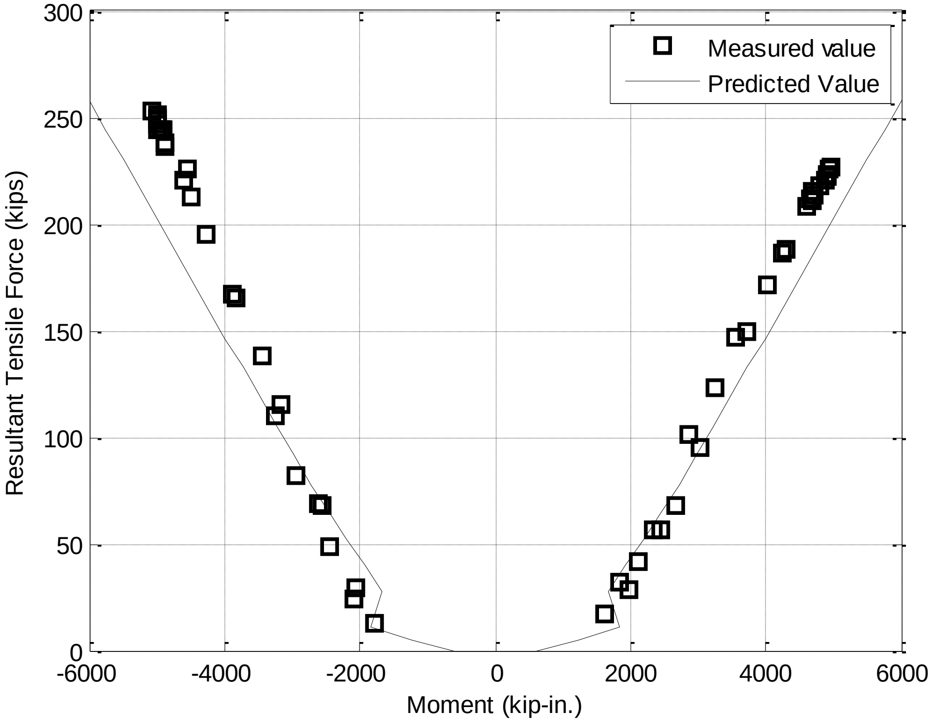

Figure 6-17. Flexural tensile resultant force of shaft at the bottom of connection – DS-3

6.2.5 Locations of Flexural Resultant Forces

Unlike a rectangular column, in which the location of the tensile reinforcement uniquely defines the location of the tension resultant, the location of the tensile force resultant in a circular column depends on the distribution of forces among the reinforcing bars. Then, the location of compressive force is determined using moment and force equilibrium requirement. The locations of the resultant forces are shown in Figure 6-18, Figure 6-19, and Figure 6-20 for the column at the column-shaft interface. Similarly, Figure 6-21, Figure 6-22, and Figure 6-23 shows locations for the shaft cross-section at its base. In both cases, the location is plotted against moment.

In general, for both the magnitudes and the locations of the resultant forces the results of the section analyses are in good agreement with the measured values. Therefore, section analyses can be used to determine the forces acting at the boundary of the transition region. The forces acting at the boundary of the connection are shown in Figure 6-24.

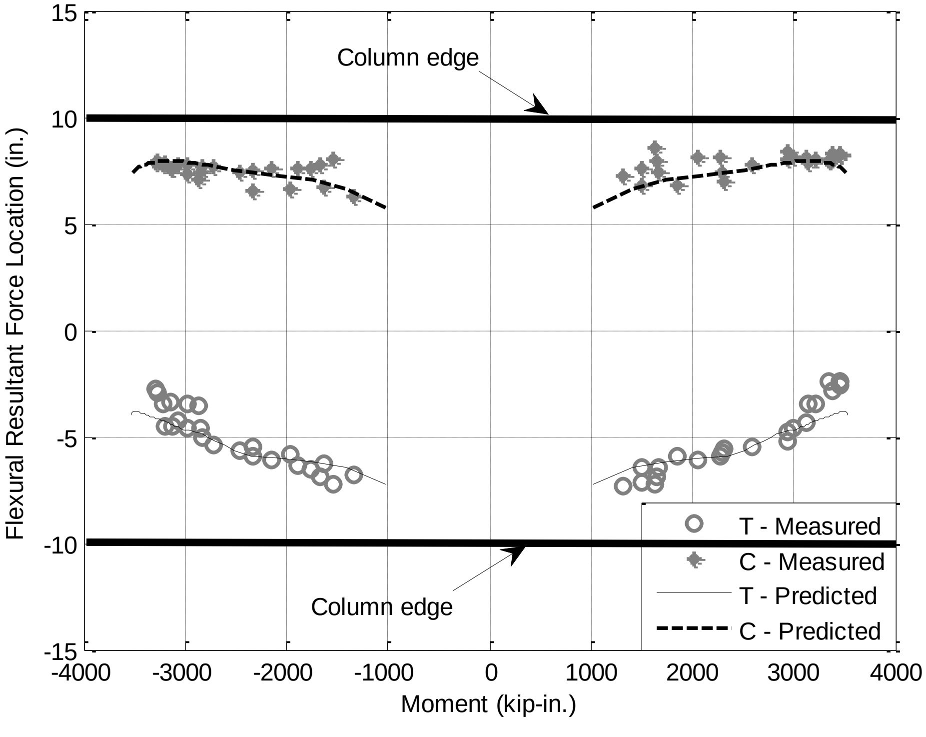

Figure 6-18. Flexural resultant force location at the column-shaft interface – DS-1

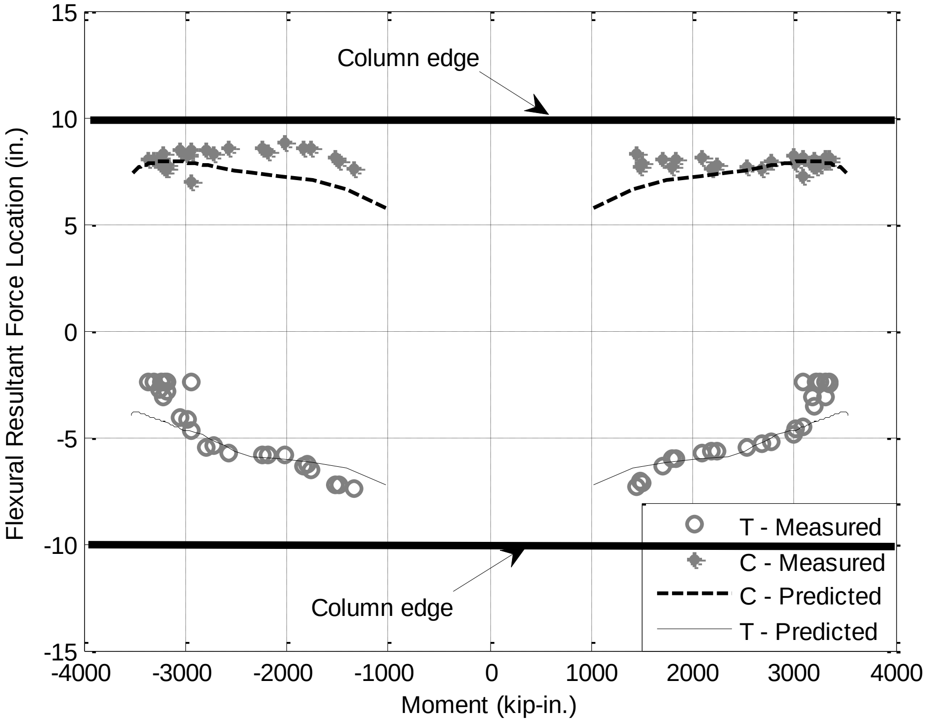

Figure 6-19. Flexural resultant force location at the column-shaft interface – DS-2

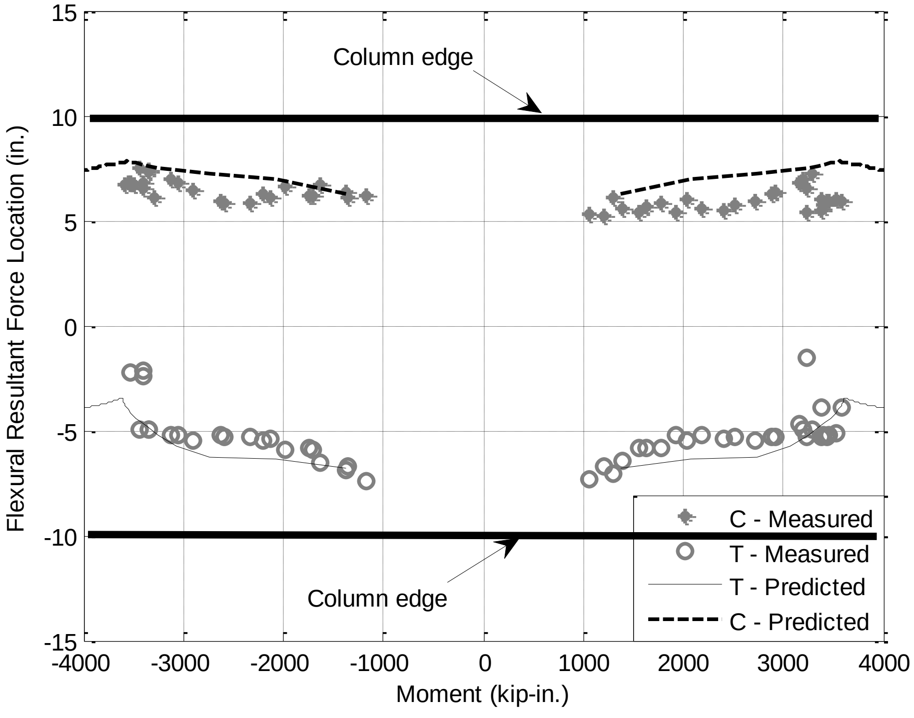

Figure 6-20. Flexural resultant force location at the column-shaft interface – DS-3

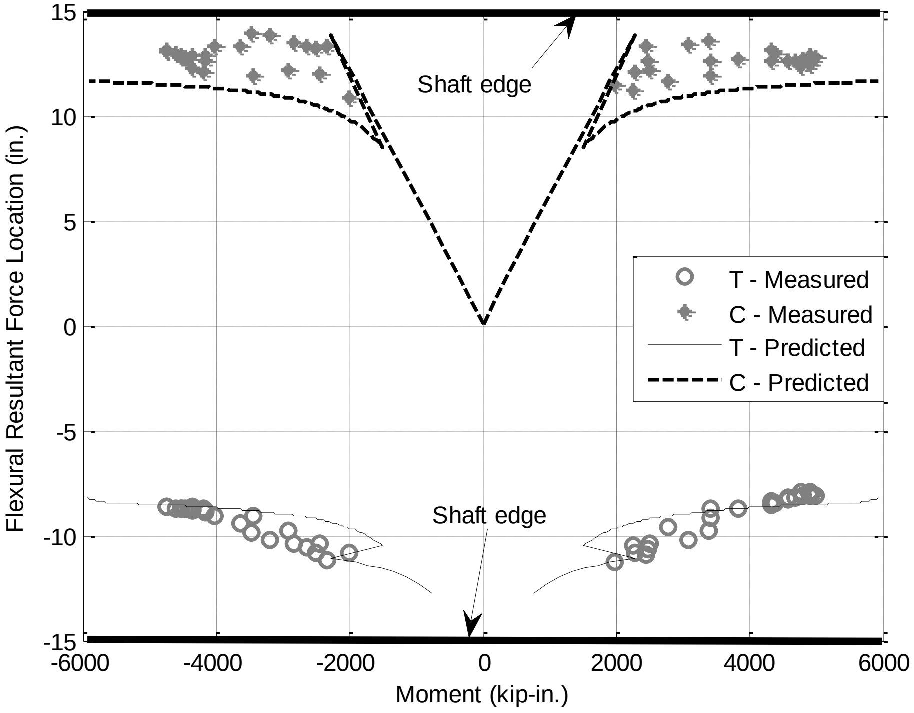

Figure 6-21. Flexural resultant force location at the bottom of the connection – DS-1

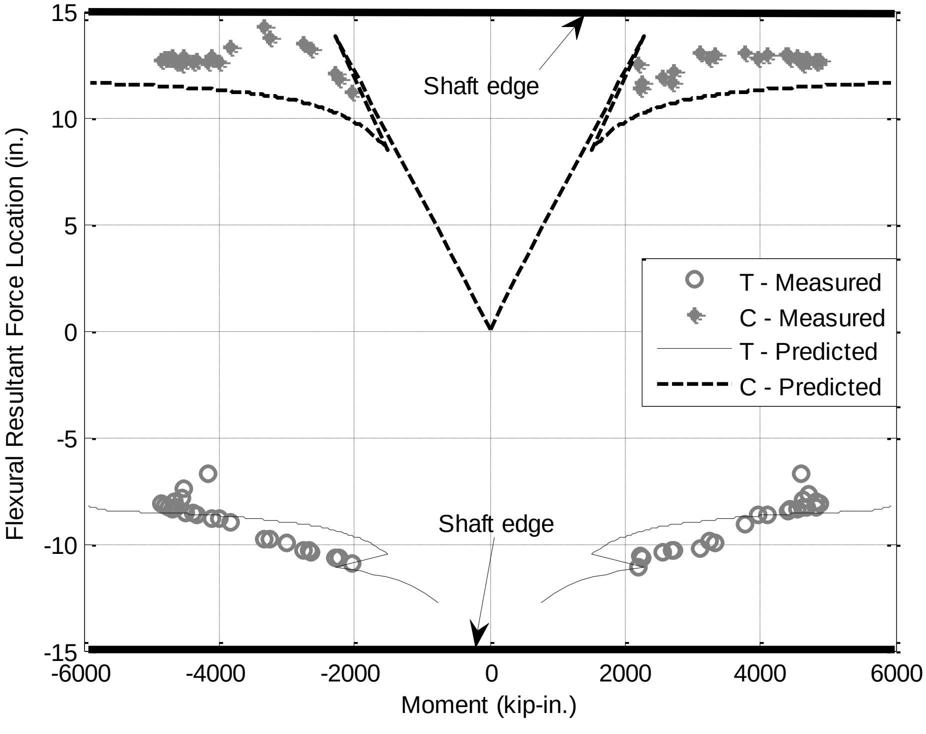

Figure 6-22. Flexural resultant force location at the bottom of the connection – DS-2

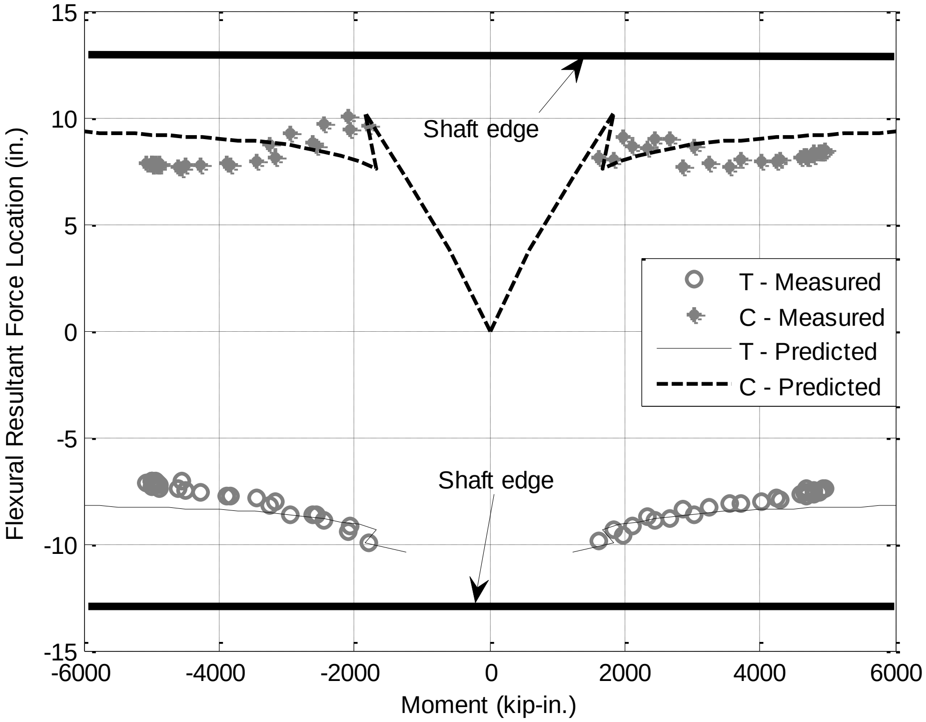

Figure 6-23. Flexural resultant force location at the bottom of the connection – DS-3

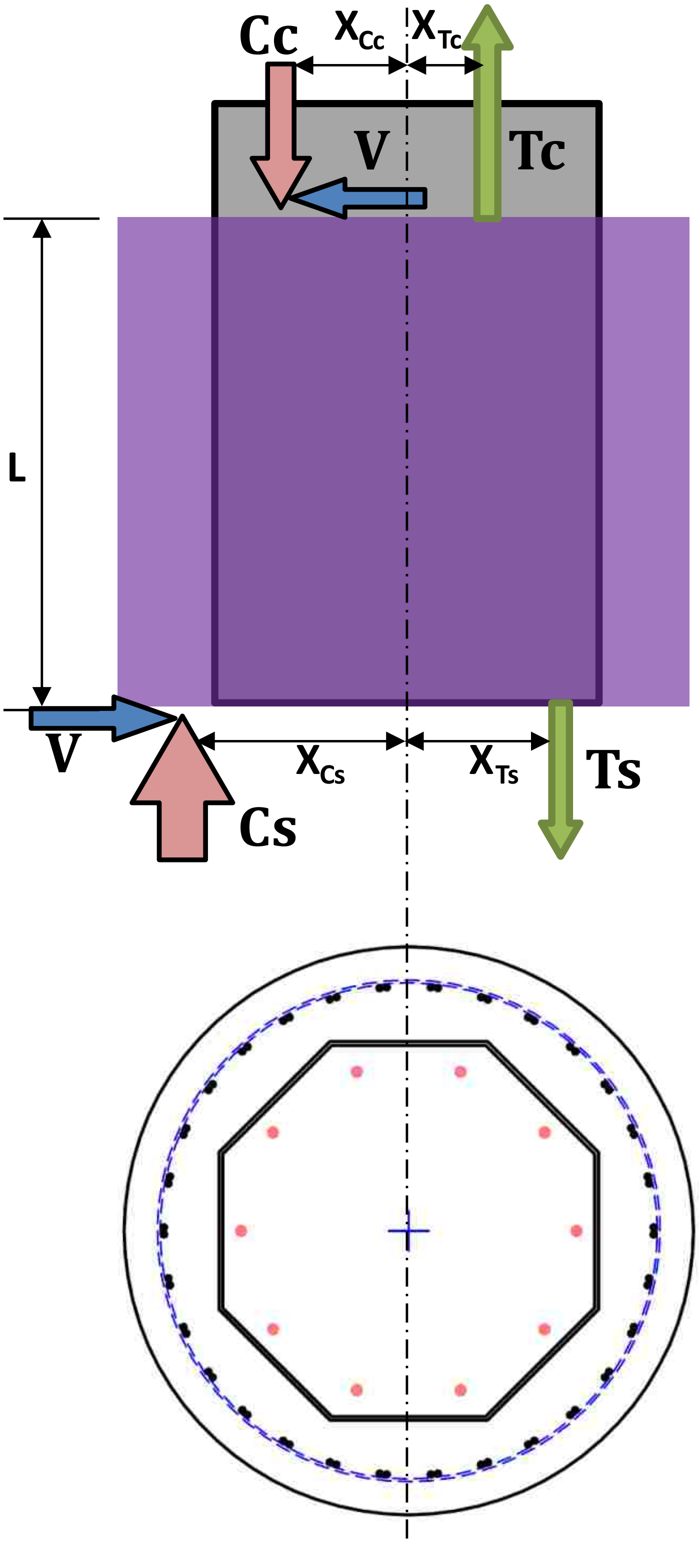

Figure 6-24. The forces acting at the boundary of the column-shaft connection.

6.3 PROPOSED STRUT-AND TIE MODEL

In the previous section, it was shown that sectional analysis can be used to establish the forces and their locations acting at the boundary of the column-shaft connection. At a given curvature and moment, the predicted values agree with the measured ones. In this section, transfer of these forces through the transition region is investigated. A strut-and-tie model is proposed and compared with measured data in the next section.

6.3.1 Free-body diagram before failure

As discussed in Chapter 5, Specimen DS-2 failed in the transition region. The damage levels for Specimen DS-2 just before and after the measured lateral load resistance decreased below 80% of the maximum resistance obtained earlier in the test, is shown in Figure 6-25. The behavior of this specimen was characterized by the opening of large vertical and diagonal cracks in the transition, and followed subsequently by fracture of the spirals.

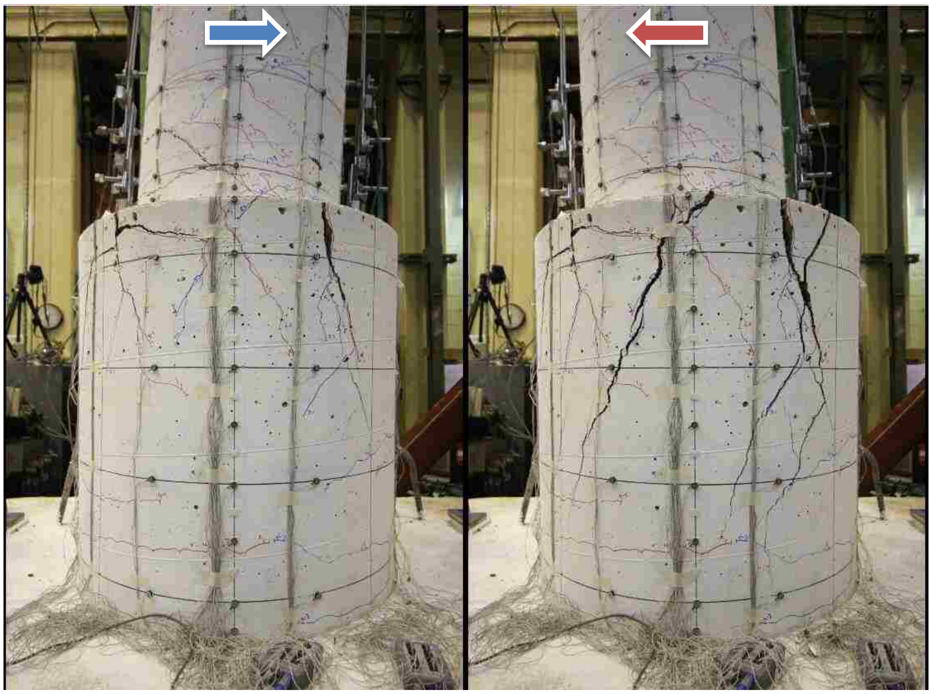

a). Cycle 9-2 Peak - drift +6.8 %   b). Cycle 9-2 Valley - drift -6.8 %

Figure 6-25. Specimen DS-2: before and after failure

The free-body diagram of the left-had part of Specimen DS-2 before failure gives an interpretation of the behavior and failure mode of the column-shaft connection. Based on the prying failure of Specimen DS-2 (Figure 6-25b), the free body diagram of the left part of the transition is demonstrated in Figure 6-26.

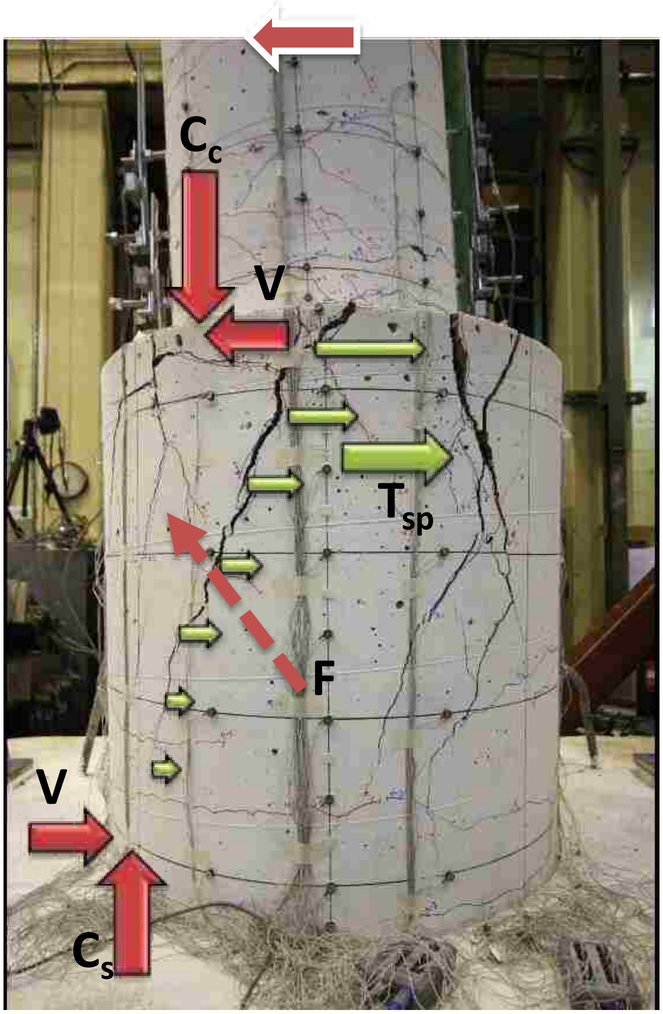

Figure 6-26. Free-body diagram – DS2

As shown in the free body diagram, the applied forces include compressive resultant force of column and shaft ($\boldsymbol{C_c}$ and $\boldsymbol{C_s}$ respectively), shear forces, $\boldsymbol{V}$, at the top and bottom, and spirals tensile forces (marked as green arrow) distributed along diagonal cracks with resultant at $\boldsymbol{T_{sp}}$. The diagonal face includes both column and shaft part. The spirals tensile force was acting at the shaft part .Because the column diameter was smaller than shaft diameter, normally, $\boldsymbol{C_c}$ was larger than $\boldsymbol{C_s}$. For equilibrium, force $\boldsymbol{F}$, which has vertical part is equal to $\boldsymbol{C_c - C_s}$ and horizontal part is equal to $\boldsymbol{T_{sp}}$,is needed at the column part of the diagonal face.

6.3.2 Strut-and-Tie Model

Based on the forces acting at the boundary region and free-body diagram, the force transferred from the column to the shaft is represented by a proposed strut-and-tie model as shown in Figure 6-27.

The boundary conditions for the strut-and-tie model were determined as follows:

- The column tension force $\boldsymbol{Tc}$ was represented by a tie element. The location ($\boldsymbol{X_{Tc}}$) and magnitude of this tie was equal to the column tensile resultant force's location and magnitude that were estimated from the moment-curvature analysis of the column section.

- Similarly, the locations of nodes **E** and **F** were identified at the calculated locations of the column and shaft compression resultant force respectively using moment and force equilibrium requirement.

- The shaft tension force $\boldsymbol{Ts}$ was represented by a tie element, which is located ($\boldsymbol{X_{Ts}}$) at the shaft tensile resultant force estimated from the moment-curvature analysis of the shaft section.

The internal elements of the model were determined as follows:

- The elevation of node **A** was assumed to be at the end of column headed bars.

- The transition transverse reinforcement was represented by tie **BC**. This tie was placed horizontally at the location of the transition transverse resultant force. In the analysis model, this location is determined based on the strain data attached on the transverse reinforcement. In the design model, it is determined based on the assumed parabolic strain distribution of the transverse reinforcement assumption which will be discussed more in the design model section.

- Struts **CE** and **DF** were identified based on equilibrium considerations of nodes **E** and **F**.
- Node **B** and **C** were placed at the intersection between tie **BC** and **Ts**, **EC** respectively
- Strut **AB** represented the lap splice force transfer mechanism between column and shaft reinforcement. This strut is not a real strut in the transition region. It was the resultant force of all compressive struts transferred from column to shaft reinforcement which were uniformly distributed inside the peripheral hoops or spirals. Strut **AB** was also needed to maintain equilibrium at nodes **A** and **B**.
- To maintain equilibrium at node **A**, strut **AD** was established.
- Node **D** was placed at the intersection between struts **DF** and **AD**.
- Strut **CD** was located to maintain equilibrium at nodes **C** and **D**.

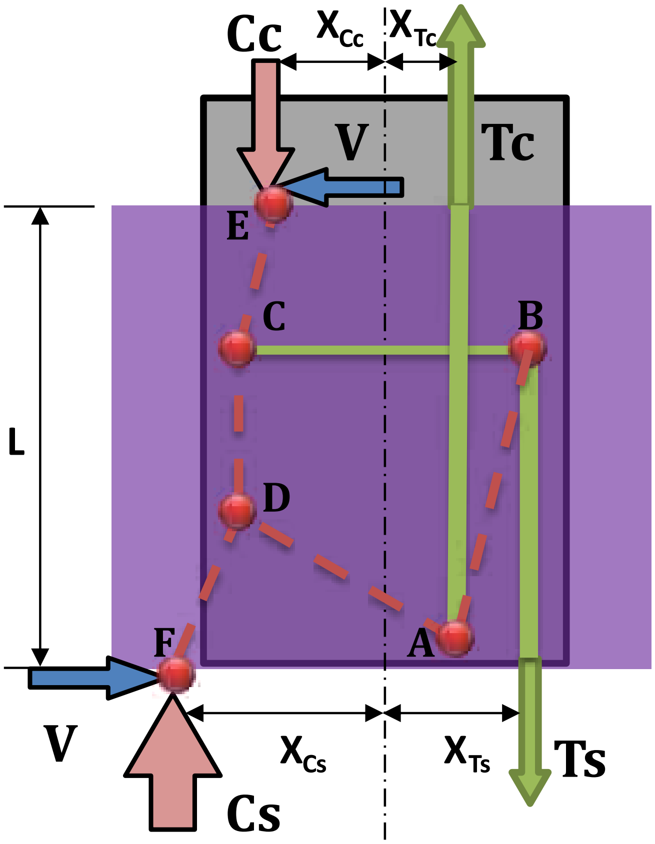

Figure 6-27. The proposed strut-and-tie model.

6.4 VERIFICATION OF STRUT-AND TIE MODEL

Various transition failure modes and the lateral-load capacity of the system are evaluated in terms of the capacities of the proposed struts and ties in this section.

6.4.1 Compression Failure

The system investigated here is the connection between a column and an enlarged shaft. Thus, the compressive stress in the column is larger than in the shaft. Therefore, in general, the compression failure will not happen in the transition.

6.4.2 Tension Failure

A tension failure is developed in the column when the hinge forms in the column and the column longitudinal reinforcement is subjected to large inelastic strain. This is the desired mode of failure of the column-shaft connection. In the strut-and-tie model, this mode of failure is represented when the column tensile resultant force **Tc** is more than the tensile resultant force estimated from the moment-curvature analysis.

6.4.3 Anchorage Failure

In order to obtain a satisfactory performance of the column-shaft connection, it is essential that the column longitudinal reinforcement is sufficiently anchored into the transition. If an anchorage failure of column reinforcement occurs, a tensile failure cannot and the desired response mode of a column flexural above the shaft cannot be achieved. Since it is desirable to form a plastic hinge in the column and the shaft reinforcement remains elastic, high inelastic strains with opposite sign are typically developed in the column reinforcing bars. In the investigated column-shaft connection, the ends of the longitudinal column reinforcement were terminated with rebar end anchors. Thus, the anchorage failure is not likely to happen.

6.4.4 Lap Splice Failure

The lap splice failure occurs if the confining pressure is not sufficient to prevent splitting of concrete between the column and shaft longitudinal reinforcement, so the column tension force may not be transferred to the shaft reinforcement by bond or shear friction across the precast-c.i.p interface. Thus, the transition will fail before the column reaches its flexural strength. Specimen DS-2 was designed with a small amount of transition spiral, which was expected to induce lap splice failure. However, the test result showed that even when some of the spirals were broken, the tension force in the shaft reinforcement did not change (Figure 6-28). It suggests that the splice failure can be prevented by a minimum requirement of transverse reinforcement.

The outside surface of the embedded part of precast column was intentionally roughened using the saw-tooth pattern was similar to the one required by the WSDOT BDM for the end forms for prestressed girders. This detail satisfied the AASHTO LRFD requirement for surface-transferring shear-friction in term of minimum amplitude. No sliding failure was observed during testing.

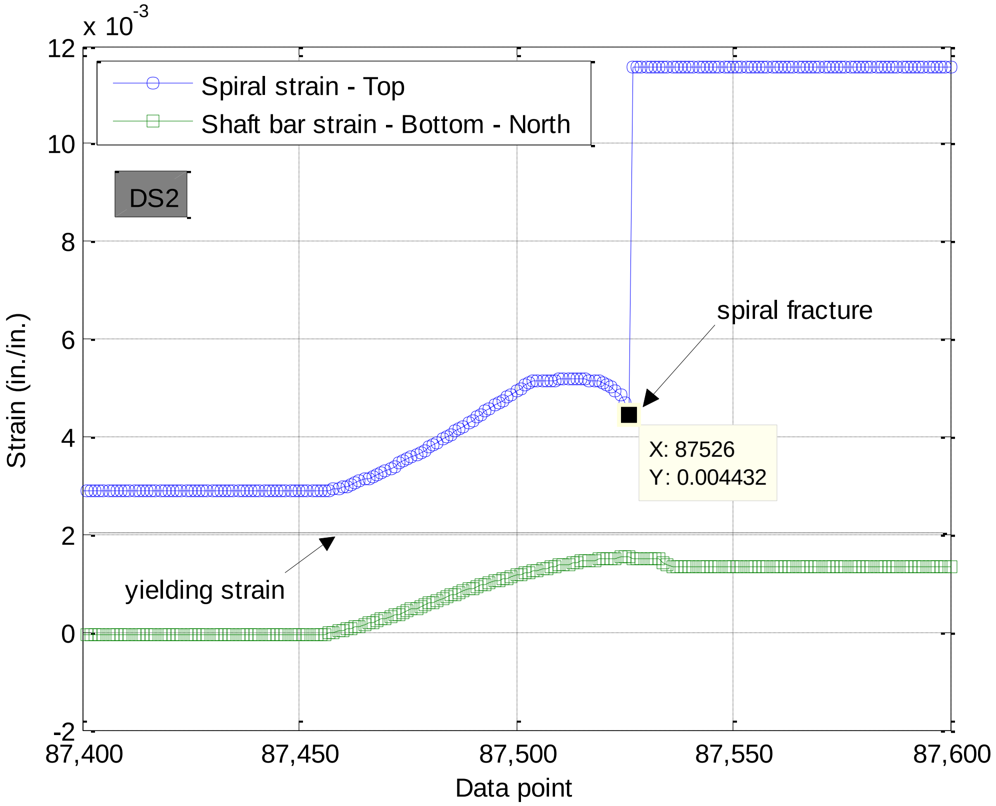

Figure 6-28. Spiral fracture point (Specimen DS-2)

6.4.5 Prying Failure

The prying failure occurs if the transverse reinforcement is not sufficient as shown in Specimen DS-2 (Figure 6-25b). In contrast with the lap splice failure, the prying failure occurs even when the tension force still can be transferred from column to shaft reinforcement. This is because only the spirals at the top part of the transition were activated in the prying behavior. When the top spirals were broken, the lower spirals were activated. This mode of failure is similar to the zip behavior as the two rows of teeth are separated if the slider moves down. Therefore, if the transverse reinforcement is uniformly distributed in the transition, the prying failure still can happen. This mode of failure is represented in the proposed strut-and-tie model when the force in tie element **BC** exceeds its strength.

6.4.6 Verification of the proposed strut-and-tie model

As shown above and in Chapter 5, the compression failure, anchorage failure, and lap splice failure did not occur in the three test specimens. The tension failure (or flexural failure) happened in specimens DS-1 and DS-3 and prying failure happened in Specimen DS-2. The criterion used to evaluate the proposed strut-and-tie model was the magnitude of tie force BC agree with the resultant force of spirals in the test results of the three specimens.

First, the tensile force in the spirals were calculated based on strain calculated by using the horizontal displacement of the shaft as follows:

- Under cyclic excitation, the shape of the shaft deformation was assumed as an ellipse shape as shown in Figure 6-29. Assuming that the semi-minor axis, **b**, is equal to the radius of the shaft spiral, **R**. The semi-major axis, **a**, is measured as a half of the distance between the North and South LED marker of Optotrak.
- The perimeter of the ellipse is calculated using Ramanujan's formula as follows:

$$p \approx \pi\left[3(a+b)-\sqrt{(3a+b)(a+3b)}\right] \tag{6-1}$$

- The average strain of spiral is calculated as:

$$\epsilon_{sp} = \frac{\Delta L}{L} = \frac{p - 2\pi R}{2\pi R} \tag{6-2}$$

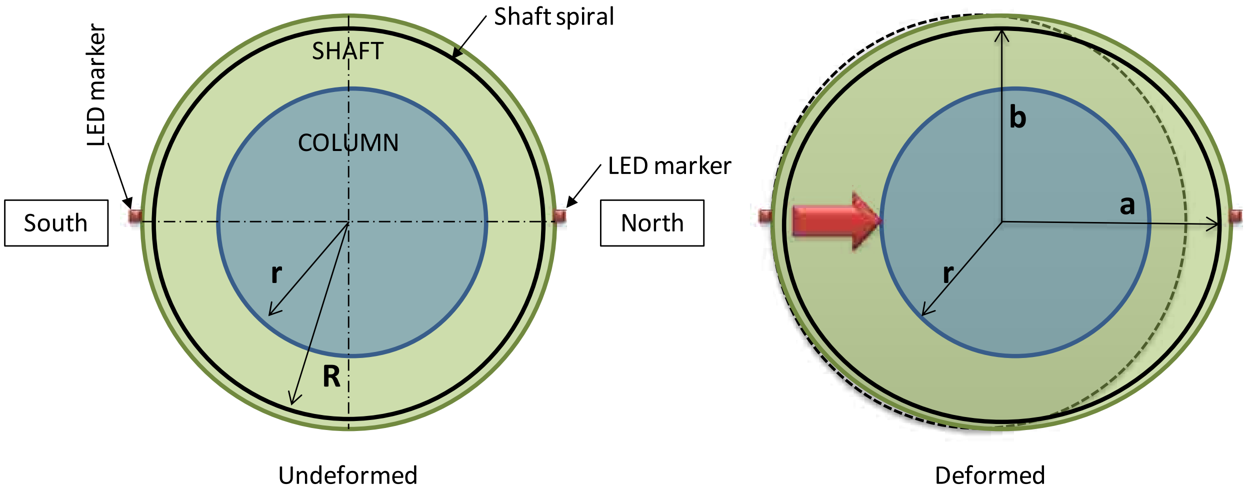

Figure 6-29. Section of column-shaft connection before and after deformed

The comparison of spiral strain measured by the above method and the strains measured by electrical strain gauges at some points are shown in Figure 6-30, Figure 6-31, and Figure 6-32 for specimens DS-1, DS-2, and DS-3 respectively. In those figures, the “calculated strain” refers to the strains calculated with the motion capture system (Optotrak) deformation data. It indicates that the strains measured by the above method are in good agreement with the strain gauge data.

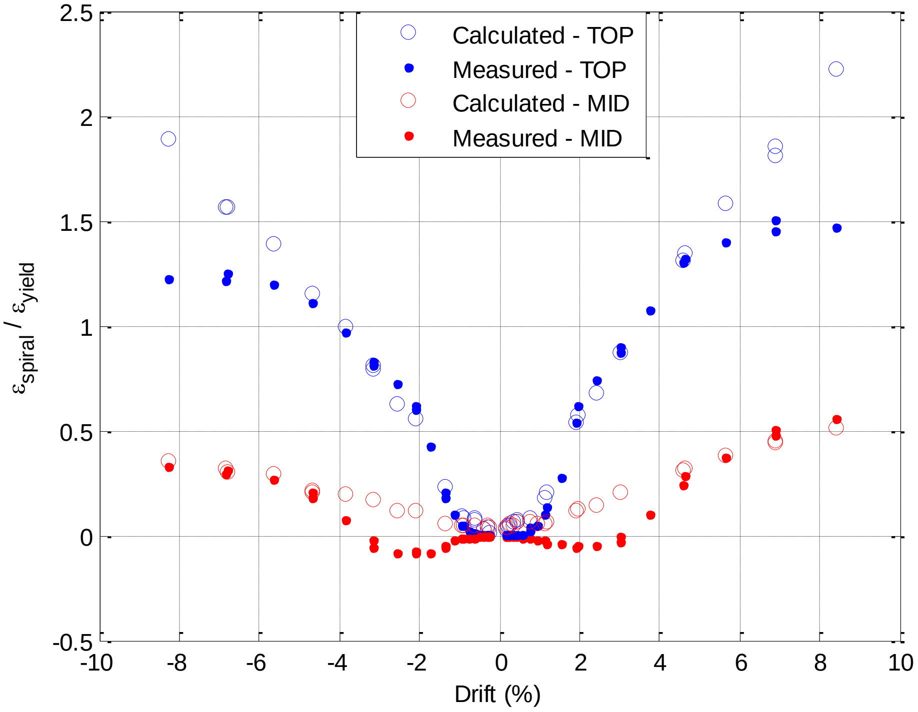

Figure 6-30. Comparison of calculated and measured spiral strain – DS-1

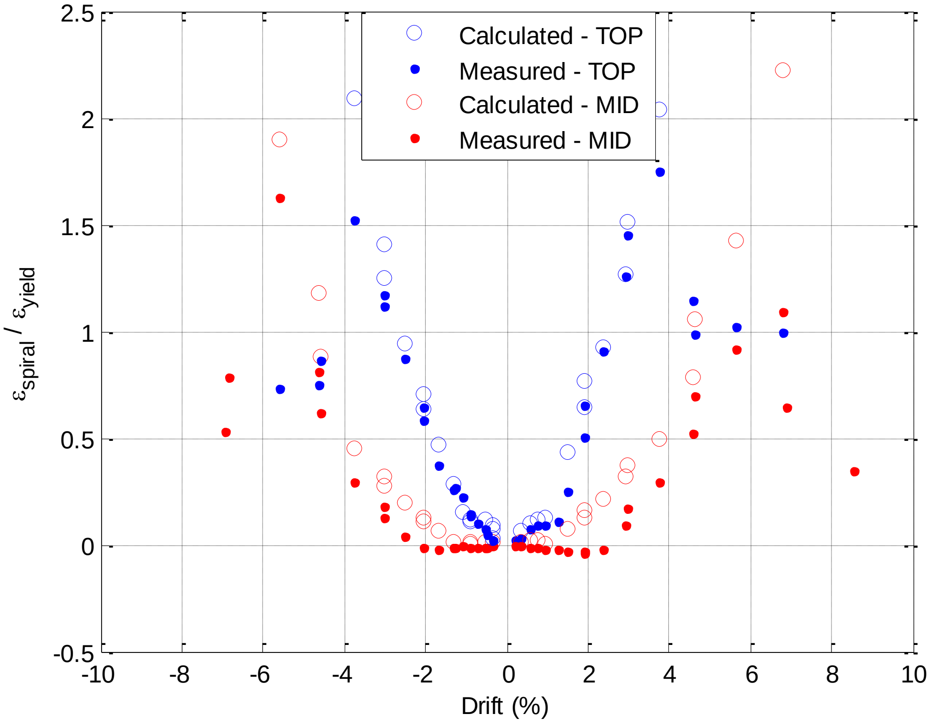

Figure 6-31. Comparison of calculated and measured spiral strain – DS-2

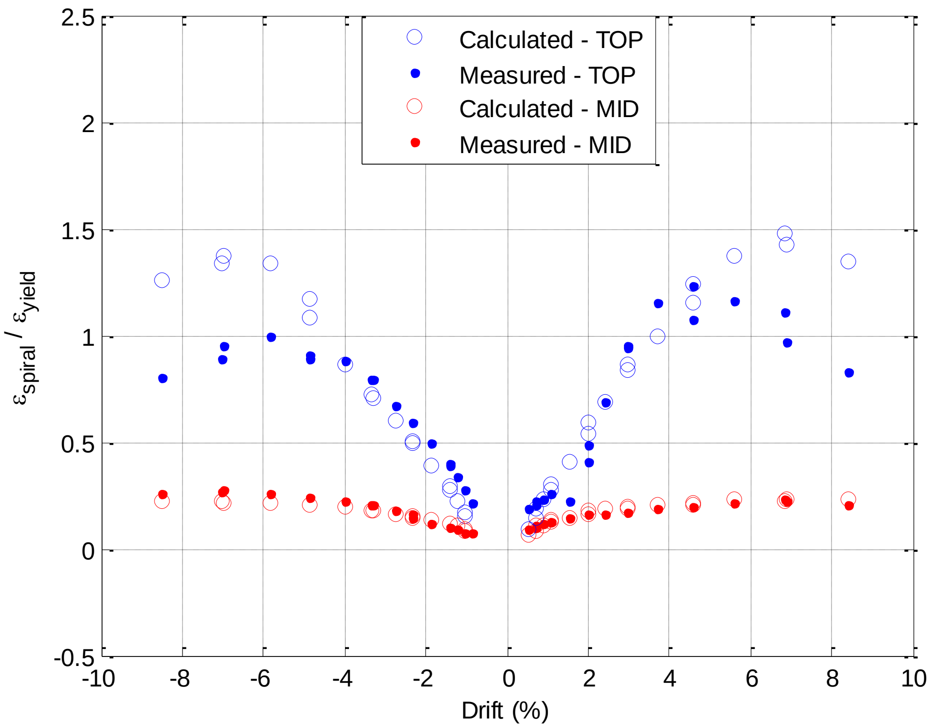

Figure 6-32. Comparison of calculated and measured spiral strain – DS-3

The stresses and tensile force of shaft spirals were calculated using the stress-strain relationship which measured in a tension test. The values of spiral force, which were calculated using strain calculated from the Optotrak data are assumed to be the measured value, since they gave a better strain distribution along the connection in comparison with using strain gauge data.

The comparison of the measured and calculated value of the spiral resultant force **Tsp** using the proposed strut-and-tie model were shown in Figure 6-33, Figure 6-34, and Figure 6-35 for specimens DS-1, DS-2, and DS-3 respectively. The difference between the measured and calculated **Tsp** in specimens DS-1 and DS-2 represents the contribution of the shaft concrete tensile strength. In Specimen DS-3, when the shaft diameter was reduced, the calculated values were close to the measured values.

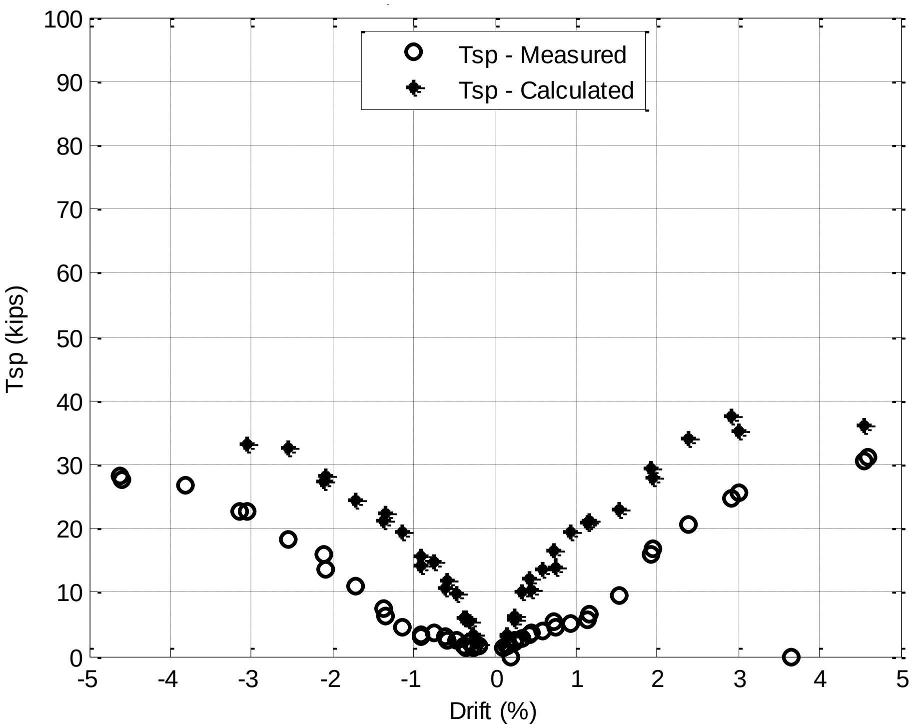

Figure 6-33. Spiral resultant force vs. drift – DS-1

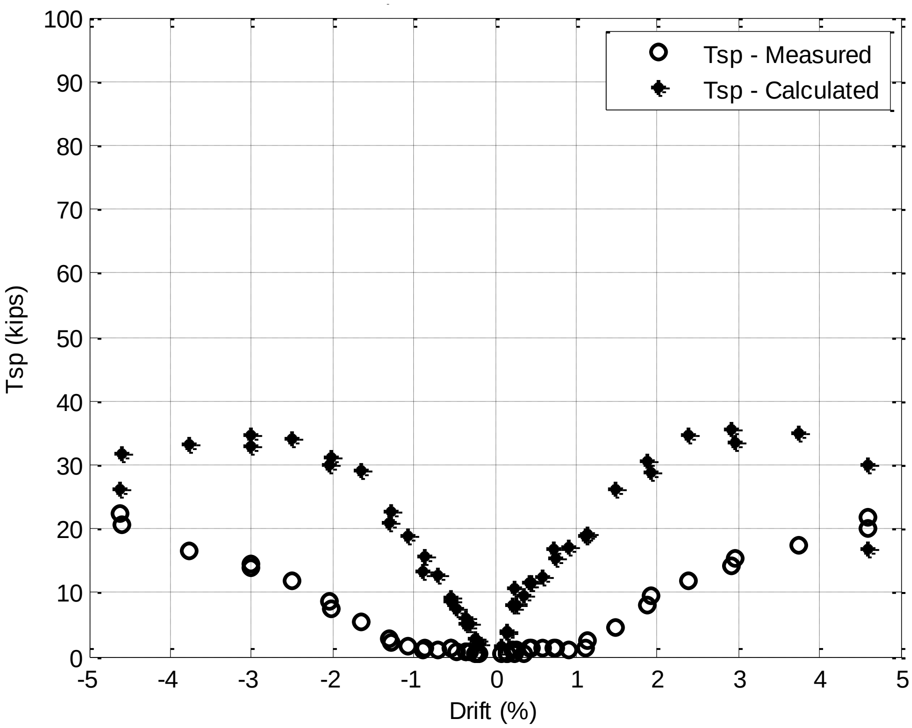

Figure 6-34. Spiral resultant force vs. drift – DS-2

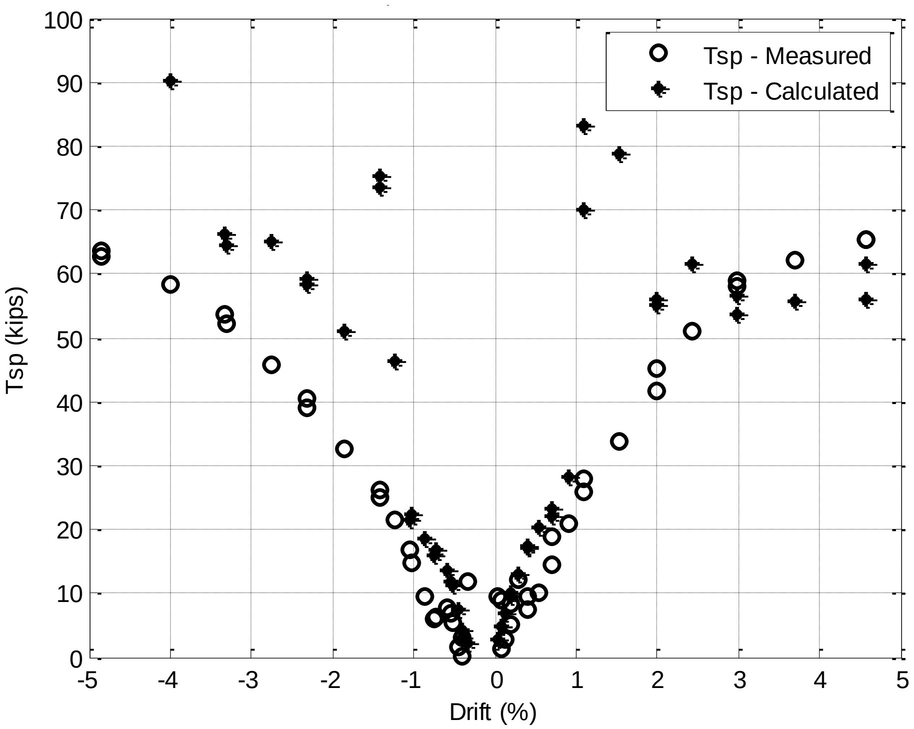

Figure 6-35. Spiral resultant force vs. drift – DS-3

As shown above, specimens DS-1 and DS-3 failed because of column bars fracture after a hinge formed in the column and the column moment strength reduced dramatically. Specimen DS-2 failed because the top shaft spirals fractured before a hinge formed in the column. Therefore, to determine the mode of failure of the column-shaft connection, the ratio of column moment to column ultimate moment (i.e. moment strength which is the maximum moment measured in specimen DS-1 and DS-3. In Specimen DS-2, moment strength is taken the same as in Specimen DS-1 since they have the same design and material) $\boldsymbol{M_c/M_{c,ult}}$ should be compared with the ratio of spiral resultant force to spiral ultimate force $\boldsymbol{T_{sp}/T_{sp,ult}}$. If the ratio $\boldsymbol{M_c/M_{c,ult}}$ reaches 1 first, the system fails in column. In contrast, if the ratio $\boldsymbol{T_{sp}/T_{sp,ult}}$ reaches 1 first, the system fails in the transition. Since it is desirable to form a plastic hinge in the column when the shaft reinforcement remains elastic, the ratio $\boldsymbol{T_{sp}/T_{sp,ult}}$ is replaced by the ratio $\boldsymbol{T_{sp}/T_{sp,yield}}$ where, $\boldsymbol{T_{sp,yield}}$ is the spiral resultant force when the strain of the top spiral turn reaches yielding strain.

The relationship between ratio $\boldsymbol{M_c/M_{c,ult}}$ and ratio $\boldsymbol{T_{sp}/T_{sp,yield}}$ for both measured and calculated values are shown in Figure 6-36, Figure 6-37, Figure 6-38 for specimens DS-1, DS-2, and DS-3 respectively. It indicates that the predicted values of strut-and-tie model were in good agreement with the measured values, and it could determine the mode of failure of all tests. However, it also can be seen that even the hinge formed in the column in specimens DS-1 and DS-3, the ratio $\boldsymbol{T_{sp}/T_{sp,yield}}$ also more than 1. It suggests that the amount of spiral designed for these tests were still not enough to keep the transition spirals remain elastic.

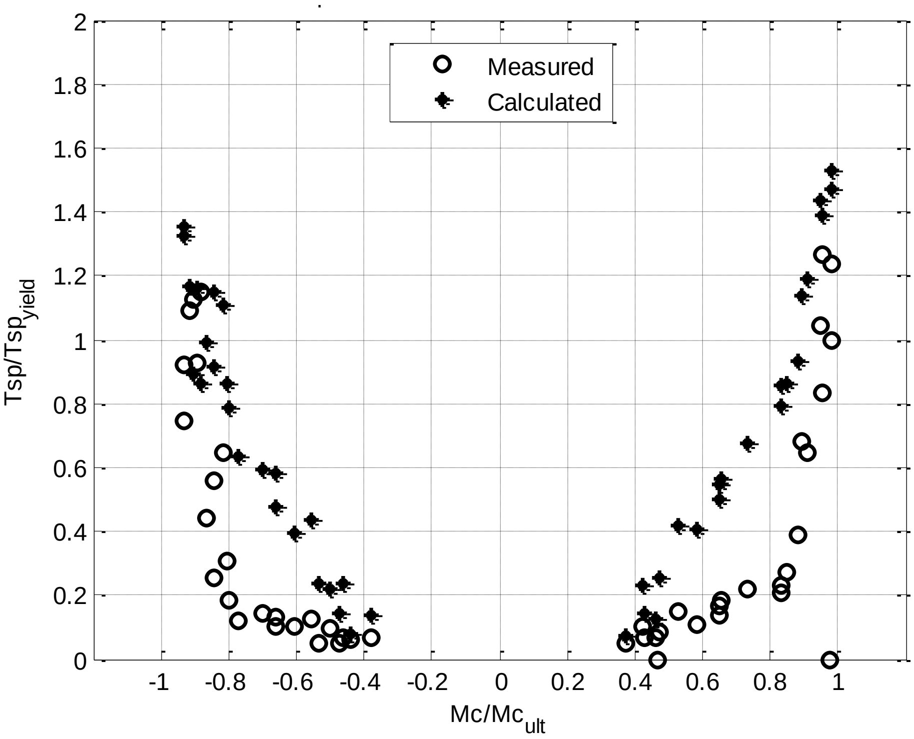

Figure 6-36. Spiral resultant force vs. column moment – DS-1

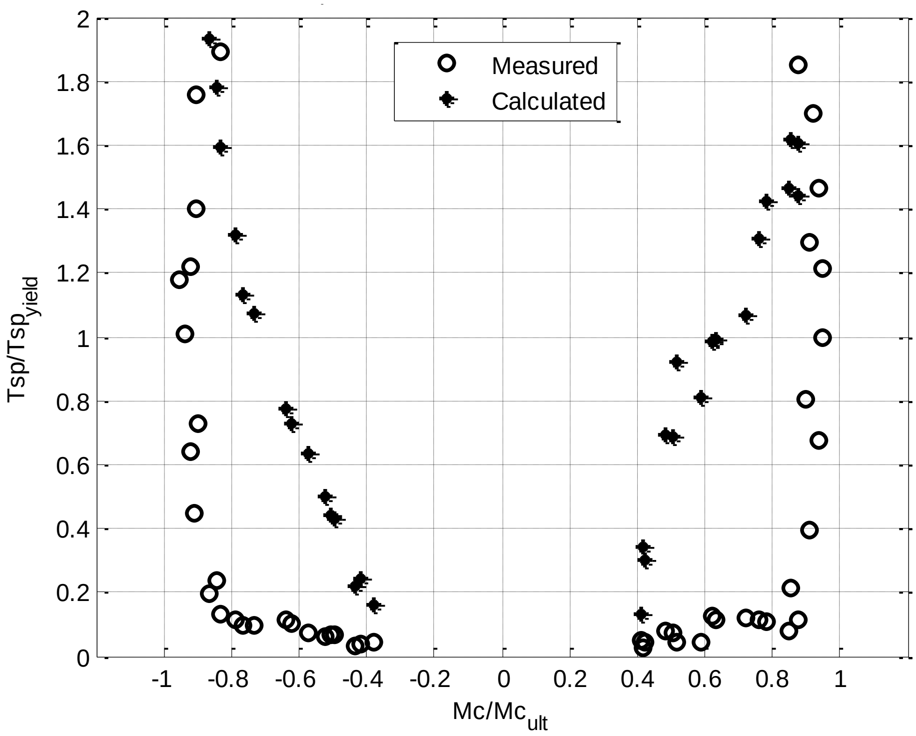

Figure 6-37. Spiral resultant force vs. column moment – DS-2

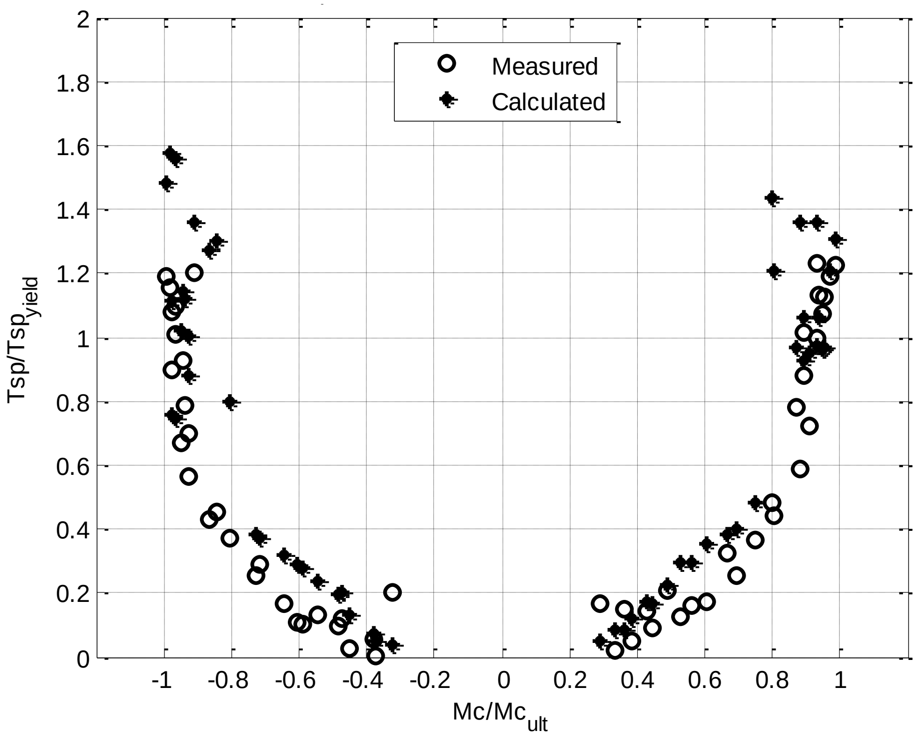

Figure 6-38. Spiral resultant force vs. column moment – DS-3

CHAPTER 7.
DESIGN PROCEDURE

The strut-and-tie model developed in the previous chapter showed good agreement with the test data. Based on that model, a design procedure of the precast column–shaft connection is presented in this chapter and applied to cast-in-place column-shaft connections too.

- First the force acting on the boundaries of the connection will be determined using flexural analysis (Section 7.1).
- Then, the connection force transfer mechanism will be specified based on assumptions and the proposed strut-and-tie model (Section 7.2).
- Finally, the design method is evaluated by comparing it with experimental data from the three specimens performed at the University of Washington and from four cast-in-place column-shaft connection specimens tested at the University of California, San Diego (Murcia-Delso et al. (2013)) (Section 7.3).

7.1 FORCES ACTING ON THE BOUNDARIES OF THE TRANSITION

The first task to be addressed when designing a connection between a precast column and a drilled shaft is the determination of the maximum forces acting on the boundaries of the transition region subjected to seismic loading. The determination of moments, axial forces, and shear forces at the top and bottom of the transition region are presented in this section.

Typically, in bridge structures, the column is designed to be the critical flexural member, and the column plastic hinge is intentionally designed to form above the column-shaft interface. This requirement is ensured by using the moment-curvature sectional analysis of the column, which is based on Bernoulli's assumption that plane sections remain plane. Strictly speaking, the column-shaft interface is in a D-region (no basis for using Bernoulli's assumption), but as indicated in the previous chapter, the experimental results showed that the column ultimate flexural strength is insensitive to the strain distribution. Sectional analysis provides a satisfactory prediction of the column flexural response.

Therefore, for design, the plastic moment capacity of the column will be calculated by moment-curvature analysis on the basis of the expected material properties, which include the effects of strain-hardening effect and concrete confinement. This moment-curvature analysis will include the axial forces due to dead load and axial forces due to overturning as required in Section 8.5 of the AASHTO Guide Specifications (2011).

To ensure the capacity protection for members (e.g., shaft) connected to a hinging member (e.g., column), an over-strength magnifier, λ_{mo}, as required by the AASHTO Specifications. According to these specifications, this magnifier shall be applied to the plastic moment capacity of the column such that:

$$M_{po\_col} = \lambda_{mo} M_{p\_col} \tag{7-1}$$

where,

M_{p_col} = plastic moment capacity of the column, using moment-curvature analysis based on expected material properties

M_{po_col} = over-strength plastic moment capacity of column

λ_{mo} = over-strength magnifier, which accounts for material strength variations

= 1.2 for ASTM A 706 reinforcement

Using the column over-strength moment, the corresponding column shear force will be determined as:

$$V_{po} = \frac{M_{po\_col}}{L_{col}} \tag{7-2}$$

where,

L_{col} = length of column from point of maximum moment (i.e. column-shaft interface) to the point of moment contraflexure.

V_{po} = column shear force corresponding to the over-strength plastic moment of the column

P-Δ effects are not considered in this calculation, so the calculated shear force value is larger than it would be if P-Δ effects were included, and therefore, this procedure treats this effect conservatively.

A similar flexural analysis is conducted for the shaft to determine its state when the column is at its over-strength capacity. Because the peak moment in the shaft will be some way down from the ground surface. The reinforcement will be designed for that moment, and will most likely be constant from there up to the top of the transition region. The shaft will be designed to work elastically under seismic excitation. Therefore the peak moment in the shaft should be smaller than the yielding moment.

From these flexural analyses, the magnitude and location of the flexural stress resultant forces will be determined. As discussed in the previous chapter, these calculated locations agreed reasonably well with the experimental results. In fact, in the column, the over-strength moment of column is larger than the plastic moment calculated by moment-curvature analysis. So the flexural resultant forces cannot be determined. Therefore, it is suggested that the location of flexural resultant forces at the column-shaft interface be the location of the flexural resultant forces calculated by moment-curvature analysis.

In the shaft, at the bottom of the transition region, the magnitude and location of the flexural resultant forces will be determined at

$$M_{sh} = M_{po} + V_{po}L \tag{7-3}$$

where,

M_{sh} = Design moment demand in the shaft at the bottom of the transition

L = Length of the transition

AASHTO allows yielding to occur in the shaft regions that are not readily accessible for inspection only with owner approval (AASHTO Guide Spec. 4.7.1). WSDOT requires that the top of shafts in typical WSDOT single column/single shaft connections that the shaft should remains elastic under seismic loads (WSDOT BDM 7.8.2.I). Therefore, these recommendations suggests that the moment at the bottom of the column-shaft connections should be designed not to yield:

$$M_{sh\_y} \geq M_{sh} \tag{7-4}$$

The magnitude and location of the flexural resultant forces will also be determined by using moment-curvature analysis and placed at the bottom of the connection as shown in Figure 7-1 where,

C_c = column compressive resultant force

T_c = column tensile resultant force

X_{Cc} = distance from compressive resultant force to the centroid of column

X_{Tc} = distance from tensile resultant force to the centroid of column

C_S = shaft compressive resultant force

T_s = shaft tensile resultant force

X_{Cs} = distance from compressive resultant force to the centroid of shaft

X_{Ts} = distance from tensile resultant force to the centroid of shaft

V = column shear force

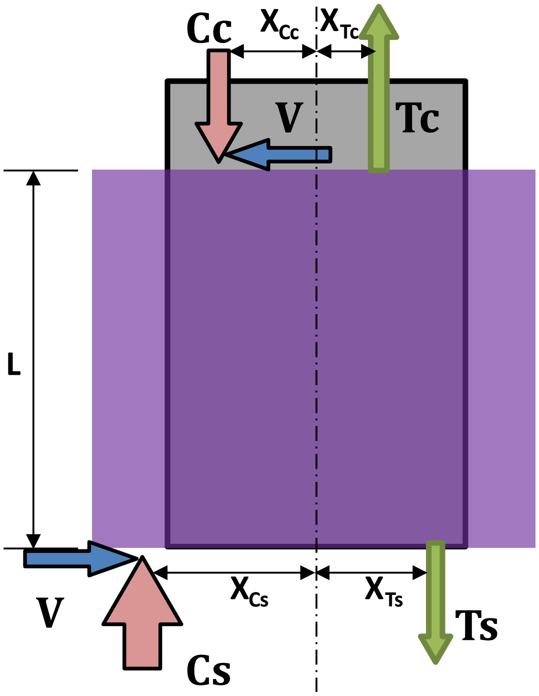

Figure 7-1. The forces acting at the boundary of the column-shaft connection.

7.2 DESIGN STRUT-AND-TIE MODEL

Methods for determining the forces acting on the boundary of the transition were proposed in the previous section. The proposed strut-and-tie model, which forms the core of the rational design procedure, is presented in this section based on the investigated analyses in the previous chapter.

7.2.1 Lateral Deformation of Transition Region

As shown in the previous chapter, the distribution of lateral deformation of the transition plays an important role in the force transfer mechanism from the column to the shaft. It allows the spirals in the transition to be designed in way that ensures the capacity protection of the connection. Based on experimental results, the lateral strain in the transition is assumed to be distributed parabolically with zero value at the bottom of the transition (Figure 7-2) as follows:

$$\varepsilon(y) = \varepsilon_t \left(\frac{y}{L}\right)^2 \tag{7-5}$$

where,

ϵ_t = lateral strain at the top of the transition

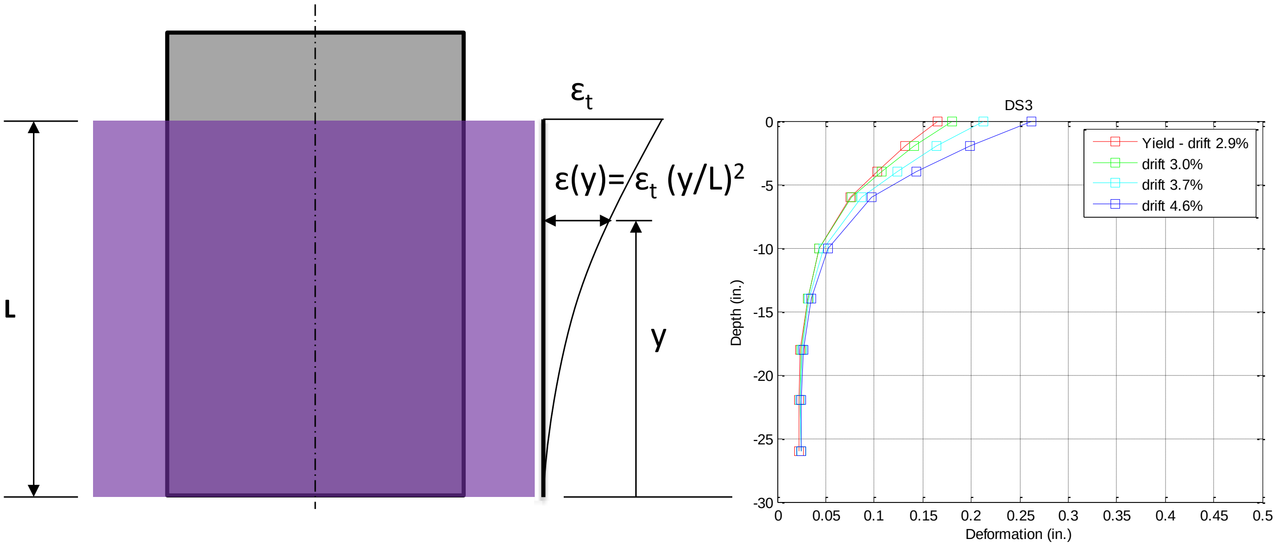

Figure 7-2. Assumed and measured lateral strain distributions in Specimen DS-3

According to this assumed distribution of lateral deformations, spiral is used most efficiently if it is concentrated at the top of the transition. If the spiral is designed with a constant spiral spacing, and the spiral is designed to respond elastically, the centroid of the spiral force would be located 3/4 up the transition length from the bottom of the transition region. In fact, WSDOT (and presumably other DOTs) will require a minimum amount of spiral that is to be spaced uniformly. If that is enough for the transition region, so be it. If not, a good choice might be to use the minimum of uniform spiral, and place the rest in a band at the top. Furthermore, placing spiral in a band at the top would have another advantage, which is that it would confine the top of the vertical reinforcement in the shaft and thereby improve the bond conditions there.

7.2.2 Strut-and-Tie Model

The proposed strut-and-tie model and the assumed boundary forces are shown in Figure 7-3.

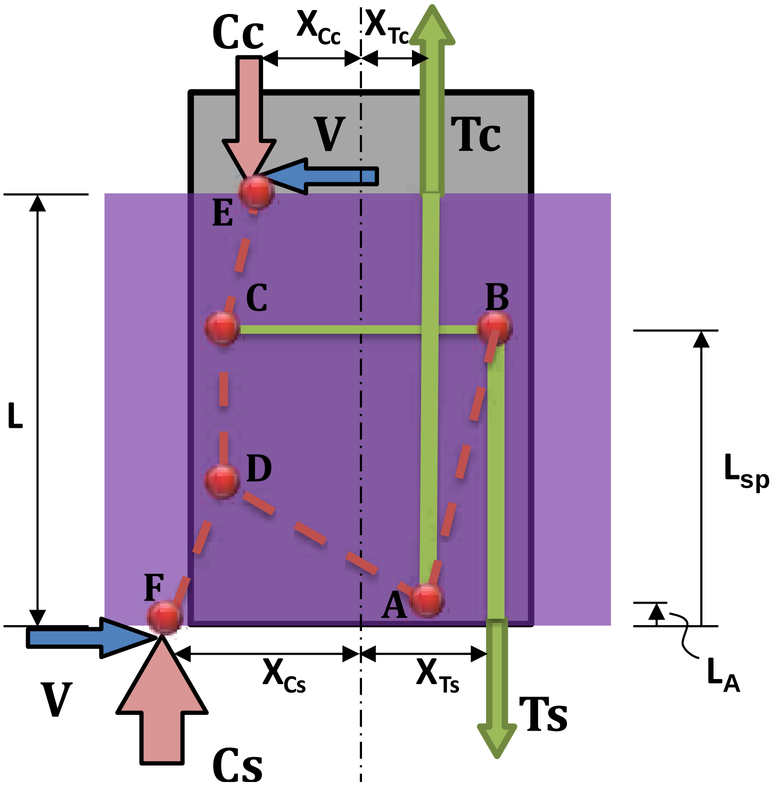

Figure 7-3. Proposed strut-and-tie model.

The procedure adopted for developing the joint force transfer model in the connection is similar with the model proposed in the previous chapter except that the position of transition transverse resultant element (**BC**) is determined based on the assumed lateral-deformation distribution (Section 7.2.1). The model is formulated as follows:

- The column tension force $\boldsymbol{Tc}$ is carried by a tie element to node **A**. The horizontal location ($\boldsymbol{X_{Tc}}$) and magnitude of this tie force is equal to the column tensile resultant force's location and magnitude, which are estimated from the moment-curvature analysis of the column.

- Node **A** is located at the end of column headed bars.

  If headed bars are not used, the bottom of the effective anchorage length is assumed to be a distance $l_a + s + c$ below the top of the transition region, s is the radial center-to-center distance between the longitudinal bars of the column and those of the shaft, and c is the concrete cover at the top of the transition, and l_a is the required anchorage length (Priestley et al. 1993)

  $$l_a = \frac{0.025 d_{b,col} f_y}{\sqrt{f_c'(psi)}} \tag{7-6}$$

  where, f_y is yield strength of the column bars (psi). For design, the above anchorage length formula implies that the column bars subjected to a stress of $1.4 f_y$, which approximates f_u, at the column-shaft interface.

  Ingham et al. (1995) suggested that node **A** could be located at the center of the effective anchorage length of the column bar from the bar end. The effective anchorage length was determined by assuming a uniform bond stress of $30\sqrt{f_c'\text{ (psi)}}$ as follows:

  $$l_{a,eff} = \frac{f_u A_{b,col}}{\pi d_{b,col}\left(30\sqrt{f_c'(psi)}\right)} \tag{7-7}$$

  where, $A_{b,col}$ = column bar area, and $d_{b,col}$ = column bar diameter.
  Combining these equations, node A is located a distance $l_a + s + c - l_{a,eff}/2$ bellow the top of the transition region.

- The shaft tension force $\boldsymbol{Ts}$ is carried by a vertical tie element to node **B**, which is located horizontally at the location of shaft tensile resultant force ($\boldsymbol{X_{Ts}}$) estimated from the moment-curvature analysis of the shaft section.

- The transition transverse reinforcement is represented by horizontal tie **BC**. This tie (and node **B**) are placed vertically at the elevation of the transition transverse resultant force. This location is determined based on the parabolic strain distribution of the transverse reinforcement assumption and transverse reinforcement placement (Section 7.2.1).

- The horizontal locations of nodes **E** ($\boldsymbol{X_{Cc}}$) and **F** ($\boldsymbol{X_{Cs}}$) are placed at the location of the column and shaft compression resultant force respectively.

- The angles of struts **CE** and **DF** are identified based on equilibrium requirements for nodes **E** and **F**.

- Node **C** is placed at the intersection between horizontal tie **BC** and diagonal strut **EC**.

- Strut **AB** represents the lap splice force transfer mechanism between column and shaft reinforcement. This strut is not a real strut in the transition region. It was the resultant force of all compressive struts transferred from column to shaft reinforcement which were distributed inside the peripheral hoops or spirals. Strut **AB** is also needed to maintain equilibrium at nodes **A** and **B**.

- The angle of strut **AD** is established to maintain equilibrium of node **A**. This compressive strut is assumed to form inside the column.

- Node **D** is placed at the intersection between struts **DF** and **AD**.

- Strut **CD** is required to maintain equilibrium at nodes **C** and **D**.

The tensile force of tie **BC** (i.e. T_{sp}) then is used to calculate the required amount of spiral to ensure that the maximum spiral strain at the top of the transition will be less than the yielding strain.

7.3 VERIFICATION OF DESIGN STRUT-AND-TIE MODEL

In order to verify the proposed strut-and-tie model for column-shaft connections, comparisons between amount of spirals of the transition suggested by the strut-and-tie model and those used in the test specimens are presented. The comparisons are performed for the three precast column/cast-in-place drilled shaft connection specimens tested at the University of Washington (Chapter 3), and four cast-in-place column/cast-in-place shaft connection specimens performed at UCSD by Murcia-Delso et al. (2013). Then, the proposed strut-and-tie model recommendations for the minimum spiral reinforcement are compared to those recommended by McLean et al. (1997), by the WSDOT BDM (2012), and by Murcia-Delso et al. (2013) which are presented in Chapter 2.

The dimensions and reinforcing details of the seven test specimens are summarized in Table 7-1. The four UCSD tests were conducted on cast-in-place column-to-shaft specimens. The key variables in these tests were the bar size, embedment length and amount of spiral reinforcement. Figure 7-4 shows a typical specimen. All of these specimens failed by hinging in the column, but some had significant inelastic strains in the transition region.

Figure 7-4. Cast-in-place column-shaft connection specimen (Murcia-Delso et al. 2013)

Table 7-1. Details of test specimens

Specimen	DS-1	DS-2	DS-3	UCSD-1	UCSD-2	UCSD-3	UCSD-4
Col. Diameter	20 in.	20 in.	20 in.	48 in.	48 in.	48 in.	48 in.
Clear Col. Height	60 in.	60 in.	60 in.	192 in.	216 in.	216 in.	192 in.
Span-to-depth Ratio	3	3	3	4	4.5	4.5	4
Column Longitudinal Reinf. Ratio	1.0 % (10#5)	1.0 % (10#5)	1.6 % (16#5)	1.6% (18#11)	2.2% (18#14)	2.2% (18#14)	1.4% (16 of 2#8)
Shaft Diameter	30 in.	30 in.	26 in.	72 in.	72 in.	72 in.	60 in.
Shaft Height	30 in.	30 in.	30 in.	108 in.	96 in.	96 in.	72 in.
Transition Length	28 in.	28 in.	28 in.	90 in.	72 in.	72 in.	37 in.
Shaft Longitudinal Reinf. Ratio	0.9 % (30 bundles of 2#3)	0.9 % (30 bundles of 2#3)	2.7 % (24 bundles of 3#4)	1.6% (28#14)	2.6% (26#18)	2.6% (26#18)	2.2% (20 bundles of 2#11)
Shaft Transverse Reinf. Ratio	0.17 % (2 gage-9 @ 3.0 in. pitch)	0.09 % (1 gage-9 @ 3.0 in. pitch)	0.60 % (3 gage-9 @ 1.5 in. pitch)	0.82% (2#6 @ 6.5 in.)	1.04% (2#7 @ 7.0 in.)	1.65%[1] (#8 @ 6.5 in. + 0.25-in. steel casing)	1.62% (2#7 @ 5.5 in.)

[1] Total equivalent amount of Grade 60 transverse reinforcement.

The magnitude and location of the forces acting at the boundary of the connection were calculated using moment-curvature sectional analysis (Table 7-2). For the precast concrete/shaft connection specimens performed at UW, the bottom of the transition was assumed at the level of the bottom of the column. For the cast-in-place column/shaft connection specimens performed at UCSD, the bottom of the transition were assumed to be located at the depth of $l_a + s + c$.

Table 7-2. Magnitudes and locations of the forces acting at the transition boundaries

Specimen	DS-1	DS-2	DS-3	UCSD-1	UCSD-2	UCSD-3	UCSD-4
Axial Load (kips)	159	159	159	800	800	800	800
Shear force (kips)	59	59	70	281	336	336	318
L (in.)	28	28	28	56	71	71	37
Tc (kips)	206	206	279	1644	2400	2400	1851
Cc (kips)	365	365	438	2444	3200	3200	2651
X_{Tc} (in.)	4.1	4.1	3.8	9.1	9.0	9.0	10.0
X_{Cc} (in.)	7.4	7.4	7.2	16.0	15.9	15.9	16.0
Ts (kips)	167	167	272	1040	1611	1611	1442
Cs (kips)	326	326	431	1840	2411	2411	2242
X_{Ts} (in.)	8.5	8.5	8.2	21.6	21.6	21.6	17.5
X_{Cs} (in.)	11.5	11.5	9.3	26.3	25.8	25.8	21.8

The results of the strut-and-tie model are shown in Table 7-3. In this table L_{sp} is the distance from the bottom of the transition to the centroid of the force in the shaft spiral in the transition, and L_A is the distance to node A.

Table 7-3. Results of strut-and-tie model

Specimen	DS-1	DS-2	DS-3	UCSD-1	UCSD-2	UCSD-3	UCSD-4
L_{sp} (in.)	22.6	22.6	21.5	42.0	54.2	54.0	27.4
L_A (in.)	2.0	2.0	2.0	17.5	26.2	26.2	11.4
T_{sp} (kips)	35.7	35.7	61.4	528.6	724.2	729.5	674.6
$f_{y,sp}$ (ksi)	80	80	80	68.4	68.4	47	68.4
$\left(\frac{A_{sp}}{s}\right) used\ (\frac{in.^2}{in.})$	0.0115	0.0057	0.0344	0.1354	0.1714	0.3715	0.0115
$\left(\frac{A_{sp}}{s}\right)\ STM\ model$ $(in.^2/in.)$	0.0159	0.0159	0.0358	0.2061	0.2122	0.4829	0.0213
$\frac{\left(\frac{A_{sp}}{s}\right) used}{\left(\frac{A_{sp}}{s}\right) req.}$	0.72	0.36	0.96	0.66	0.81	0.77	0.54
Measured maximum strain of spiral	0.0035	0.0116	0.0028	0.0024	0.0030	0.0027	0.0220
Maximum spiral strain to yielding strain ratio	1.27	4.21	1.02	1.02	1.27	1.67	9.33

The relationship between the ratio of maximum measured spiral strain-to-yielding strain and the ratio of (A_{sp}/s)_required to (A_{sp}/s)_used are shown in Figure 7-5. For specimens DS-2 and UCSD-4, the values of spiral strain were larger than could be measured reliably, and the spirals of Specimen DS-2 fractured.

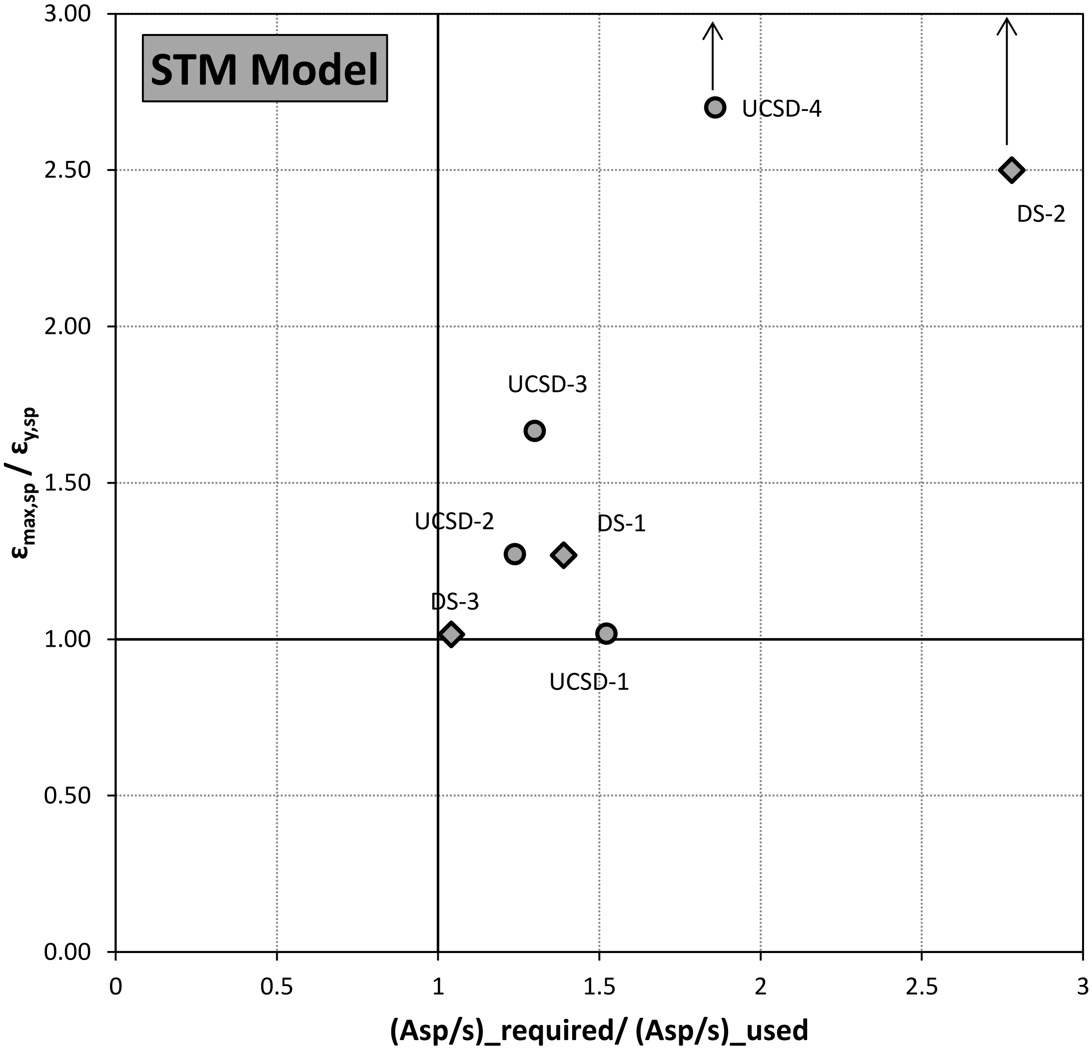

Figure 7-5. Spiral strain vs. transverse reinforcement (STM model)

The plots are divided into 4 regions as given:

$$(1)\begin{cases}\dfrac{\varepsilon_{max,sp}}{\varepsilon_{y,sp}} \le 1\\[2ex] \dfrac{\left(\dfrac{A_{sp}}{s}\right)_{required}}{\left(\dfrac{A_{sp}}{s}\right)_{used}} \le 1\end{cases} \qquad (2)\begin{cases}\dfrac{\varepsilon_{max,sp}}{\varepsilon_{y,sp}} \le 1\\[2ex] \dfrac{\left(\dfrac{A_{sp}}{s}\right)_{required}}{\left(\dfrac{A_{sp}}{s}\right)_{used}} \ge 1\end{cases}$$

$$(3)\begin{cases}\dfrac{\varepsilon_{max,sp}}{\varepsilon_{y,sp}} \ge 1\\[2ex] \dfrac{\left(\dfrac{A_{sp}}{s}\right)_{required}}{\left(\dfrac{A_{sp}}{s}\right)_{used}} \le 1\end{cases} \qquad (4)\begin{cases}\dfrac{\varepsilon_{max,sp}}{\varepsilon_{y,sp}} \ge 1\\[2ex] \dfrac{\left(\dfrac{A_{sp}}{s}\right)_{required}}{\left(\dfrac{A_{sp}}{s}\right)_{used}} \ge 1\end{cases}$$

If data points are in region 1 or 4, the model is good because it shows that if the connection is designed with enough amount of transverse reinforcement, the transverse reinforcement will work in the elastic range (Region 2). If the transverse reinforcement is not enough, the transverse reinforcement will yield (Region 4). If data points are in region 2, even the model can not predict the outcome exactly, but the design is conservative and still can be used. If data points are in region 3, the model is not suitable because even when the design uses more transverse reinforcement than required by the model, the transverse reinforcement is still yielding. The proposed strut-and-tie model provides all seven data points in region 2. It suggests that this model will be suitable for designing the column-shaft connection.

Similarly, in Figure 7-6, Figure 7-7, and Figure 7-8 respectively, the measured strains are compared with the recommendations for the minimum transverse reinforcement proposed by McLean et al. (1997), by WSDOT BDM (2012), and by Murcia-Delso et al. (2013) (Table 7-4).

Table 7-4. Comparison of transverse reinforcement equations

McLean et al. (1997)	WSDOT BDM	UCSD (Murcia-Delso et al. 2013)
$\frac{A_{tr}}{s} = \frac{A_l f_u}{2\pi f_{y,tr} l_s}$	$\frac{A_{tr}}{s} = \frac{k A_l f_u}{2\pi f_{y,tr} l_s}$ where k = 0.5	$\frac{A_{tr}}{s} = \frac{N_{col} d_{b,col} \tau_u}{2\pi f_{y,tr}} = \left(\frac{A_l f_u}{2\pi f_{y,tr} l_s}\right)\left(\frac{\tau_u}{f_u}\right)\left(\frac{l_s}{d_{b,col}}\right)\left(\frac{4}{\pi}\right)$ where τ_u is the ultimate bond strength of column longitudinal reinforcement, which can be taken to be 2.4 ksi for 5-ksi concrete

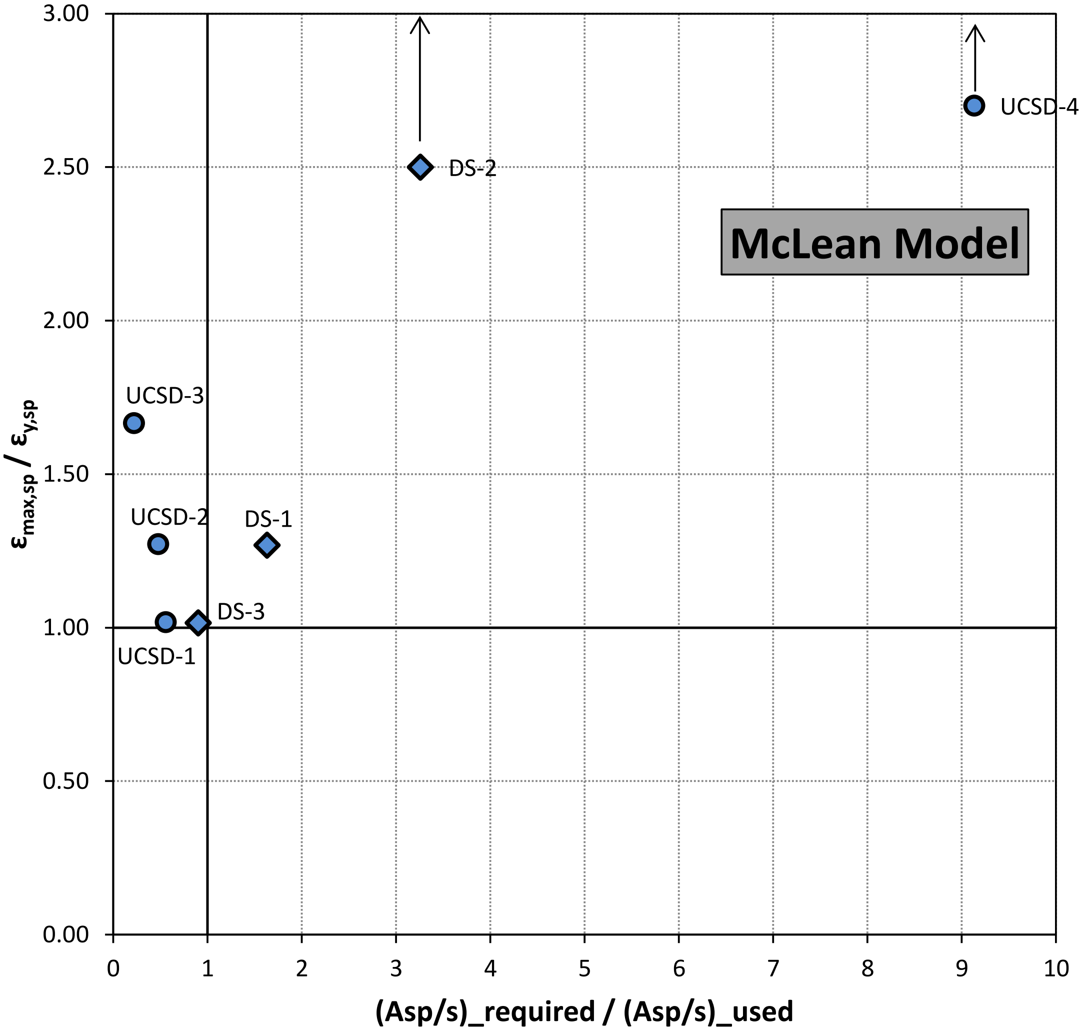

Figure 7-6. Spiral strain vs. transverse reinforcement (McLean's model)

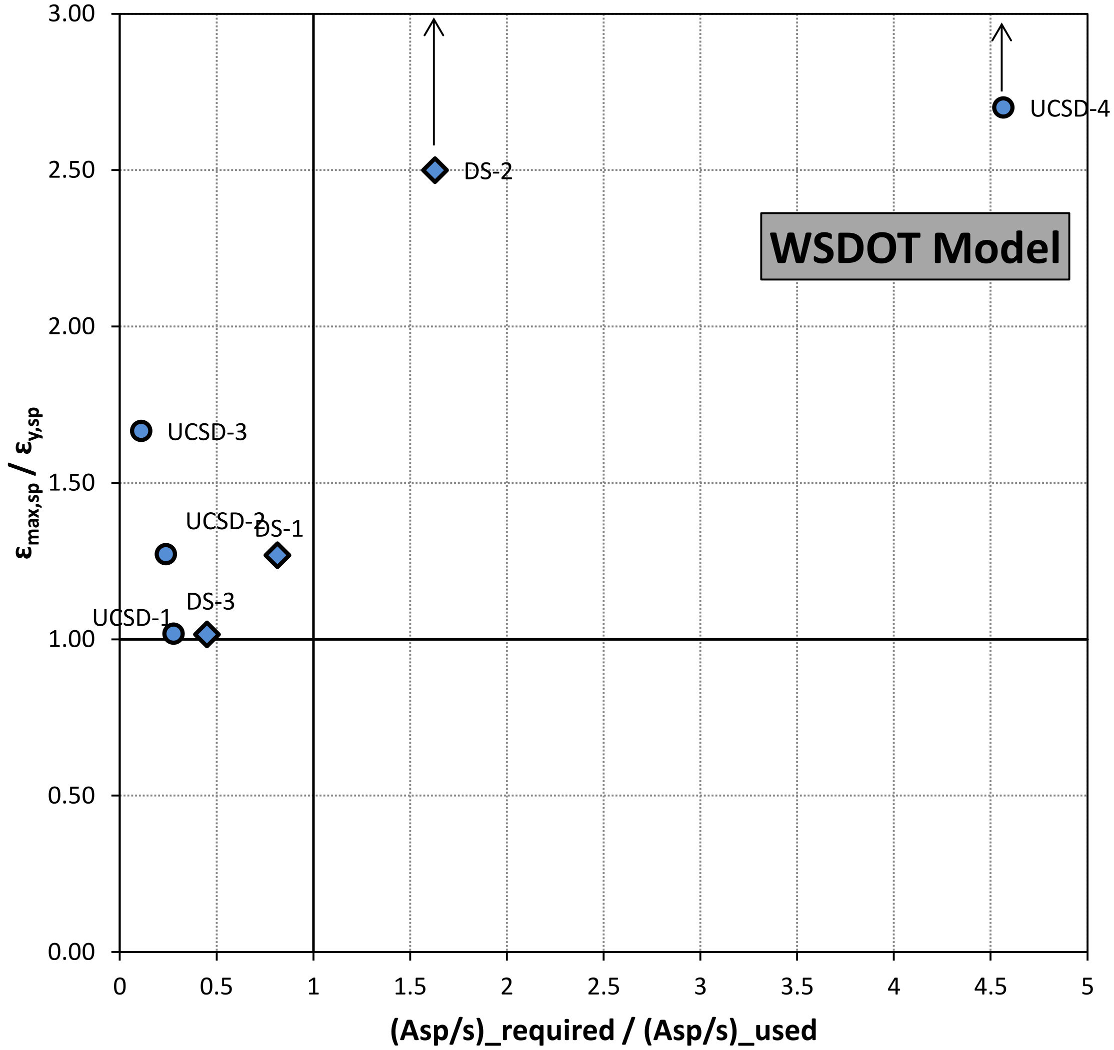

Figure 7-7. Spiral strain vs. transverse reinforcement (WSDOT's model)

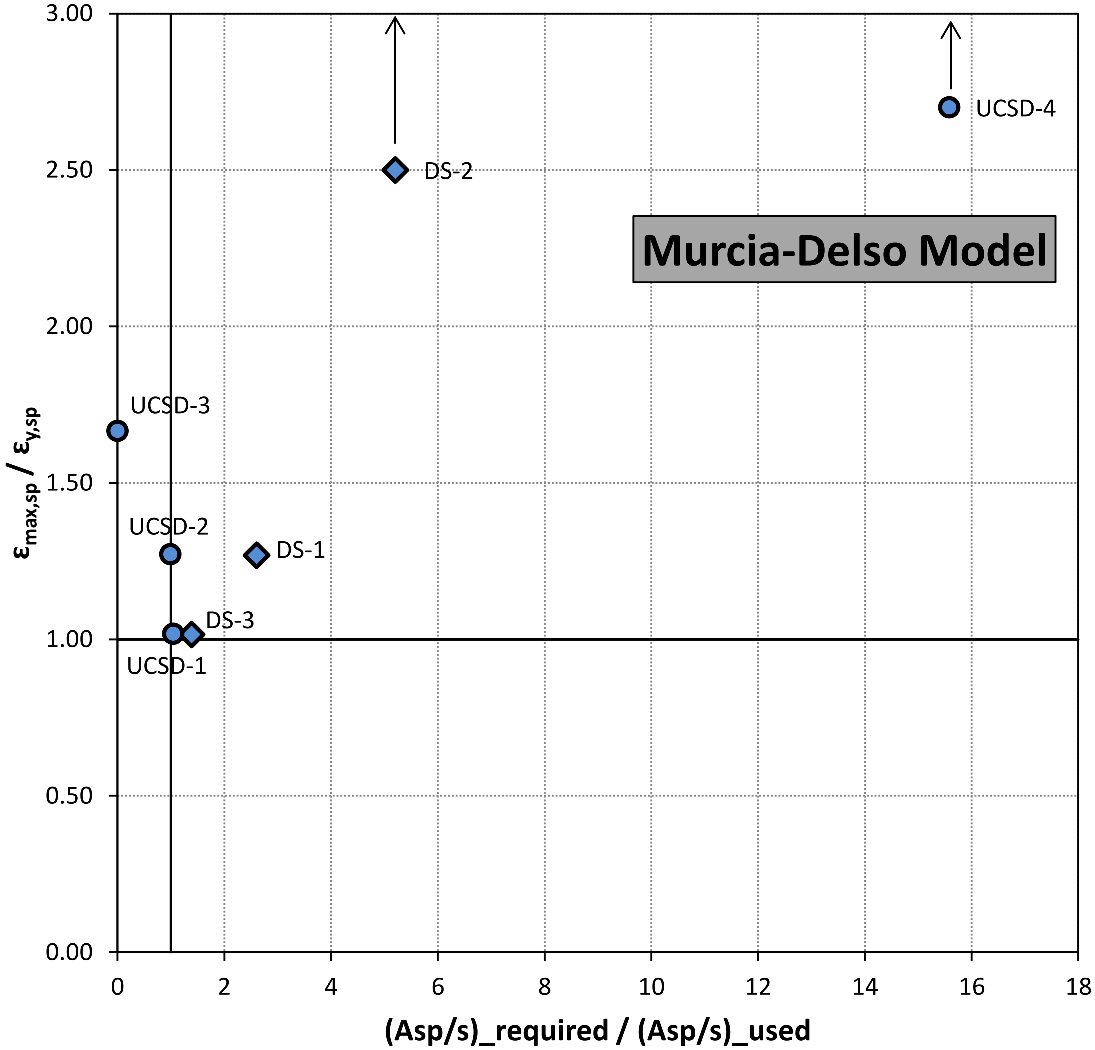

Figure 7-8. Spiral strain vs. transverse reinforcement (Murcia-Delso's model)

The figures shows that McLean's model and WSDOT's model are not suitable modal since most of their data points are in region 3. The model proposed by Murcia-Delso et al. (2013) seem to be a suitable model when only one data point (Specimen UCSD-3) is in region 3. The model expects that with the steel casing outside the connection, no spiral is required. However, the strain gauges indicated that the top of the tube yielded.. Besides, this model also require too much amount of spirals which cannot fit in the space for Specimen UCSD-4. A closer result comparison between Murcia-Delso's model and the proposed strut-and-tie model are shown in Figure 7-9.

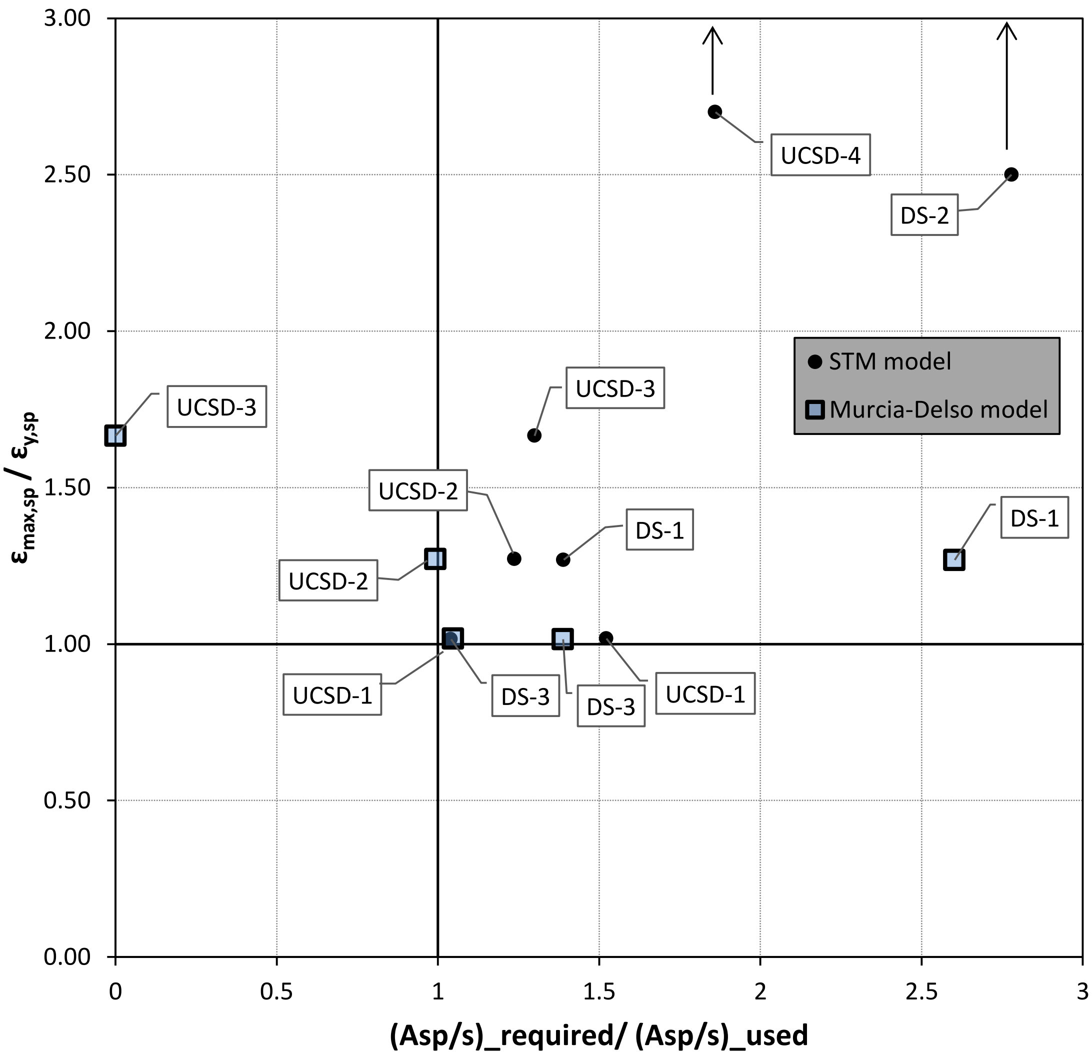

Figure 7-9. Comparison of STM model and Murcia-Delso's model

In comparison with the other models, the proposed strut-and-tie model better correlates with the observed test performance. When the amount of spiral used in specimens was close to the required values, the maximum strain of spiral was close to the yielding strain. In contrast, as the difference between amount of required and provided spiral increased, the maximum strain of spiral increased rapidly over the yielding strain.

Furthermore, the strut-and-tie model predicted well in case when steel casing was used as an additional spiral. In the Specimen UCSD-3, a 0.25-in thick steel casing (72-in diameter) was used together with No. 8 at 6.5 in. pitch spiral in the connection, which was an equal amount of

1.65% volumetric ratio of Grade 60 transverse reinforcement. In this case, the other models predict that almost no spirals needed. Only strut-and-tie model predicts that more spirals is needed to ensure that no yielding strain in the connection. In fact, the steel casing was yield at the top of connection as predicted.

CHAPTER 8.
SUMMARY AND CONCLUSIONS

8.1 SUMMARY

A new system is proposed for connecting drilled shafts to precast columns in bridge bents. It is adapted from the "socket" connection proposed for connecting a precast column to a cast-in-place spread footing by Haraldsson et al. (2011), and consists of embedding a precast column into the cast-in-place transition region of the drilled shaft. The connection was design to facilitate rapid on-site construction through the use of pre-fabricated elements. The system is suitable for use in seismic regions.

Three drilled shaft specimens (DS-1, DS-2 and DS-3) were fabricated and tested at the University of Washington. This chapter summarizes the construction procedure, the design methodology, the test specimens and performance, and an analytical model used to study the connection. Later, a design model was proposed and verified not only with 3 specimens tested at the University of Washington, but also with 4 cast-in-place column-to-shaft connection specimens tested at the University of California, San Diego. This design model was also compared to other current design models.

8.1.1 Construction Sequence

The connection was developed to accelerate the construction bridges. The field construction sequence (Figure 1-2) is as follows:

- A precast column is cast. The surface is roughened in the region where the column will be embedded in the cast-in-place drilled shaft.
- The hole for the shaft is bored, the reinforcing cage is placed, and the shaft is cast up to the bottom of the transition region (approximately ten feet below grade).

- The precast column is positioned in the transition region of the drilled shaft, leveled and braced.
- The concrete of the transition region is cast around the precast column.

8.1.2 Test Specimens

Three specimens were tested as part of this research. The first two specimens were designed to represent a 6-ft (72-in.) diameter column embedded in a 9-ft (108-in.) diameter shaft. The scale factor (1/3.6, or 28%) was chosen to match the 20-in. diameter of column specimens tested by previous researchers (e.g., Haraldsson et al. 2011, and Janes et al. 2011). At 28% scale, the shaft diameter of the laboratory specimens was 30 in.

Both specimens DS-1 and DS-2 had a shear span ratio of 3.0, a column longitudinal reinforcement ratio of 1.0%, and a shaft longitudinal reinforcement ratio of 0.9%. The only difference between specimens DS-1 and DS-2 was that DS-1 contained the full amount of spiral specified by WSDOT for a cast-in-place system (0.17%), and DS-2 contained half that amount (0.09%). These amounts of spiral were selected to promote failure in the column in Specimen DS-1 and in the shaft transition region in Specimen DS-2, in order to develop an understanding of the load transfer mechanism there.

Specimen DS-3 was not a prototype-based specimen. It was designed, after the first two had been tested, to investigate the mechanism of force transfer within the transition region, and in particular the contribution of the concrete to hoop tension strength. Consequently, its transition region had a smaller diameter (26 in.) but more column longitudinal reinforcement (1.60%) and more shaft reinforcement than the other two specimens (Table 7-1).

In all specimens, a cast-in-place base was built monolithically with the transition region in order to attach the specimen to the self-reacting testing frame.

8.1.3 Test Performance

Quasi-static, cyclic lateral load tests were performed to evaluate the seismic performance of the three specimens.

In each test, the specimen was subjected to a constant, axial load of 159 kips (which represented the unfactored dead load at laboratory scale), accompanied by a cyclic, displacement-controlled lateral loads. The displacement history was a modification of a loading history for precast structural walls recommended in NEHRP, which had been used in previous tests at the University of Washington.

The behavior of specimens DS-1 and DS-3 were controlled by column behavior. Failure occurred by plastic hinging in the column (Table 5-1) while the connection region in the shaft remained largely undamaged. Testing was stopped when almost all the column longitudinal reinforcement had fractured. In Specimen DS-2, a prying failure occurred (Figure 6-25b) in the connection between the column and the shaft. Testing was stopped when all the spiral reinforcement in the shaft had fractured.

The prying failure in DS-2 occurred because the transverse reinforcement was not sufficient. In contrast with lap splice failure, the prying failure occurs even when the tension force still can transferred from the column reinforcement to the shaft reinforcement. The prying failure occurred, because only the spirals at the top part of the transition were activated. When the top spirals were fractured, the lower spirals were then activated. This behavior is different with most current predicting models that assume a uniform spiral strain distribution in the connection.

8.1.4 Response Data

The specimens were heavily instrumented. The measured data included transverse loads and displacements, deflections and rotations of column and shaft (measured by potentiometers and a motion-capture system), strains in the column and shaft longitudinal reinforcement, and strains in the shaft spiral.

The measured data was consistent with the observed modes of failure for the three specimens. For specimens DS-1 and DS-3, the columns contributed most to the overall specimen deformations. By contrast, the deformations in Specimen DS-2 were dominated by deformation of the shaft at large displacements.

8.1.5 Strut-and-Tie Model

Based on the test observations and measurement, the load transfer within the transition region was modeled using a strut-and-tie model. This model is necessarily a simplification of the true behavior, but it provides reasonable agreement with the experimental results and helps to identify the probable load paths. Besides, the proposed model can predict several modes of failure (includes prying failure) by checking the capacity of each elements of the model. It also provides the basis for a design methodology.

8.1.6 Design Procedure

A design procedure was proposed based on the strut-and-tie model. This method uses moment-curvature sectional analysis to determine forces acting at the boundary of the transition region. Then a strut-and-tie model is built in the transition region to transfer forces from the column to the shaft for (1) a specified distribution of spiral in the transition, and (2) an assumed parabolic distribution of spiral strains. Based on the internal forces of strut-and-tie model, the amount of spiral area is chosen to ensure that the maximum strain of spiral is equal or less than yielding strain, and that the plastic hinge forms above the transition region.

This design procedure was applied to 3 specimens tested at the University of Washington and 4 cast-in-place column/ cast-in-place shaft connection specimens tested at the University of California, San Diego (Murcia-Delso et al. 2013), and compared to other design models' results. It shows that the new design method predicted the specimen behavior better than the other models.

8.2 CONCLUSIONS

From the results obtained in these tests and analyses, the following conclusions can be drawn for the behavior and design of the column-to-shaft connection.

(1) Provision of the amount of spiral reinforcement required for conventional column-to-drilled shafts connection cannot ensure to form the desired behavior for all configurations. In some cases, the results of current methodologies are too conservative, and in other cases they are not enough. Current methods do not

consistently predict the observed modes of failures and spiral strains in the connections.

(2) Variations in the amount of transverse shaft reinforcement can cause the failure mechanism to change from the column to the connection. In this study, use of half of the conventional amount of shaft spiral caused failure to occur in the shaft, by prying action of the concrete shell surrounding the precast column.

(3) The vertical distribution of the spiral used in the transition region of the test specimens was uniform. However, the strains in the spiral steel were higher at the top and lower at the bottom of the transition. This variation in strains suggests that a more efficient design could be achieved by using a non-uniform distribution of spiral, with the majority of spiral reinforcement concentrated near the top of the transition.

(4) The test specimens contained no external confining steel shell around the top of the transition region. If one were used, it provide some of the benefits of additional spiral, and may offer the possibility of reducing the amount of spiral as seen in one test specimen (UCSD-3) performed at the University of California, San Diego for CIP column-shaft connection (Chapter 7).

(5) The vertical reinforcement in the shaft is likely to be controlled by the peak moments, which typically occur at some distance below the transition region. It is therefore unlikely to prove critical in the design of the transition region.

(6) Mechanical anchor heads provide a convenient and reliable means of anchoring the column longitudinal bars. In this study, mechanical anchor heads were used at the ends of the column longitudinal reinforcement to allow the shortest possible transition region. No anchorage failure occurred. Anchor heads were not used for the shaft bars, and the bars showed no sign of anchorage failure.

(7) The concrete contributes most to the hoop tensile strength of the transition region at small drift ratios. However, under large cyclic excitation, it cracks extensively and its contribution reduces dramatically.

(8) The proposed strut-and-tie model predicted the mode of failure in, and provided satisfactory agreement with, the experimental results of three specimens constructed with precast columns.

(9) The proposed design procedure provides a method for designing the connection between a precast column and a cast-in-place shaft. It was verified against the three precast specimens tested at the University of the Washington. Because no other data were available for precast columns, the method was also applied to four cast-in-place column-shaft connections tested at UCSD. In all cases it provided better correlation with measured results than did the three available methodologies proposed by others.

(10) The method is also applicable to cast-in-place connections, because none of the failure modes envisaged in it depends on the precast-cip interface.

(11) The model was compared only with shafts containing uniformly spaced spiral. However, it can be applied to spiral with any distribution, and the test results suggest that it would be advantageous to place the majority of the spiral at the top of the shaft.

(12) If a steel casing is left in place at the top of the shaft, its contribution to hoop tension strength may be taken into account in the model and added to the resistance offered by the shaft spiral. In determining the casing's strength, due consideration should be paid to the effects of corrosion over time.

8.3 RECOMMENDATIONS FOR FUTURE RESEARCH

Due to the high cost of the experiments, only a small range of parameters can be evaluated experimentally. The proposed strut-and-tie model cannot predict the ductility, displacements and deterioration progress of the whole system under repeated cyclic loading. More complex models are needed to reliably predict the response of other specimen details and configurations.

An analytical investigation using three-dimensional finite element software did not successfully reproduce key observed behavior, including the failure modes. These investigations should be continued until they can reproduce the column-shaft connection experimental behavior. The model should predict the right force capacities, spiral strains, deformation distribution and modes of failures for the tested specimens.

Once the model has been shown to be reliable, it could be used to study the influence of other parameter such as: transition length, column-shaft diameter ratio, and column reinforcement ratio.

ACKNOWLEDGEMENTS

A debt of gratitude is due to professors John F. Stanton and Marc O. Eberhard, for their inspiration, friendship and guidance. Thanks to Vietnamese Education Foundation (VEF) for giving me a great chance in my life. Thanks to my friends Todd Janes, Olafur Haraldsson, Bo-Shiuan Wang, Po-Chien Hsio, Patricia Clayton, Tu Nguyen, Travis Thonstad, Max Stephens, and Andy Sen for making graduate school an enjoyable experience. Thanks to my family for always being so supportive and encouraging. Last but not least, this research could never have been achieved without the patience, encouragement, and understanding of my wife, Hang, and I apologize for the many long nights and lost weekends.

REFERENCES

AASHTO (2009). “*LRFD Bridge Design Specifications*” 4th ed., American Association of State Highway and Transportation Officials, Washington, DC.

“*AASHTO Guide Specification for LRFD Seismic Bridge Design*” (2009). AASHTO, Washington DC.

ACI Committee 318 (2008). “*Building Code Requirements for Structural Concrete and Commentary*.” *ACI 318-08*, American Concrete Institute, Farming Hills, MI.

Berry, M. P., and Eberhard, M. O. (2004). “*PEER Structural Performance Database User’s Manual.*” Pacific Earthquake Engineering Research Center Report 2004, <www.ce.washington.edu/~peeral>, University of California, Berkeley, CA.

Brown, W. (2008). “*Bar Buckling in Reinforced Concrete Bridge Columns.*” Master’s Thesis, University of Washington, Seattle, WA.

Building Seismic Safety Council for the FEMA. (2004) “*NEHRP Recommended Provisions for Seismic Regulations and for New Buildings and Other Structures (FEMA 450) 2003 Ed.*,” Washington D.C.

Caltrans (2006). “*Seismic Design Criteria Version 1.4*”. Caltrans, Sacramento, CA.

Cohagen, L.S. Pang, J.B.K., Steuck, K.P., Eberhard, M.O. and Stanton, J.F. (2008), “*A Precast Concrete Bridge Bent Designed to Re-center after an Earthquake*,” Washington State Department of Transportation Report, WA-RD 684.3, Olympia, Washington, October, 184 pp.

FHWA (2006). “*2006 Condition and Performance Report*.” U.S. Department of Transportation, Federal Highway Administration.

Haraldsson, O. (2011). “*Spread Footing Socket Connections for Precast Columns.*” Master’s Thesis, University of Washington, Seattle, WA.

Hieber, D.G., Wacker, J.M., Eberhard, M.O. and Stanton, J.F. (2005), "*Precast Concrete Pier Systems for Rapid Construction of Bridges in Seismic Regions*," Washington State Department of Transportation Report WA-RD 611.1, Olympia, Washington, March, 312 pp.

Hieber, D.G., Wacker, J.M., Eberhard, M.O. and Stanton, J.F. (2005), "*State-of-the-Art Report on Precast Concrete Systems for Rapid Construction of Bridges*," Washington State Department of Transportation Report WA-RD 594.1, Olympia, Washington, March, 112 pp.

Ingham, J., (1995), "*Seismic performance of bridge knee joints,*" Doctoral dissertation, Univ. of California, San Diego, USA.

Janes, T. (2011). "*Precast Column Socket Connections for Thin Spread Footings*." Master's Thesis, University of Washington, Seattle, WA.

Kent, D.C., and R. Park (1971). *"Flexural Members with Confined Concrete,"* Journal of the Structural Division, ASCE, Vol. 97, No. 7, July, pp. 1969-1990.

Mander, J.B., M.J.N. Priestley, and R. Park (1988). *"Theoretical Stress-Strain Model for Confined Concrete,"* Journal of the Structural Division, ASCE, Vol. 114, No. 8, August, pp. 1804-1826.

Marsh, L. (2009). Personal communication with J. Stanton.

Matsumoto, E., Waggoner, M., Sumen, G., Kreger, M., Wood, S., and Breen, J. (2001). *"Development of a Precast Bent Cap System,"* Center for Transportation Research, Research Project 0-1748, University of Texas at Austin.

McLean, D.I. and Smith C.L. (1997), "*Noncontact Lab Splices in Bridge Column-Shaft Connections*," Washington State Department of Transportation Report WA-RD 417.1, Olympia, Washington, July.

Moustafa, S., (1989). "*Ductile Pullout Connections*". Concrete Technology Associates, CTA Bulletin 74B11. Now available from the Precast and Prestressed Concrete Institute, Chicago, IL.

Murcia-Delso, J., Shing, P. B., Stavridis, A., Liu, Y. (2013), “ *Required embedment length of column reinforcement extended into type II shafts*,” Structural Systems Research Project, Rep. No. SSRP 13/05, Univ. of California, San Diego, USA.

Nakaki, S.D., Stanton, J.F., Sritharan, S. (1999). “*Overview of the PRESSS Five Story Precast Test Building*,” *PCI Jo.*, 44(2), March-April 1999, pp 26-39.

Osanai, Y., Watanabe, F. and Okamoto, S., (1996). “*Stress Transfer Mechanism of Socket Base Connections with Precast Concrete Columns*”. ACI Structural Journal, ACI, Chicago. IL. May-June, pp. 266-276.

Pang, B.K., Eberhard, M.O., and Stanton, J.F. (2010), “*Large-Bar Connection for Precast Bridge Bents in Seismic Regions*,” Journal of Bridge Engineering, ASCE, May-June, pp 231-239.

Pang, J.B.K., Steuck, K.P., Cohagen, L.S., Eberhard, M.O. and Stanton, J.F. (2008), “*Rapidly Constructible Large-Bar Precast Bridge-Bent Connection*,” Washington State Department of Transportation Draft Report, WA-RD 684.2, Olympia, Washington, October, 184 pp.

Precast/Prestressed Concrete Institute (2004). “*PCI Design Handbook*”. 6th ed. Chicago, IL.

Priestley, M. J. N., Seible, F. and Calvi, G. M. (1996), “ *Seismic Design and Retrofit of Bridges*,” John Wiley & Sons, Inc., Hoboken, NJ, USA.

Priestley, M. J. N., (1993), “ *Assessment and design of joints for single-level bridges with circularc columns*,” Structural Systems Research Project, Rep. No. SSRP 93/02, Univ. of California, San Diego, USA.

Raynor, D.J., Lehman, D.L. and Stanton, J.F. (2002). “*Bond-Slip Response of Reinforcing Bars Grouted in Ducts*”. *ACI Str. Jo.* 99(5), Sept. pp 568-576.

Schlaich, J., Schäfer, K., and Jennewein, M. (1987). “*Toward a Consistent Design of Structural Concrete*”. *PCI Journal*,V. 32, No. 3, May-June, pp. 74-150.

Schlaich, J. and Schäfer, K., "*Design and Detailing of Structural Concrete Using Strut-and-Tie Models*," The Structural Engineer, Vol. 69, No. 6, March 1991, pp. 113-125.

Sritharan, S., (1998), "*Analysis of concrete bridge joints subjected to seismic actions*," Doctoral dissertation, Univ. of California, San Diego, USA.

Stanton, J.F. (2010), Moment-curvature program, University of Washington, Seattle, WA.

Steuck, K.P., Pang, J.B.K., Eberhard, M.O. and Stanton, J.F. (2008), "*Anchorage of Large-Diameter Reinforcing Bars Grouted into Ducts*," Washington State Department of Transportation Report, WA-RD 684.1, Olympia, Washington, July, 148 pp.

Steuck, K., Stanton, J.F. and Eberhard, M.O. (2009) "*Anchorage of Large-Diameter Reinforcing Bars in Ducts*," *ACI Str. Jo.*, July-August, pp 506-513.

Wacker, J.M, Hieber, D.G., Eberhard, M.O. and Stanton, J.F. (2005), "*Design of Precast Concrete Piers for Rapid Construction in Seismic Regions*," Washington State Department of Transportation Report, WA-RD 629., Olympia, Washington.

Xiao, Y., Priestley, M.J.N., and Seible, F. (1996). "*Seismic Assessment and Retrofit of Bridge Column Footings*". *ACI Str. Jo.*, ACI, Farmington Hills, MI. Jan-Feb., pp. 79-94.

APPENDIX A: SPECIMEN CONSTRUCTION DRAWINGS

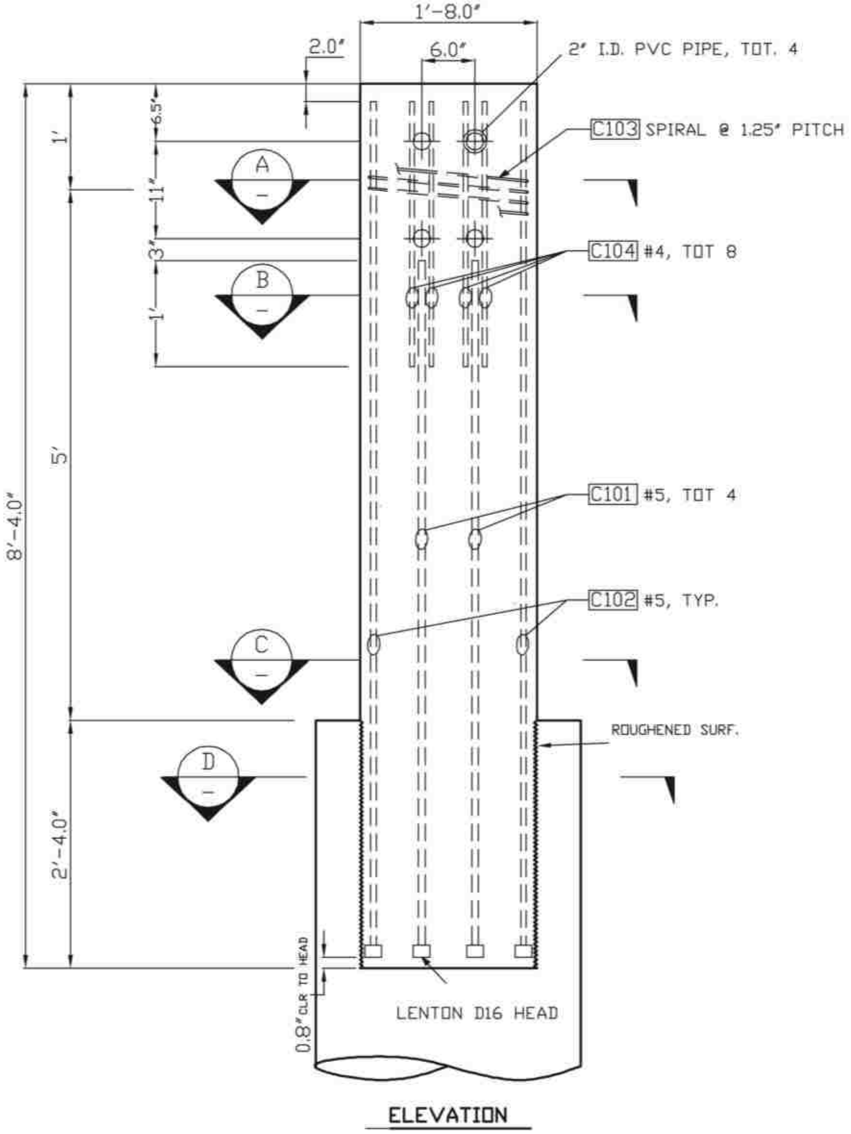

Figure A-0-1.Column elevation

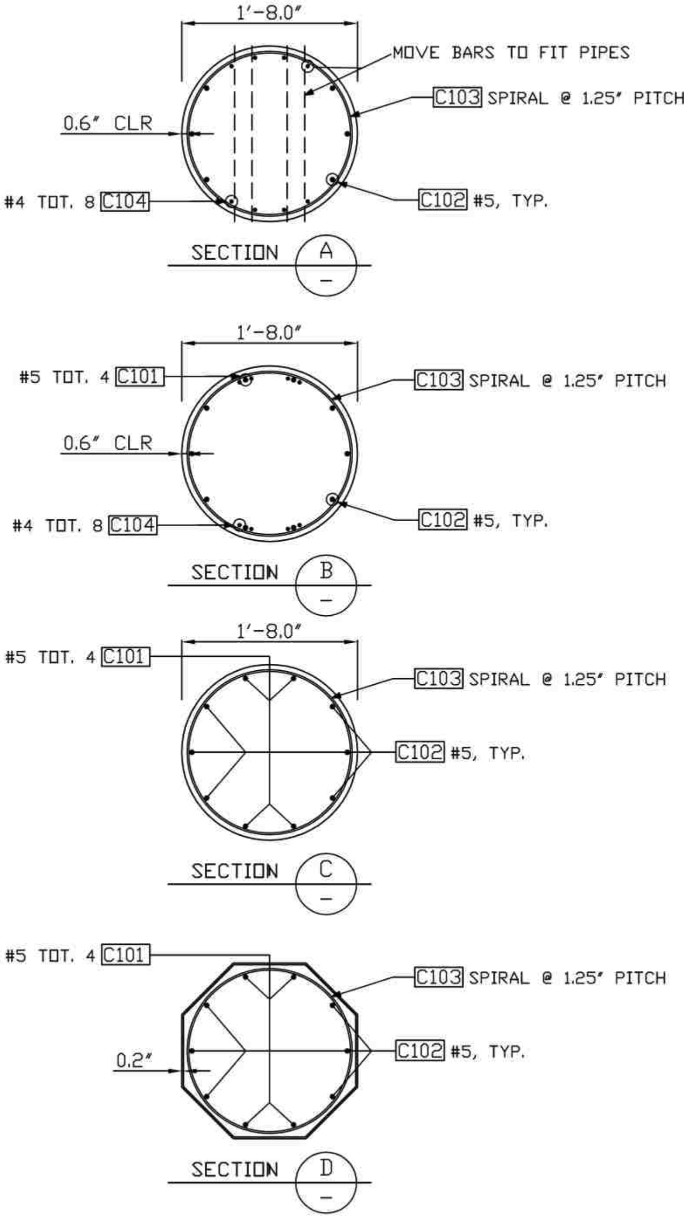

Figure A-0-2.Column sections

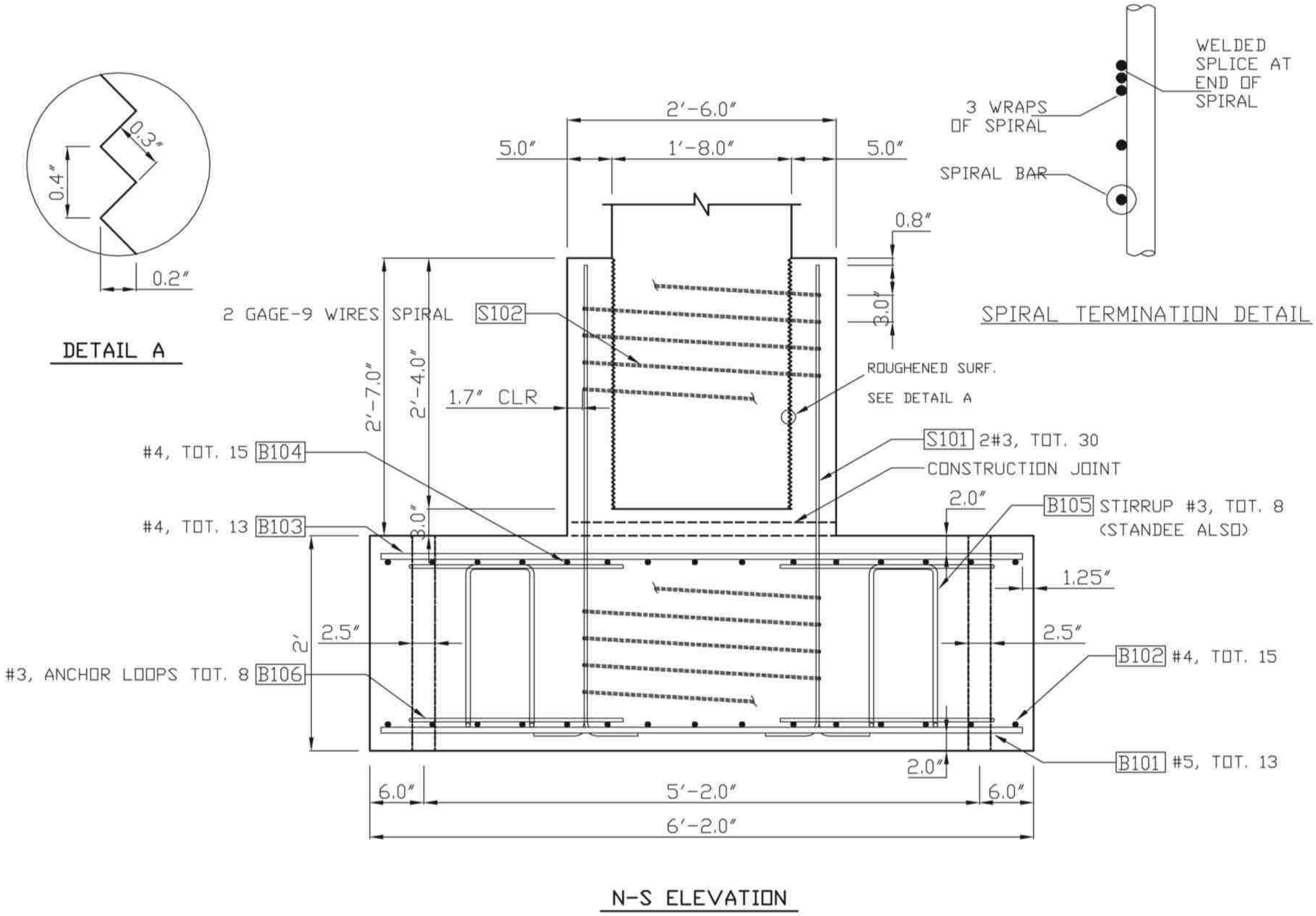

Figure A-0-3.Shaft & base – Longitudinal section

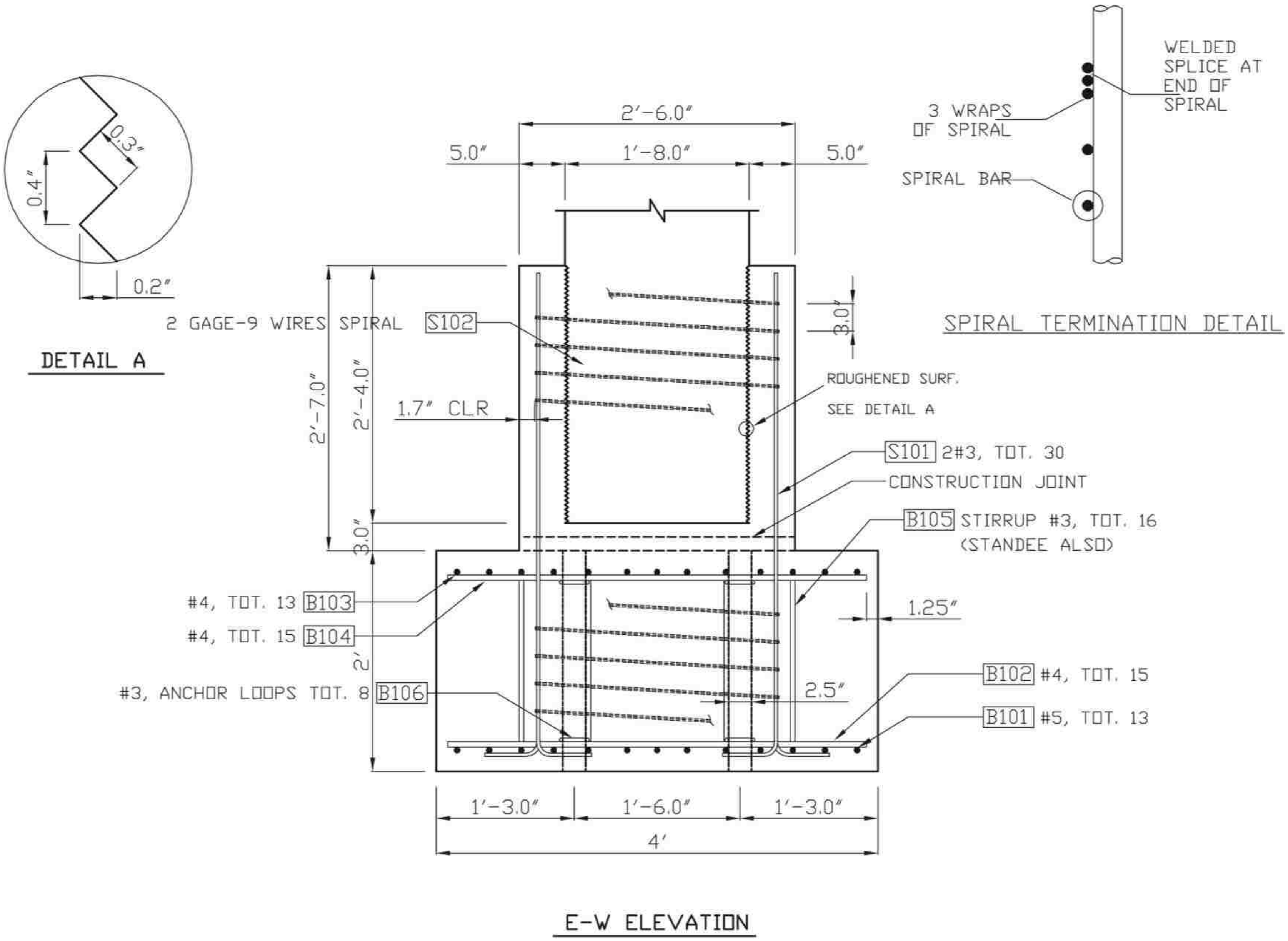

Figure A-0-4.Shaft & base – Transverse section

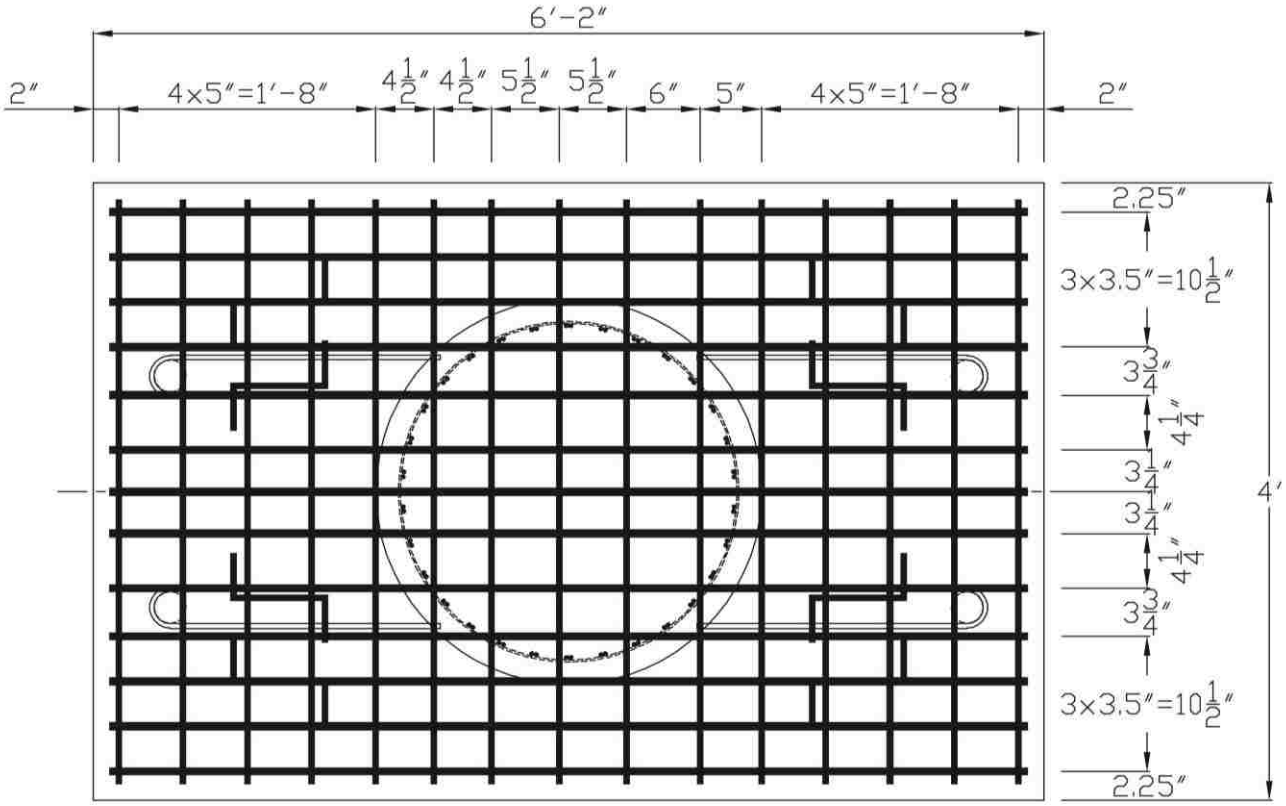

Figure A-0-5.Shaft & base reinforcement arrangement

APPENDIX B: MATERIAL TESTS

B.1 CONCRETE STRENGTHS

All specimens DS-1, DS-2 and DS-3 used the common concrete mix with code 09468 provided by Calportland Company. The concrete design strength was 6000 psi. It used 3/8-in aggregate pea gravel and had a specified slump of 5-in.

The concrete compressive strength at 7, 14, 28 day and testing day are provided in the following table.

Table B-0-1. Concrete compressive strength

Time	7-Day (psi)	14-Day (psi)	28-Day (psi)	Day of Test (psi)
DS-1 Column	5130	5820	6250	7770
DS-1 Shaft	5320	6350	6600	7360
DS-2 Column	4780	6350	6600	7170
DS-2 Shaft	5270	5790	6400	6450
DS-3 Column	4072		6147	7211
DS-3 Shaft	4737		6451	8388

B.2 REINFORCEMENT

Reinforcement used in the footing and column conformed to ASTM Standard 706. The column spiral used the 3-gauge wire (0.244-in dia.), which was the same as that used by Haraldsson et al. (2011) and Janes et al. (2011). The shaft spiral used the 9-gauge wire (0.148-in dia.). All spirals conformed to ASTM Standard A82.

The tension tests were performed using MTS system machine and the elongation was measured by an extensometer. The tension specimen was loaded slowly until the load reached its maximum and started reducing. The extensometer was then removed to prevent damage to the equipment. The specimen was then loaded until failure, after which the length was measured to obtain a strain at failure.

Results of the tension tests for longitudinal bars are shown in Figure B-0-1, Figure B-0-2, Figure B-0-3, and Figure B-0-4. Because the spirals were too small and extensometer cannot be used to measure the elongation, only the ultimate stresses of spirals were found (Table B-0-2).

Table B-0-2. Tensile strength of spirals

9-gauge wire (psi)	3-gauge wire (psi)
109,860	95,050

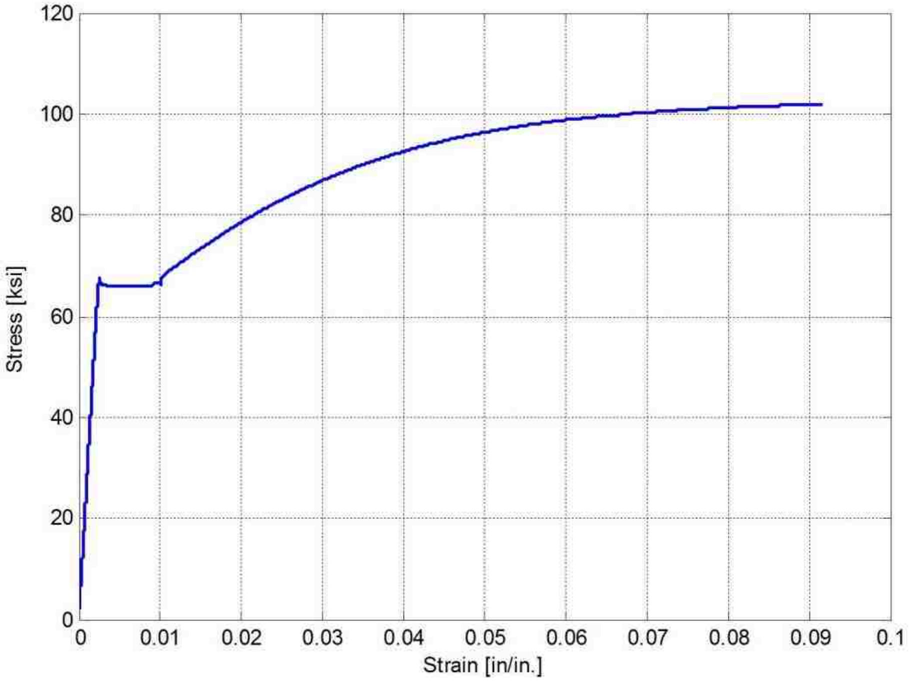

Figure B-0-1. Stress-strain curve for No. 3 bar (for DS-1 and DS-2)

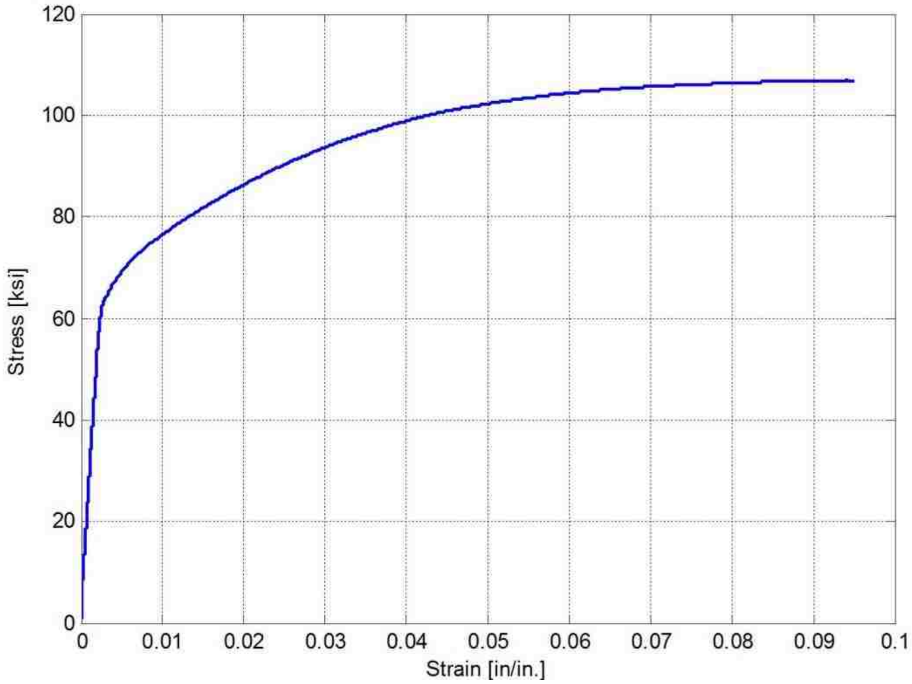

Figure B-0-2. Stress-strain curve for No. 5 bar (for DS-1 and DS-2)

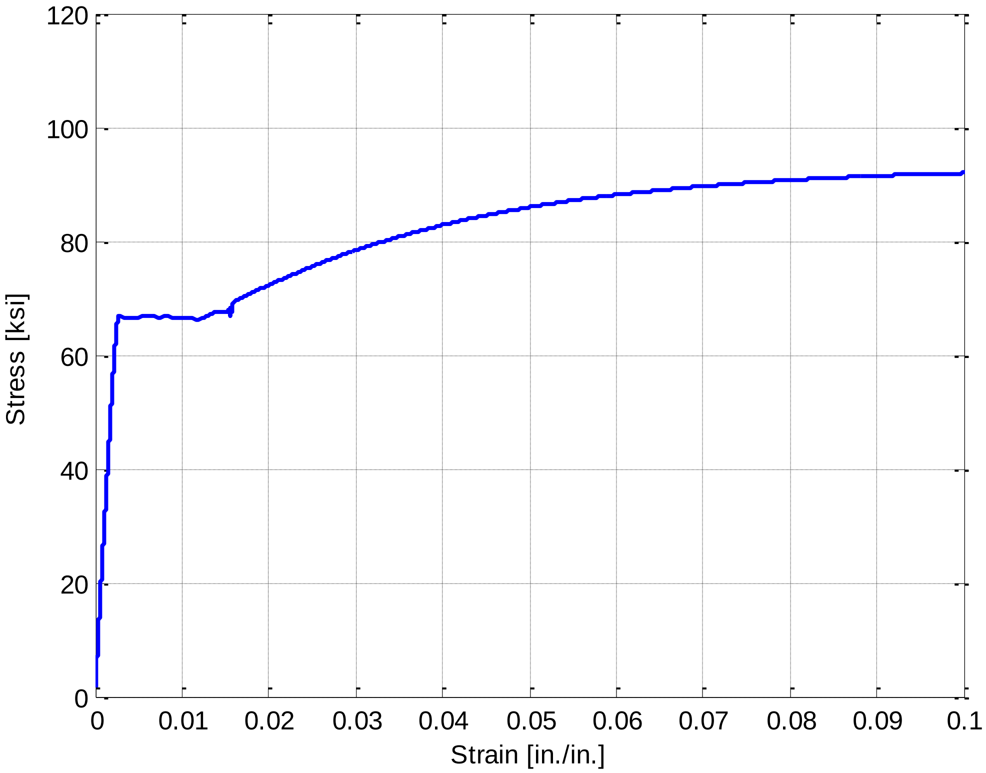

Figure B-0-3. Stress-strain curve for No. 4 bar (for DS-3)

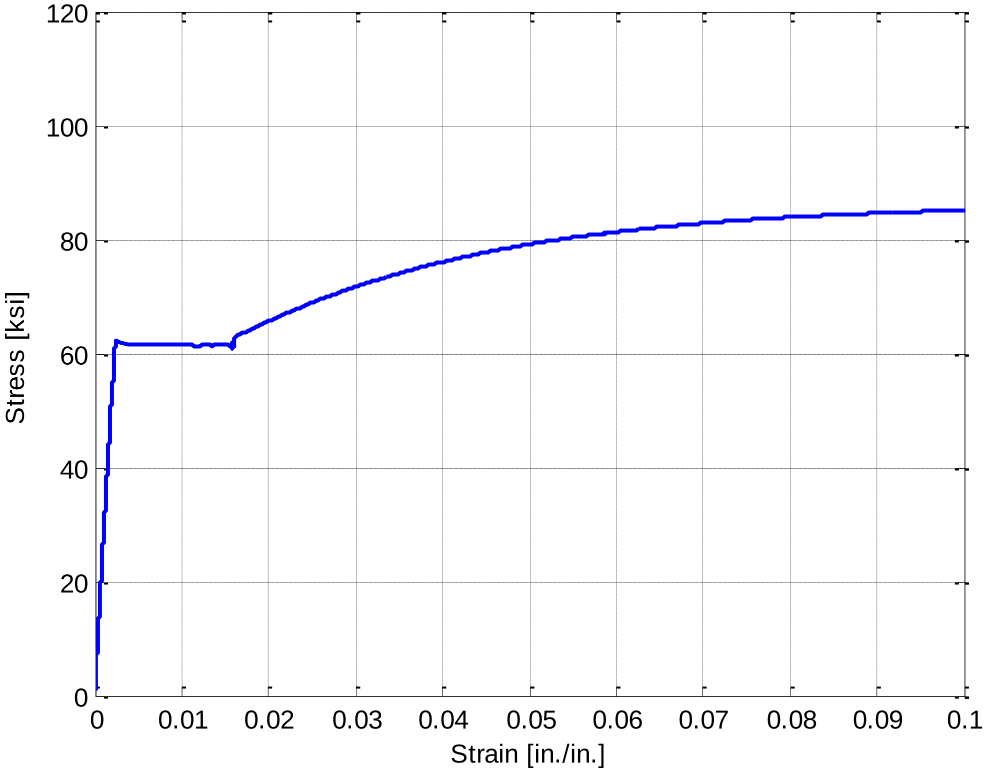

Figure B-0-4. Stress-strain curve for No. 5 bar (for DS-3)

APPENDIX C: DAMAGE PROGRESSION

C.1 SPECIMEN DS-1

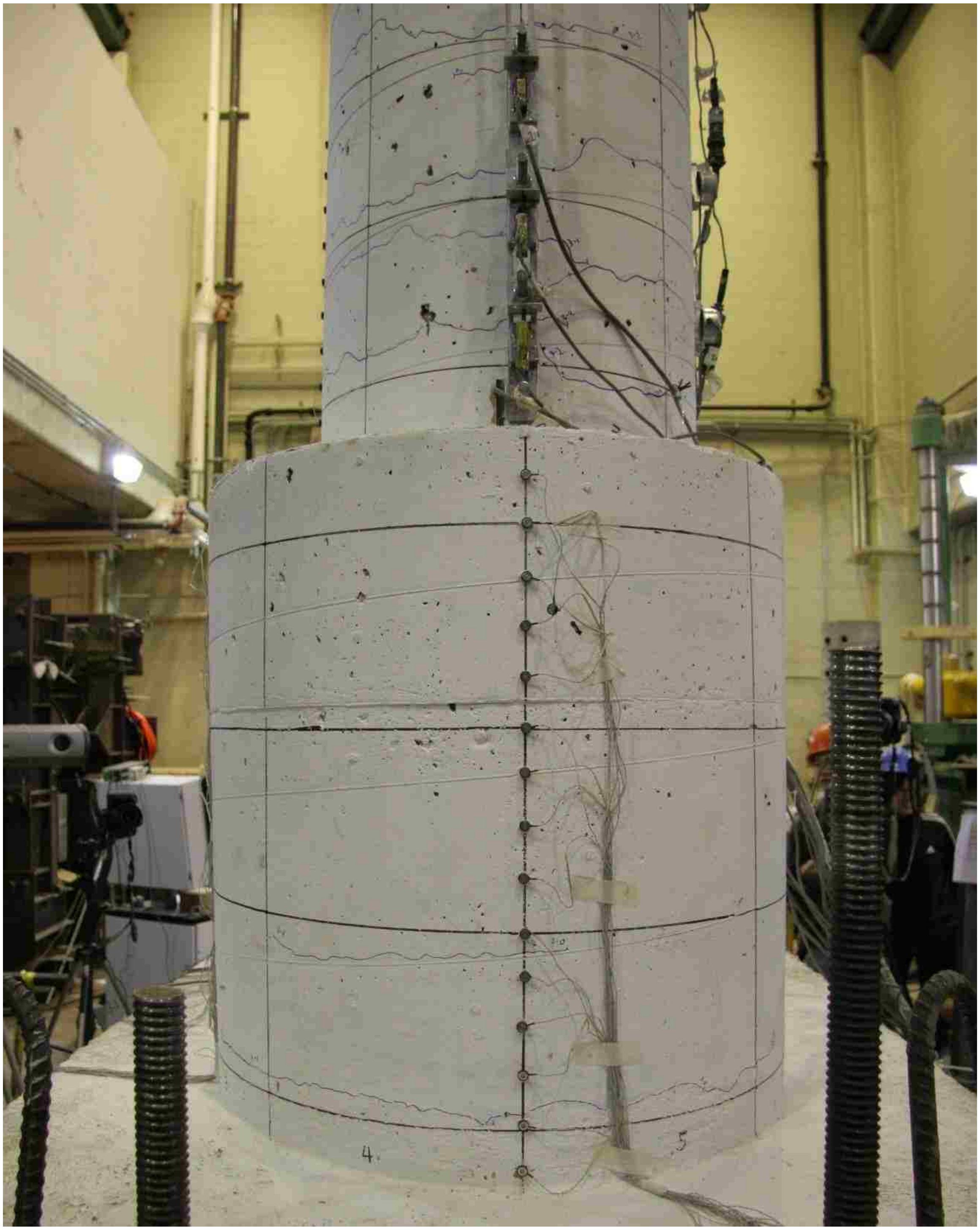

Figure C-0-1. DS-1 – Significant horizontal crack at 0.56/-0.75 percent drift

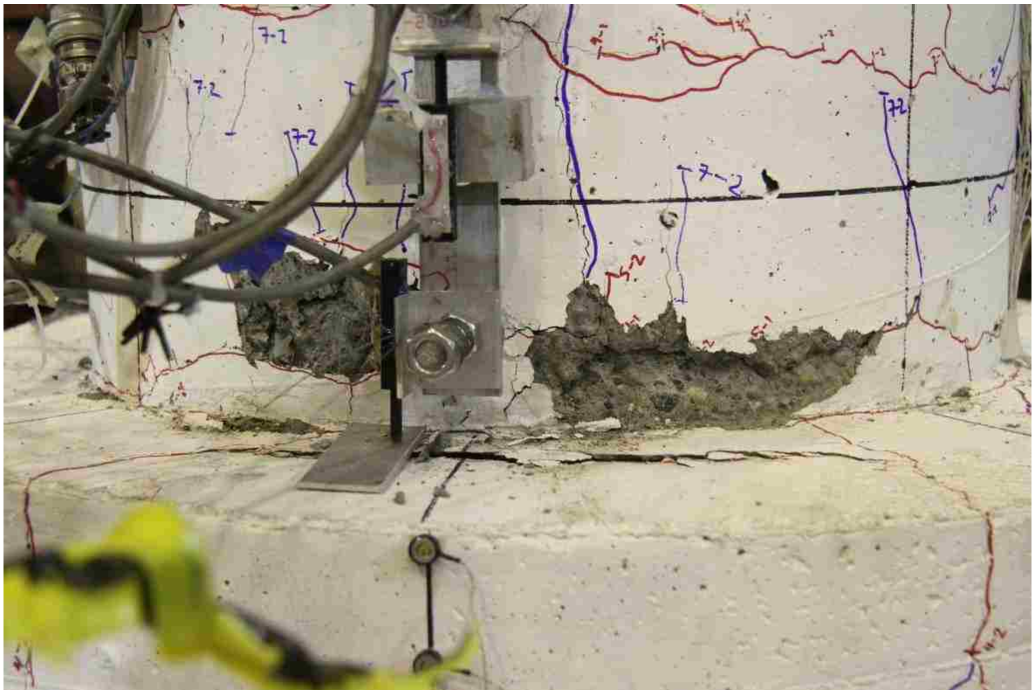

Figure C-0-2. DS-1 – First significant spalling occurred in the column at 3.00/-3.14 percent drift

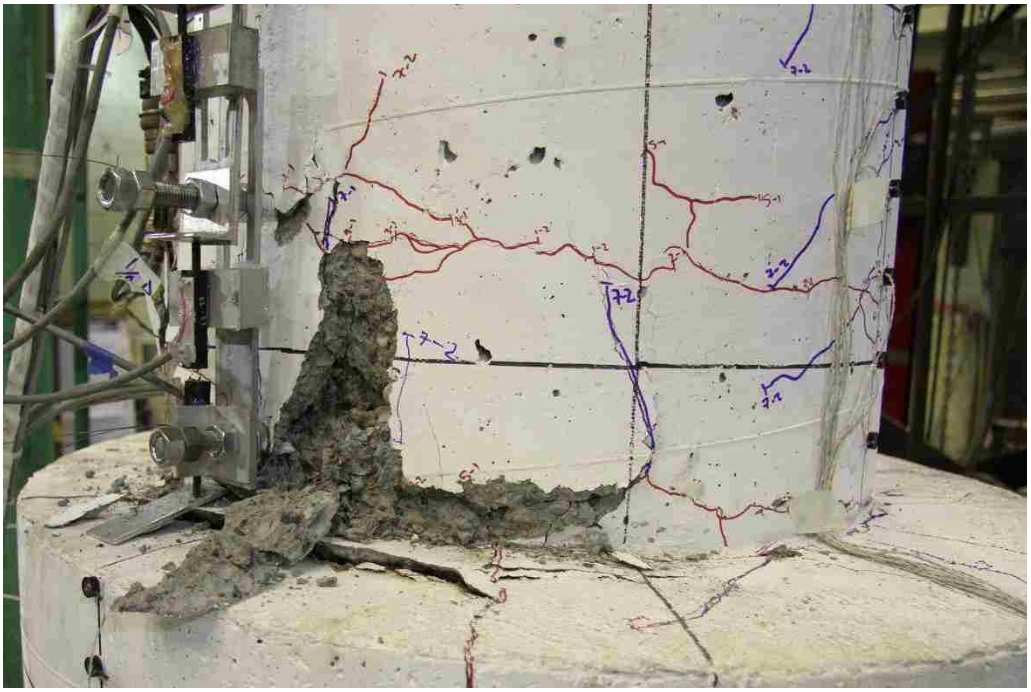

Figure C-0-3. DS-1 – Plastic hinge formed in the column at 4.60/-4.68 percent drift

Figure C-0-4. DS-1 – First noticeable bar buckling in the column at 6.90/-6.81 percent drift

Figure C-0-5. DS-1 – First column spiral fractured at 8.43/--8.27 percent drift

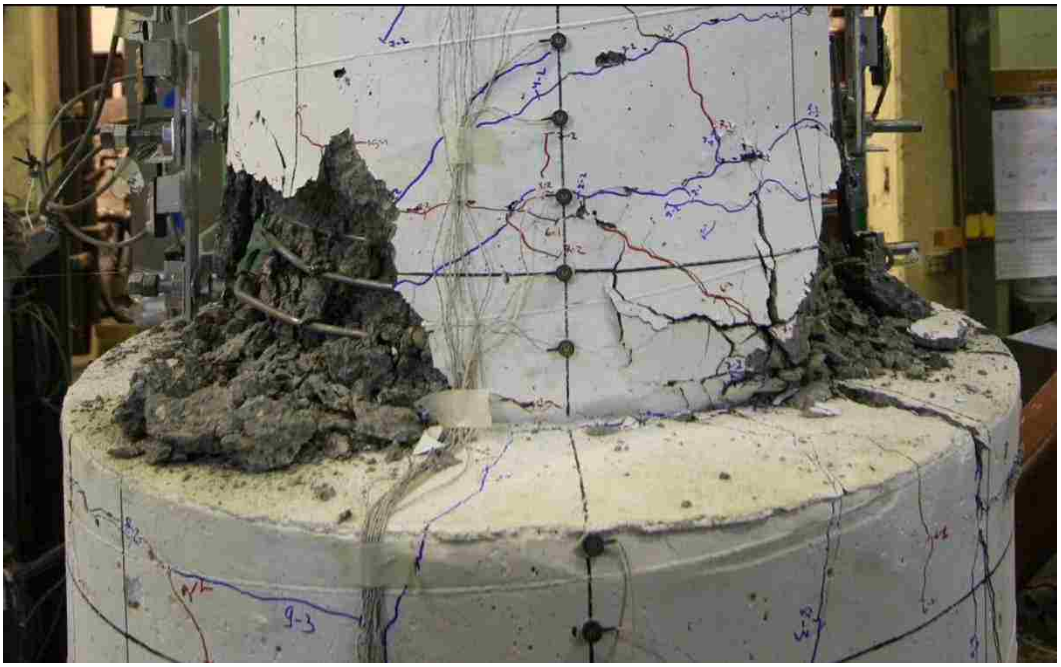

a). East side

b). West side

Figure C-0-6. DS-1 – Column damage after cyclic testing

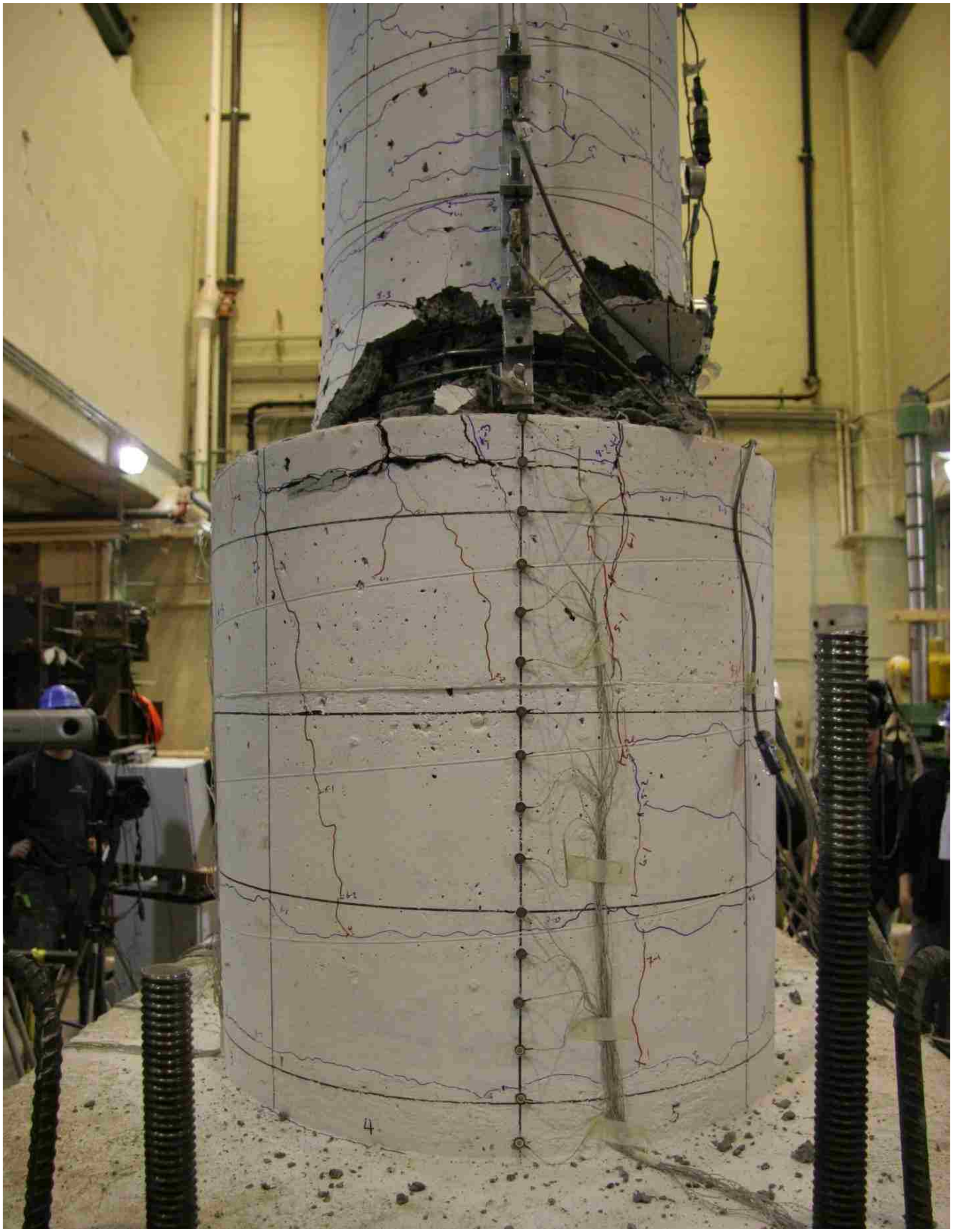

Figure C-0-7. DS-1 – Shaft damage after cyclic testing

C.2 SPECIMEN DS-2

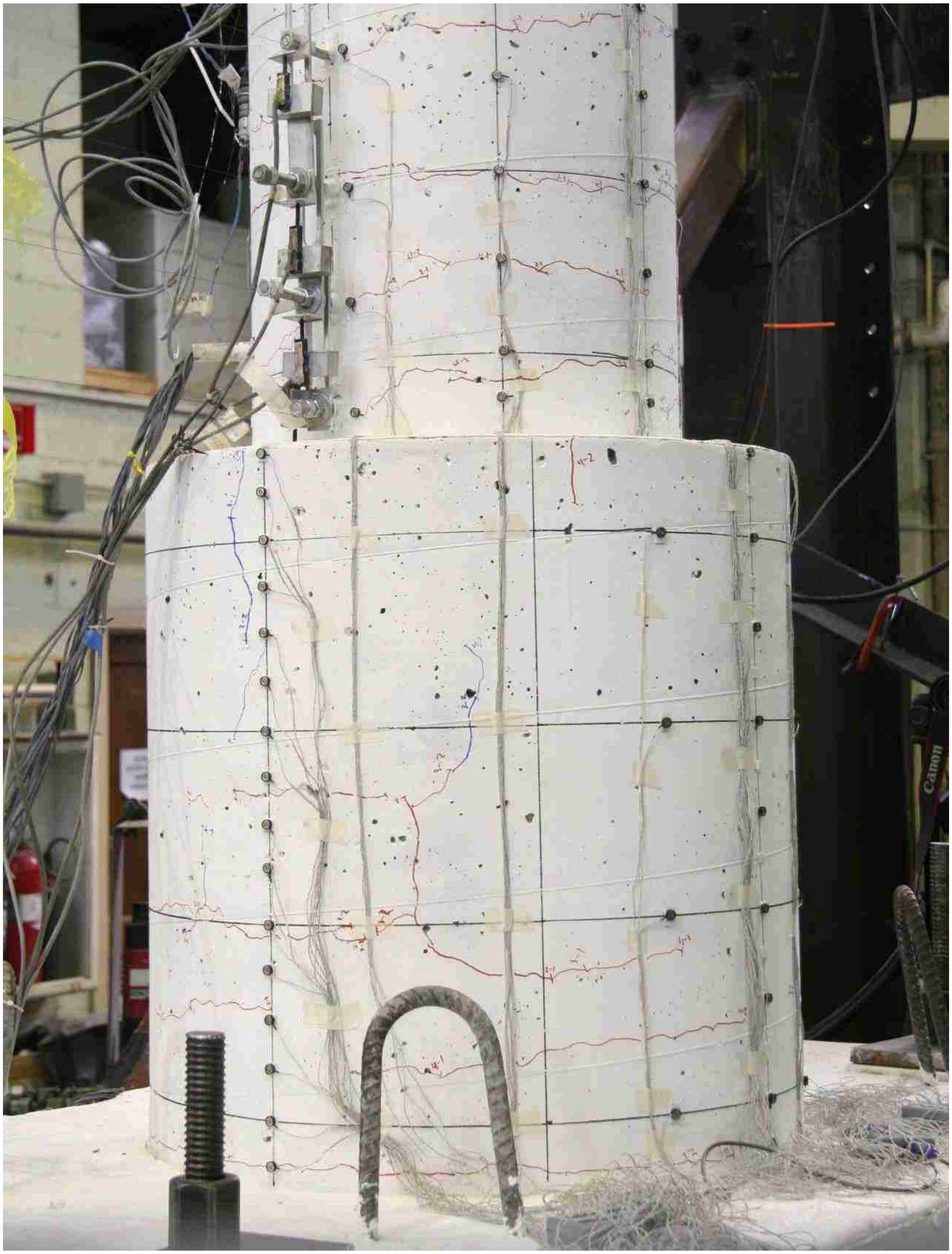

Figure C-0-8. DS-2 – Significant horizontal crack at 0.73/-0.87 percent drift

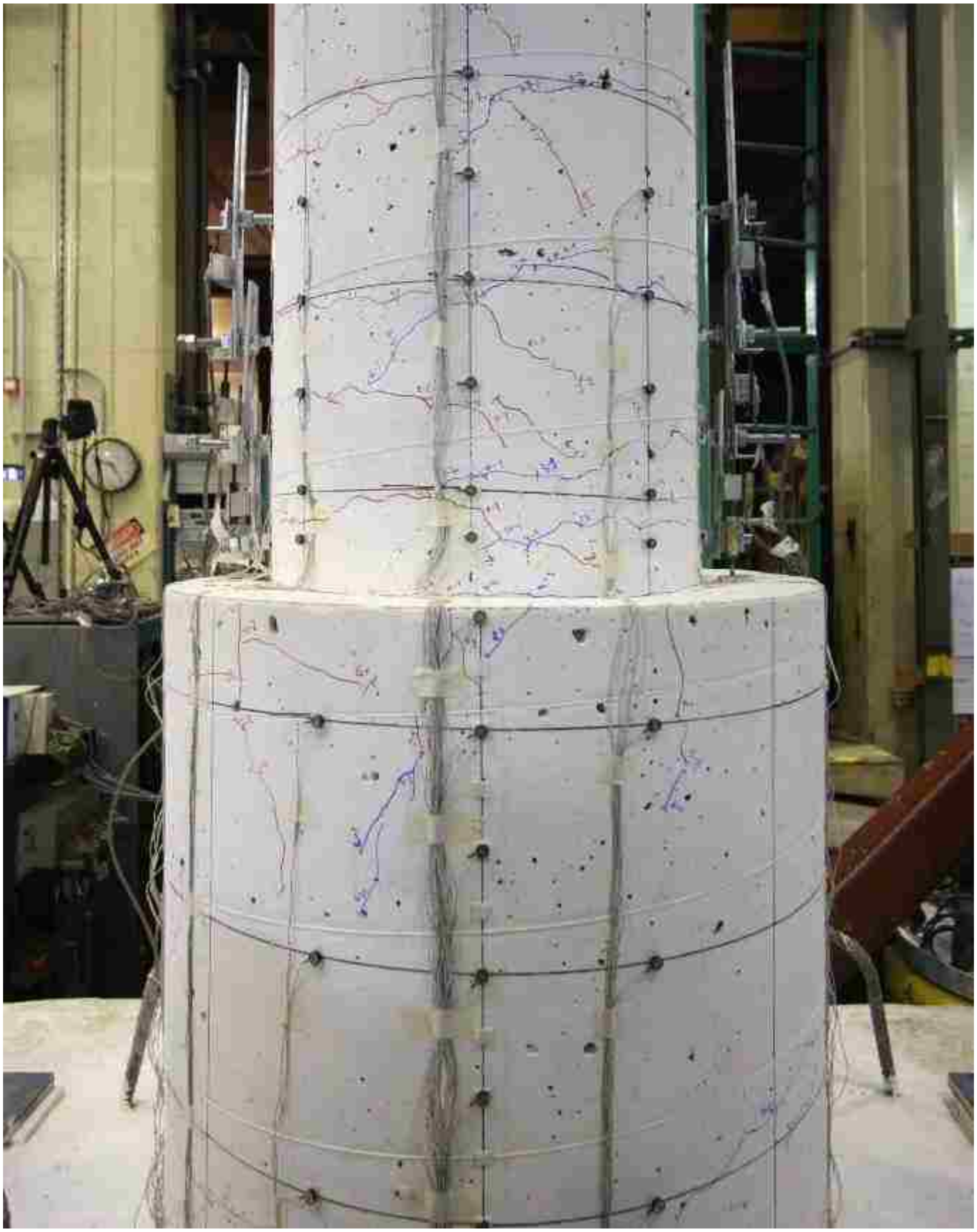

Figure C-0-9. DS-2 – First diagonal crack in the shaft at 1.87/-2.02 percent drift

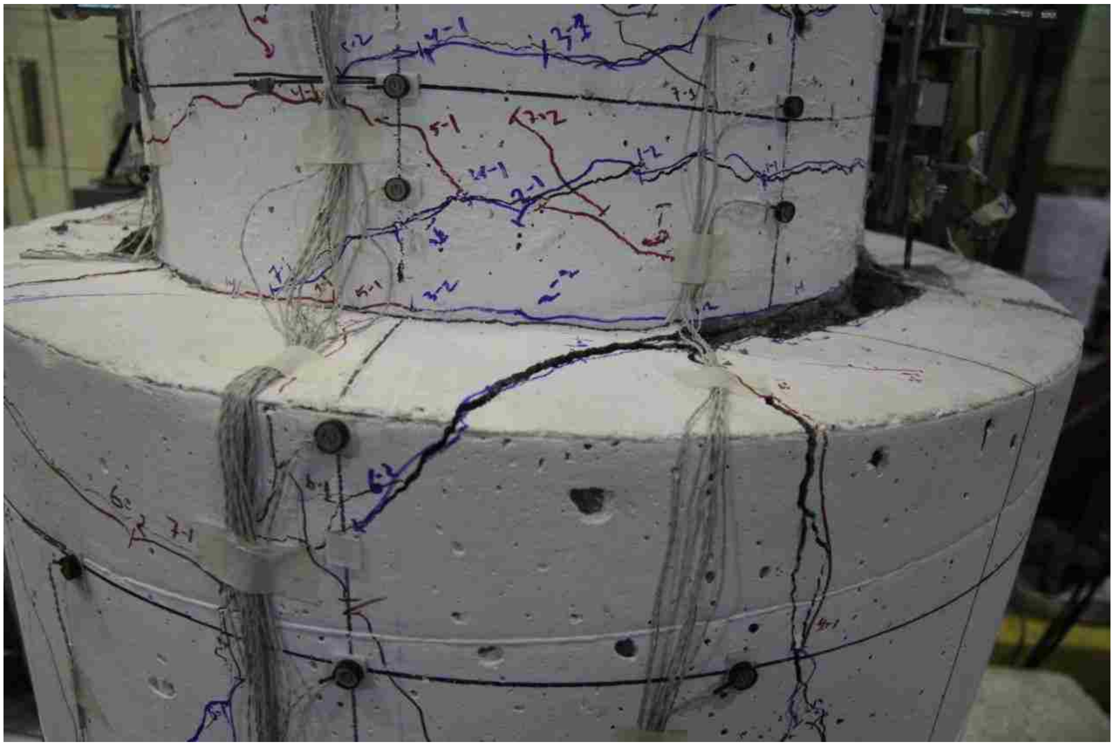

Figure C-0-10. DS-2 – Shaft damage when first shaft spiral fractured at 4.59/-4.59 percent drift

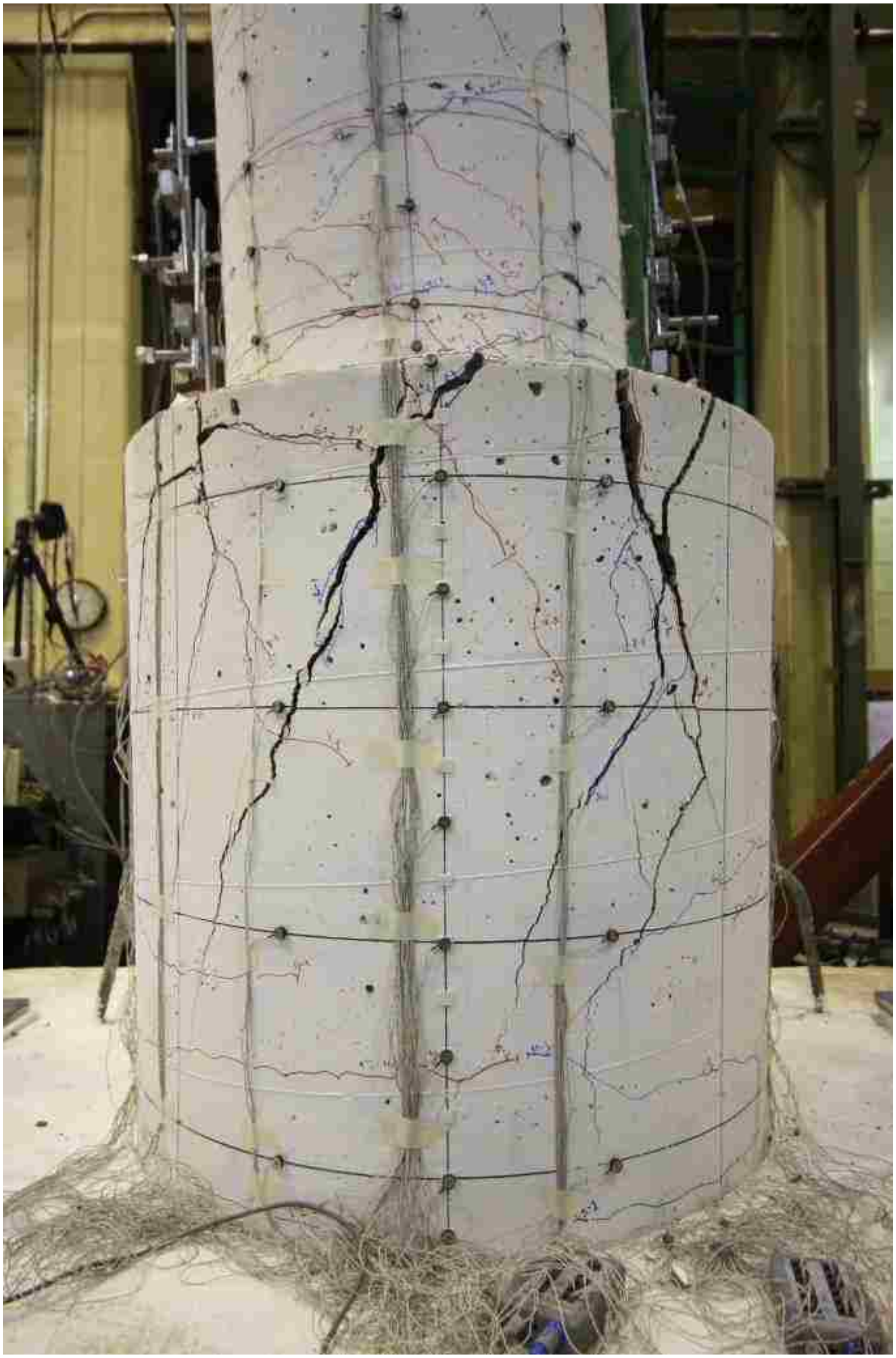

Figure C-0-11. DS-2 – First noticeable prying action in shaft at 6.72/-6.83 percent drift

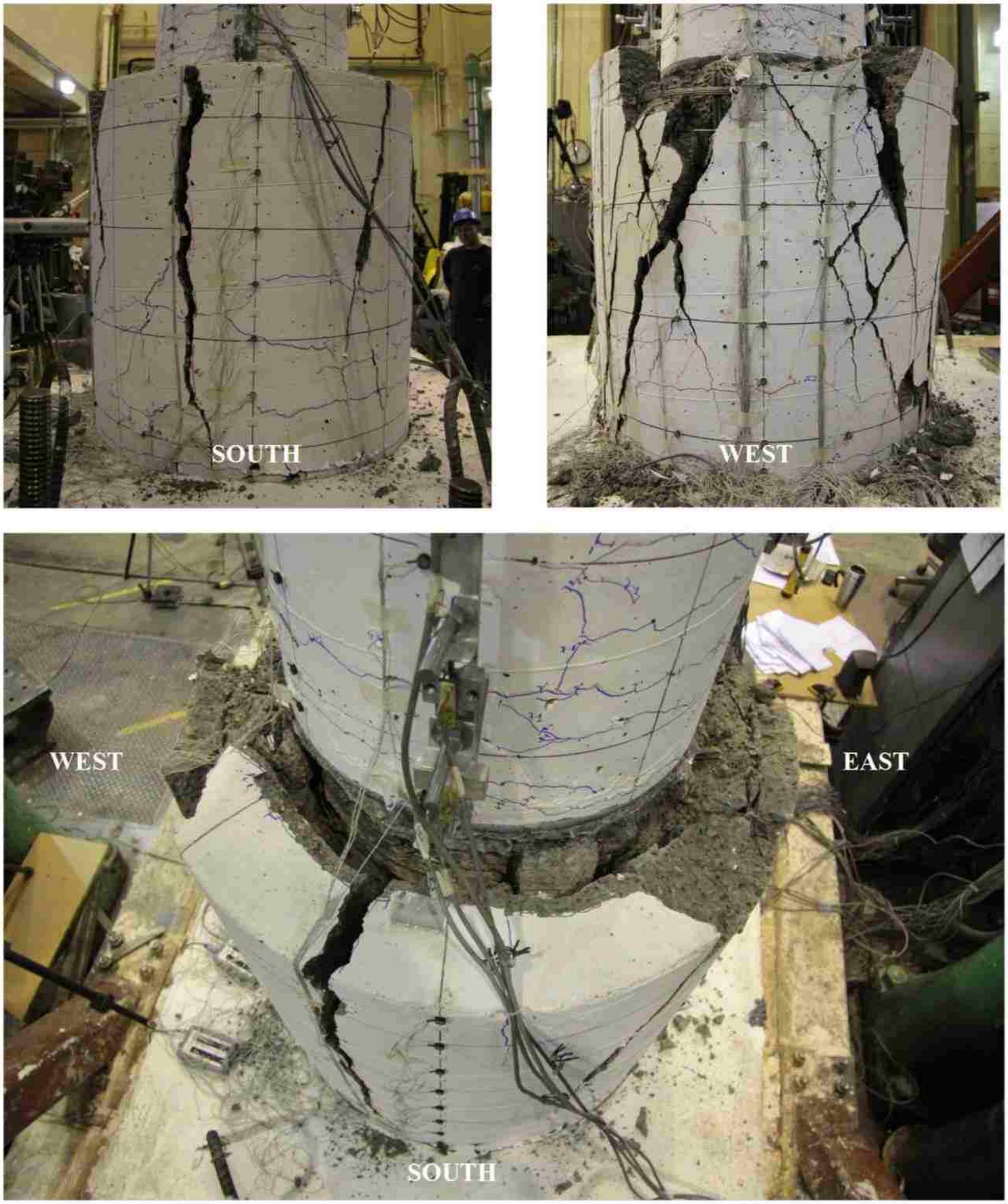

Figure C-0-12. DS-2 – Shaft damage after cyclic testing

Figure C-0-13. DS-2 – Column damage after cyclic testing

C.3 SPECIMEN DS-3

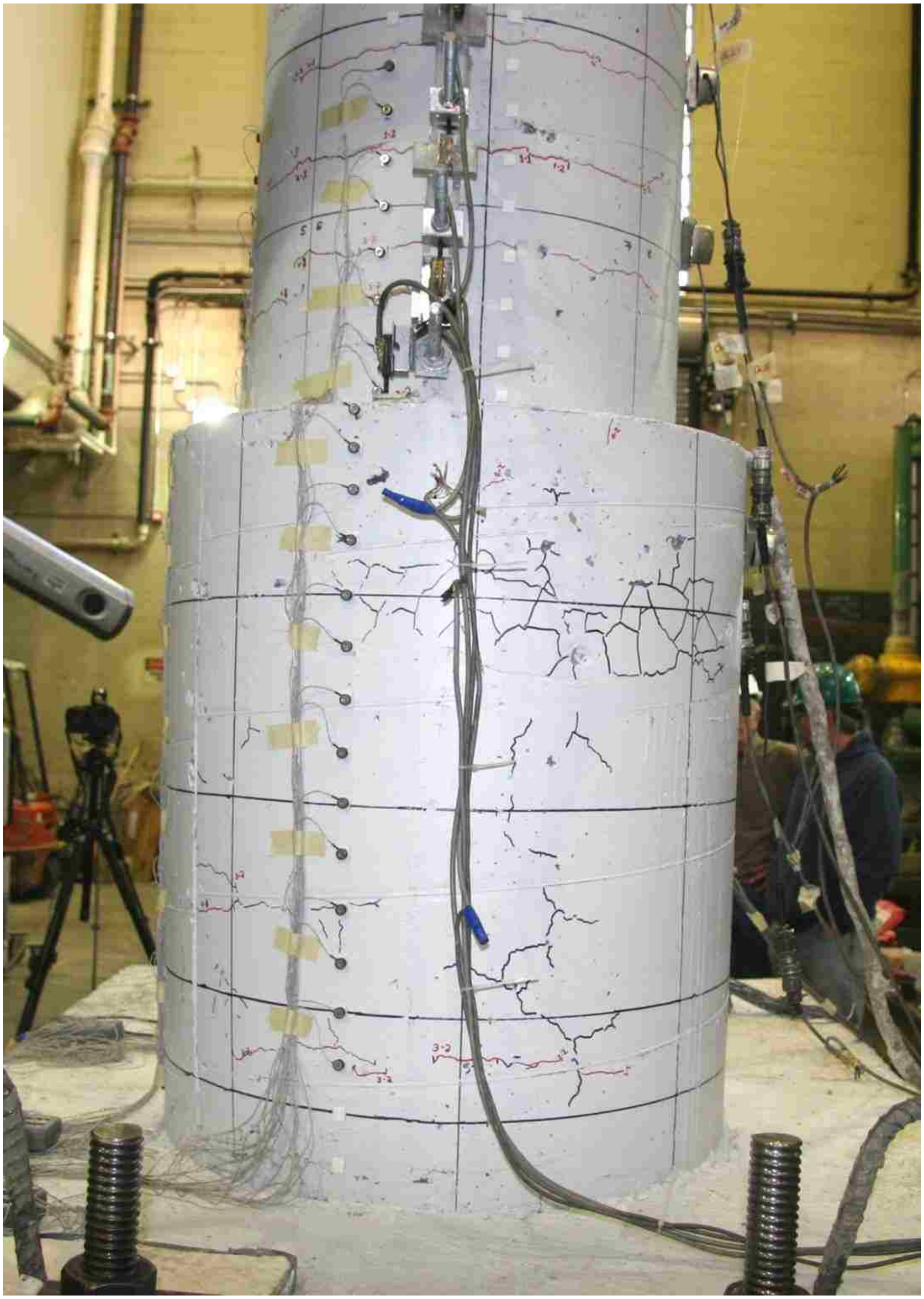

Figure C-0-14. DS-3 – Significant horizontal crack at 0.53/-0.86 percent drift

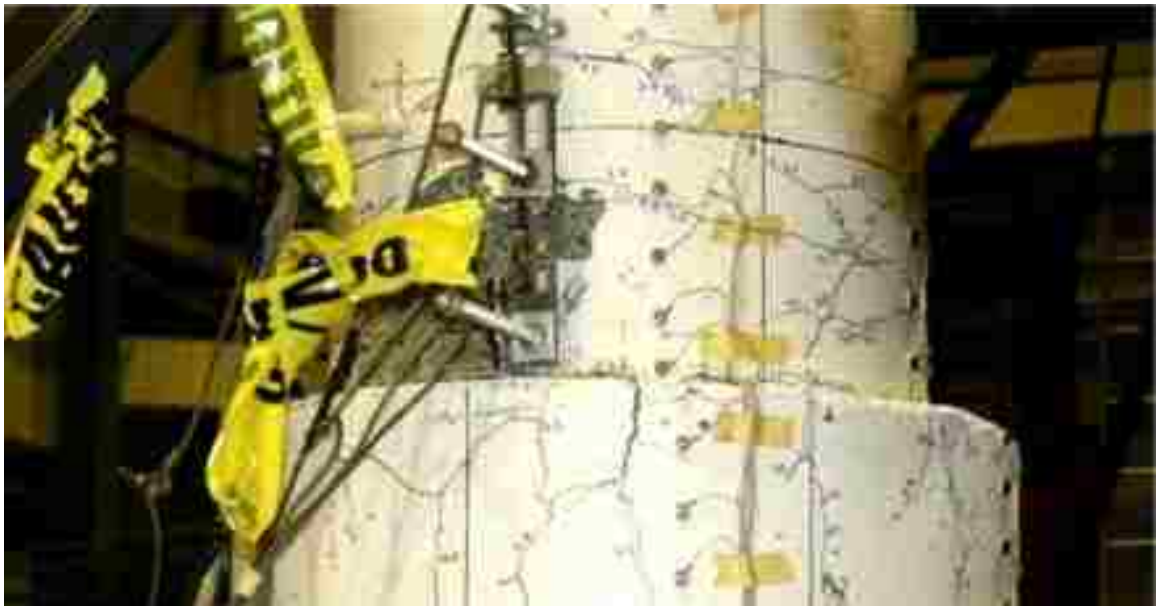

Figure C-0-15. DS-3 – First significant spalling occurred in the column at 2.98/-3.32 percent drift

Figure C-0-16. DS-3 – Plastic hinge formed in the column at 4.57/-4.84 percent drift

Figure C-0-17. DS-3 – First noticeable bar buckling in the column at 5.59/-7.00 percent drift

Figure C-0-18. DS-3 – First column spiral fractured at 6.88/--7.03 percent drift

a). East side

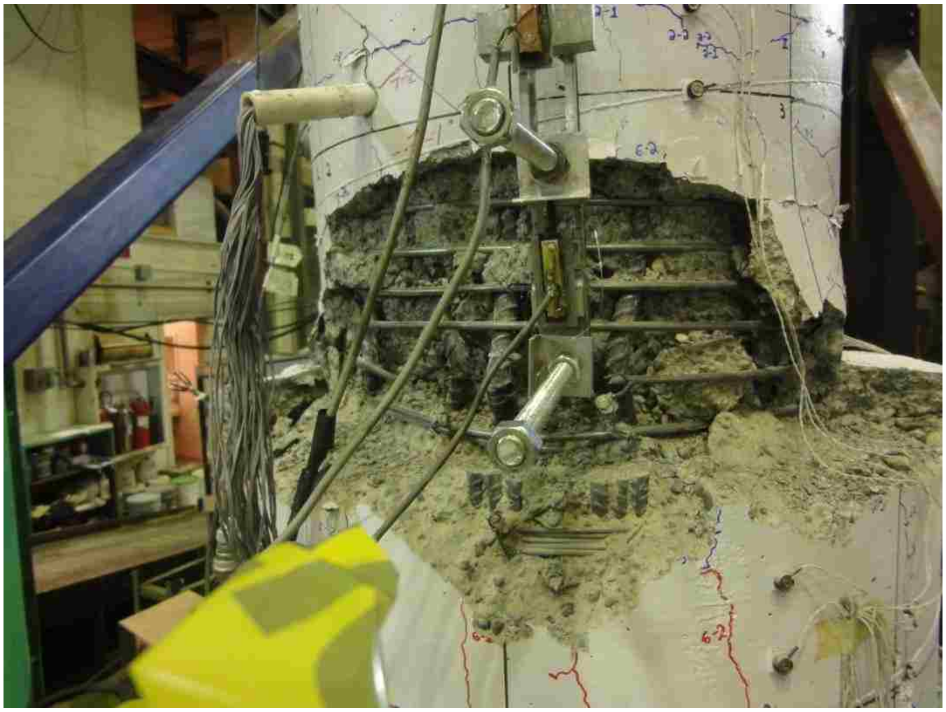

b). North side

Figure C-0-19. DS-3 – Column damage after cyclic testing

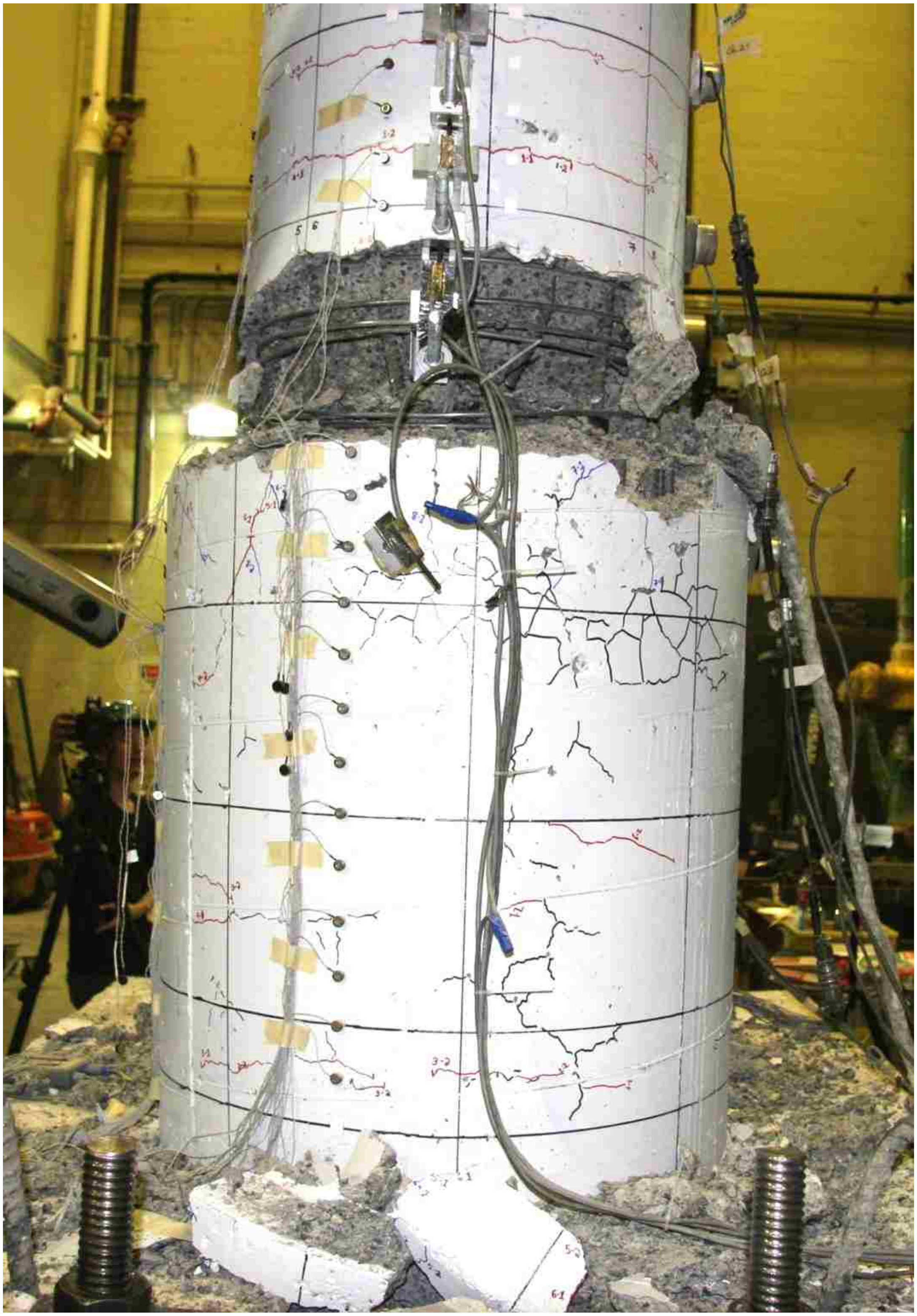

Figure C-0-20. DS-3 – Shaft damage after cyclic testing